

Multi-Level Abrasive Wear Investigation of Agricultural Tool Steels

Ádám Kalácska

Doctoral dissertation submitted to obtain the academic degree of
Doctor of Electromechanical Engineering

Supervisors

Prof. Patrick De Baets, PhD - Prof. Dieter Fauconnier, PhD

Department of Electromechanical, Systems and Metal Engineering
Faculty of Engineering and Architecture, Ghent University

June 2022



**GHENT
UNIVERSITY**

Multi-Level Abrasive Wear Investigation of Agricultural Tool Steels

Ádám Kalácska

Doctoral dissertation submitted to obtain the academic degree of
Doctor of Electromechanical Engineering

Supervisors

Prof. Patrick De Baets, PhD - Prof. Dieter Fauconnier, PhD

Department of Electromechanical, Systems and Metal Engineering
Faculty of Engineering and Architecture, Ghent University

June 2022



**GHENT
UNIVERSITY**

ISBN 978-94-6355-600-2

NUR 971, 978

Wettelijk depot: D/2022/10.500/41

Members of the Examination Board

Chair

Prof. Filip De Turck, PhD, Ghent University

Other members entitled to vote

Prof. Wim De Waele, PhD, Ghent University

Kannaki Shanmugham Pondicherry, PhD, Ghent University

Kati Valtonen, PhD, Tampere University, Finland

Prof. László Zsidai, PhD, Hungarian University of Agriculture and Life Sciences, Hungary

Supervisors

Prof. Patrick De Baets, PhD, Ghent University

Prof. Dieter Fauconnier, PhD, Ghent University

English title:

Multi-Level Abrasive Wear Investigation of Agricultural Tool Steels

Dutch title:

Multilevelonderzoek van abrasieve slijtage van staalsoorten voor landbouwwerktuigen

Hungarian title:

Talajművelő szerszámacélok abrázíós kopási folyamatai

De auteur geeft de toelating dit doctoraatswerk voor consultatie beschikbaar te stellen, en delen ervan te kopiëren uitsluitend voor persoonlijk gebruik. Elk ander gebruik valt onder de beperking van het auteursrecht, in het bijzonder met betrekking tot de verplichting uitdrukkelijk de bron te vermelden bij het aanhalen van de resultaten van dit werk.

The author gives the authorization to consult and copy parts of this work for personal use only. Any other use is limited by the Laws of Copyright. Permission to reproduce any material contained in this work should be obtained from the author.

A szerző a jelen disszertációnak csak és kizárólag személyes célból történő felhasználására és másolására ad felhatalmazást. Bármely más felhasználását a szerzői jogi törvény korlátozza. A műben szereplő anyagok reprodukálásának engedélyét a szerzőtől kell beszerezni.

Copyright © Ádám Kalácska

Gent, 2022

“If plan A does not work, the alphabet has a lot more letters... Stay cool.”

Random Google comment

“But never abandon courage and always strive forward.”

Eugène Mattelaer - Never lose courage

- *To my father* -

ACKNOWLEDGEMENT

First, I would like to express my deepest gratitude to my main promoter Prof. Dr. Patrick De Baets for his support, persistent help and guidance. I am especially grateful to Dr. Jacob Sukumaran for his support and daily supervision of my work. Without their help, expertise and encouragement I could not achieve these results.

I appreciate the valuable advices received from my co-promotor Prof. Dr. Dieter Fauconnier during my research work. I also would like to thank all of the other and former members of Soete Laboratory (Department of Electromechanical, Systems and Metal Engineering, UGent) especially Dr. Wouter Ost, Ir. Jonathan Vancoillie, Dr. Kannaki Pondicherry, Dr. Jan De Pauw, Dr. Levente Ferenc Tóth and ir. Naveenkumar Rajendhran for their valuable discussions, help and useful suggestions. Also, I would like to thank Gözdenur Toraman, Sameera Naib, Soasometh Chhith, Kaveh Samadian, Jie Zhang, Harishchandra Lanjewar, Jules Bossert, Rahul Iyer Kumar, Jean Carlos Poletto and Vitor Adriano for their cheerful support. I appreciate the effort of ir. Fabien Tailleu for his contribution towards this dissertation through his master thesis.

I appreciate the support and collaboration work with Dr. Róbert Keresztes (MATE), Dr. László Székely (MATE), Dr. Hasan Muhandes and Dr. Hayder Al-Maliki. Also, I would like to thank Dr. Florian Schramm (TUBS) and Dr. Haithem Ben Hamouda (OCAS) for the material support and the fruitful research cooperation.

I acknowledge the financial support received through Research Fund for Coal and Steel (RFCS) project RFSR-CT-2015-00010 (IMMARS) and IWT 150999 (ViRoRe) project.

I am particularly grateful for the kind administrative support received from Georgette D'hondt and Muriel Vervaeke. I am thankful for the ever-helpful technical support from Sam Demeester, Tonino Vandecasteele, Hans Van Severen, Johan Van Den Bossche, Lieven Van West, Luc Berckmoes and Michel De Wale.

I owe a deep gratitude to my family and friends (Bálint, Márk, Marci, Tamás, András, Pali, Miki, Zsófi, Bandi, Misi, Anna, Böröcz, Peti, Donát, Gábor...) for their support, advices and encouragement as well as providing a cheerful and positive environment for me. I would like to especially thank Klára Bartha for her continuous support and patience during these years. Finally, I am eternally grateful to my parents Magdolna Kalácska and Prof. Dr. Gábor Kalácska, as well as my sister Erika Kalácska for believing in me and for their endless support in my whole life. Their love and encouragement helped me through tough times.

TABLE OF CONTENTS

Acknowledgement.....	IX
Symbols and units	XV
Acronyms.....	XVIII
Summary	XIX
Samenvatting (<i>Dutch summary</i>).....	XXIII
Összefoglalás (<i>Hungarian summary</i>).....	XXVII
1 Chapter 1 Introduction	1
1.1 Background.....	2
1.1.1 Wear	4
1.1.2 Abrasion.....	5
1.1.3 Wear in soil engaging agricultural implements.....	7
1.2 Problem definition and motivation of the research.....	9
1.3 Basics of abrasive wear investigation.....	11
1.4 Investigation goals and thesis structure.....	14
2 Chapter 2 Field Investigation of cultivator tines	16
2.1 Introduction.....	17
2.1.1 Wear process in soil engaging tools	17
2.1.2 Wear influencing parameters.....	18
2.1.3 Wear investigation approaches.....	20
2.2 Material and investigation method.....	22
2.3 Field investigation results.....	25
2.3.1 Mass loss and dimensional change	25
2.3.2 Soil investigation	29
2.3.3 Surface characterization.....	31
2.3.3.1 Top surface.....	31
2.3.3.2 Cutting side (edge)	32
2.3.3.3 Surface fatigue.....	35
2.3.4 Hardness measurements.....	36
2.3.5 Particle flow investigation with DEM	37
2.4 Conclusions from field investigation	38
3 Chapter 3 Investigated Materials	39
3.1 Materials.....	40

4	Chapter 4 Micro level single-asperity contact abrasion investigation	43
4.1	Introduction.....	44
4.1.1	Abrasive micro-wear process	44
4.1.2	Wear investigation approaches.....	45
4.2	Experimental procedure.....	46
4.3	Parameters influencing wear micro-mechanisms in single-asperity scratch testing	47
4.4	Results of scratch testing.....	49
4.4.1	Wear modes	49
4.4.2	Groove depth.....	50
4.4.3	Degree of penetration (Dp)	52
4.4.4	Parametric study, specific wear rate	53
4.4.5	Multiple linear regression models and sensitivity analysis	54
4.4.6	Coupling to material properties	60
4.5	Conclusions from single-asperity scratch testing	61
5	Chapter 5 Macro level multi-asperity contact abrasion investigation	62
5.1	Introduction.....	63
5.2	Experimental procedure.....	64
5.3	Parameters influencing wear micro-mechanisms in multi-asperity contact testing	65
5.4	Results of pin-on-disk testing	66
5.4.1	Surface characterization and wear modes	66
5.4.2	Mass loss	68
5.4.3	Parametric study and wear rate	71
5.4.4	Hardness investigation	75
5.4.5	Microstructure investigation.....	77
5.4.6	Multiple linear regression models and sensitivity analysis	78
5.4.7	Coupling to material properties	83
5.5	Conclusions from multi-asperity pin abrasion testing	83
6	Chapter 6 Co-existing wear mode investigation in multi-asperity contact.....	85
6.1	Introduction.....	86
6.2	Slurry abrasion-erosion	87
6.3	Experimental procedure.....	88
6.4	Results of slurry pot testing.....	90
6.4.1	Wear rate.....	90
6.4.2	Surface characterization and wear modes	92
6.4.3	Pitting investigation.....	95

6.4.4	Hardness investigation	100
6.4.5	Multiple linear regression models and sensitivity analysis	100
6.5	Conclusions from multi-asperity slurry pot testing	104
7	Chapter 7 Conclusions	105
7.1	Connection of multi-scale testing.....	106
7.2	Main research conclusions	109
7.3	Recommendations for further study.....	112
8	References	113
9	Appendix.....	121
10	Curriculum Vitae	123

SYMBOLS AND UNITS

Latin symbols:

Notation	Name, comment, value	Unit
Δm^*	Normalized mass loss with contact area	%
A_g	Groove area	μm^2
Al	Aluminium	
A_s	Shoulder/ridge area	μm^2
B	Boron	
C	Carbon	
CMn	Carbon manganese	
$CMnSi$	Carbon manganese silicon	
Cr	Chromium	
Cu	Copper	
Dp	Degree of penetration	
d	Abrasive particle size	μm
E	Young's modulus	GPa
E_c	Compressive modulus	GPa
F_N	Normal load	N
H	Hardness	HV
h	Scratch depth	μm
k	Specific wear rate	mm^3/Nm
L	Scratch length	mm
m	Mass	kg
$m/m\%$	Mass per mass percent concentration	
Mn	Manganese	
MnB	Manganese boride	
Mo	Molybdenum	
MoB	Molybdenum boride	
Nb	Niobium	
Ni	Nickel	
P	Phosphorus	
r	Indenter tip radius	μm
R	Arm radius	mm

<i>Ra</i>	Arithmetical mean height	μm
<i>Rc</i>	Profile element average height	μm
<i>Rk</i>	Kurtosis	-
<i>Rp</i>	Highest peak	μm
<i>Rq</i>	Root mean square height	μm
<i>Rsk</i>	Skewness	-
<i>Rsm</i>	Mean width of the profile elements	μm
<i>Rt</i>	Total height of the profile	μm
<i>Rv</i>	Lowest valley	μm
<i>Rz</i>	Maximum height	μm
<i>S</i>	Sulphur	
<i>s</i>	Sliding distance	m
<i>Sa</i>	Surface arithmetic mean deviation	μm
<i>Si</i>	Silicon	
<i>SiC</i>	Silicon carbide	
<i>Sq</i>	Surface root mean square mean deviation	μm
<i>Sz</i>	Surface ten-point height	μm
<i>Ti</i>	Titanium	
<i>V</i>	Vanadium	
<i>v</i>	Velocity	m/s
<i>V_g</i>	Groove volume	mm ³
<i>V_s</i>	Shoulder/ridge volume	mm ³
<i>W</i>	Charpy ISO 148-1 (20 °C/–40 °C)	J
<i>w</i>	Half width of wear groove	μm
<i>wt%</i>	Weight percent concentration	

Greek symbols:

Notation	Name, comment, value	Unit
α	Attack/impact angle, specimen orientation angle	°
β	Degree of wear	-
γ	Indenter cone angle	°
δ	Apex angle	°
σ_c	Compressive strength	MPa
σ_Y	Yield strength	MPa
σ_M	Ultimate tensile strength	MPa
ε_M	Uniform elongation	%
ε_B	Fracture elongation	%
τ	Tine tip angle	°

ACRONYMS

3D	Three-dimensional
ADI	Austempered ductile iron
Al ₂ O ₃	Aluminium-oxide, alumina
ANN	Artificial neural network
ANOVA	Analysis of variance
ASTM	American Society for Testing and Materials
CDP	CastoDur Diamond Plates
CFD	Computational fluid dynamics
CPS	Critical particle size
DEM	Discrete Element Method
FEA	Finite-element analysis
FM	Fresh martensite
GNP	Gross National Product
IBM	International Business Machines corporation
ISO	International Organization for Standardization
MLP	Multilayer perceptrons
MP	Multiphase
pH	Potential of hydrogen
Q&T	Quenched and tempered
RA	Retained austenite
RBF	Radial basis network
RD	Rolling direction
RFCS	Research Fund for Coal and Steel
ROI	Region of interest
rpm	Rotations per minute
sd	Standard deviation
SEM	Scanning Electron Microscopy
TD	Transverse direction
TM	Tempered martensite
TRIP	Transformation Induced Plasticity
TWIP	Twinning Induced Plasticity
USA	United States of America

SUMMARY

Understanding the wear mechanisms in wear parts is a crucial element of tribological investigation, particularly in agricultural applications where the knowledge about abrasive micro-mechanisms of soil engaging tools is limited. Multiple factors contribute to wear, including materials, contact configuration, tool geometry (shape/size), soil condition including moisture content, soil constituents, and physical properties, operational aspects such as e.g. tillage speed and depth as well as other environmental parameters. In this research work, symmetrical skew wedge cultivator tines of 27MnB5 steel were wear tested to investigate the change in mass, linear dimensions, hardness and microstructure, aiming at prolonging the lifetime of these parts through better performing materials and design adjustments. Based on the mass loss measurements and change in geometrical dimensions the wear trends obtained from the in-field tests carried out in a typical European crop production land were in good agreement with literature about symmetrical goose foot tines. A linear decrease in the absolute mass was observed during the tillage operation, with a dominant dimensional reduction of the tip and edge length rather than the tine thickness. The wear mechanisms were optically identified and characterized by non-contact 3D optical profilometry. Test results clearly shows a zone specific wear micro-mechanism. The cutting edge of the tine could be segmented into a micro-cutting and a micro-ploughing zone. Vickers hardness and microstructural analysis were performed on the cross-section of the sliding interface. A tribo-layer was identified on the worn surface. Degree of penetration (D_p) of the wear scratches was calculated to justify the wear micro-mechanisms. A Discrete Element Method (DEM) model was used to investigate the soil flow during the tillage process. The model results and field test wear scars are in good agreement with each other with respect to the wear patterns. As concluded from real scale tests, co-existing micro-mechanisms were observed, amongst which micro-cutting was the dominant mechanism responsible for material removal. To enhance the operating life of the tine, newly developed materials with enhanced wear resistance against micro-cutting were proposed and wear tested.

Steel making companies are developing new steels with complex microstructure to satisfy abrasion resistance issues. The wear behaviour of a number of different steels targeted for tine material replacement and other abrasion and erosion applications in agriculture and mining industry were investigated in three abrasive test systems with different complexity.

One of the main challenges in tribology of agricultural tools is establishing a relationship between lab-scale testing and real applications. Nevertheless, the wear micro-mechanism can stand as an effective mediator amid different test scales. In this research, different scales of testing methods were applied: (1) in-field testing of agricultural tines (real scale), (2) intermediate test using adjusted soil bin (slurry

pot test on macro scale/multi-asperity test) and (3) standard tests on macro-scale using ASTM G132 pin-abrasion tester in multi-asperity contact as well as single asperity testing using scratch tester (micro-scale). A relationship was established between different scales based on the qualitative output (wear micro-mechanism) and validated using quantitative data (Dp) based on 3D profilometry.

The three newly developed steels (fresh martensitic, tempered martensitic and a multiphase steel) were investigated under single and multi-asperity abrasion test conditions on a growing scale, and their abrasive performance was linked to material properties. As the scale is closer to the real application more variables and uncertainties are included. Scratch tests were performed with different indenter radii, shapes, and loads. In the single asperity testing a spherical diamond indenter was used with different normal loads. Wear micro-mechanisms were analysed during the scratching using optical microscopy and 3D-profilometry. The fresh and tempered martensitic steels showed a transition in micro-mechanism from micro-ploughing to micro-cutting at higher loads and smaller tip radius. For the multiphase steel with retained austenite, despite its Transformation Induced Plasticity (TRIP) effect, micro-cutting was already reached at lower loads. The tempered martensitic material outperformed the fresh martensitic material despite the similar hardness and microstructure.

The material behaviour was also investigated in multi-asperity contact systems. Pin-on-disk tests were performed with various loads and abrasive particles, as well as abrasive slurry-pot tests with different sliding velocities, distances, and impact angles of the abrasive media. In the multi-asperity test, increasing the normal load and abrasive particle size resulted in increasing mass loss and in transition in micro-mechanisms from ploughing to micro-cutting. Martensitic materials showed better wear performance due to their higher hardness. As a result of the abrasive action a newly formed tribo-layer was observed in the contact zone of all steel specimen.

Test variables such as particle geometry/indenter radius (22–200 μm), attack angle (90° – 120°) and normal force (4.5–24.2 N) were adapted to obtain various micro-mechanisms. As identified from the real tine, Dp value 0.4 representing micro-cutting at the cutting edge contributes significantly to the reduction in service life of the tines. Dp corresponding to micro-cutting was prevalent in the multi-asperity pin-abrasion as well as in single asperity testing, where the intermediate slurry pot testing reproduced all the co-existing wear mechanisms identified on the tine, including micro-fatigue in the form of pitting. The cross-sectional analysis revealed the tribo-layer formation in the test material for both real scale and multi-asperity testing. The optical in-situ observations on single asperity testing elucidated the transition in micro-mechanism.

In single-asperity testing the load and the attack angle together with the shape of the abrasive particle is fixed, where in multi-asperity contact the abrasive particle size varies together with the attack angle and shape. For this reason, the connection between the three scales was the Dp extracted from wear marks. Matching Dp between different scales justified that the same wear micro-mechanism was

achieved and resulted the same wear process. Beside the micro-mechanisms, the wear rate in case of all three scales was in the same order for the regions bound within the micro-cutting zone. Hence the wear micro-mechanism and the degree of penetration is to be considered while experimentally simulating a service life of an agricultural tine subjected to abrasion.

Comparing the test systems, the tested materials ranked similarly based on their wear performance. However, in each configuration, the dominant variable of the wear mechanism differed. The significance and contributions of test parameters, the material's mechanical properties (H , σ_M , σ_Y , E , ε_M , ε_B , W , σ_C , E_C) and the dimensionless numbers derived from them on the wear behaviour and the surface deformation were investigated. Correlation between parameters was established by multiple linear regression models. The sensitivity of the tested materials to abrasion was evaluated taking into account the wide range of influencing parameters. In terms of wear resistance, the tempered martensitic steel performed best across all the investigated test systems and was proposed as potential replacement tine material. The multiphase steel resulted in the most severe material loss. This investigation aids the design of an optimized tribo-system by enabling the prediction of the wear process in complex abrasive environment for the investigated steels.

SAMENVATTING

(Dutch summary)

Het begrijpen van de slijtagemechanismen in slijtageonderdelen is een cruciaal element van tribologisch onderzoek, met name in landbouwtoepassingen waar de kennis over abrasieve micromechanismen van grondaangrijpende gereedschappen nog beperkt is. Meerdere factoren dragen bij tot slijtage, waaronder de materialen, de contactconfiguratie, de gereedschapsgeometrie (vorm/afmetingen), de bodemgesteldheid inclusief vochtgehalte, de bodembestanddelen en de operationele aspecten van de werktuigen zoals de grondbewerkingsnelheid en diepte, evenals andere omgevingsparameters. In dit onderzoekswerk werden symmetrische, schuine wigcultivatortanden van 27MnB5-staal aan abrasieve slijtage onderworpen om de verandering in massa, lineaire afmetingen, hardheid en microstructuur te onderzoeken. Finaal is het doel de levensduur van deze onderdelen te verlengen door middel van beter presterende materialen en enkele ontwerpaanpassingen. Massaverliesmetingen en observatie van de verandering in geometrische afmetingen werden verkregen uit veldtesten die werd uitgevoerd in een typisch Europees gewasproductieland. De bekomen slijtagetrends komen goed overeen met de literatuur over symmetrische ganzenvoettanden. Tijdens de grondbewerking werd een lineaire afname van de absolute massa waargenomen, met een dominante dimensionele vermindering van de punt- en randlengte in vergelijking met de afname van de tanddikte. De slijtagemechanismen op de tand werden geïdentificeerd en gekarakteriseerd door middel van contactloze 3D optische profilometrie. De testresultaten tonen duidelijk een zonespecifiek slijtagemicromechanisme. De slijtagezone aan de snijkant van de tand kan worden gesegmenteerd in een microsnij- en microploegzone. Vickers-hardheid en microstructurele analyse werden uitgevoerd op de dwarsdoorsnede van de snijkant. Op het versleten oppervlak werd een tribolaag geïdentificeerd. De penetratiegraad (D_p) van de slijtagegroeven werd berekend om de slijtagemicro-mechanismen te beschrijven. De Discrete Elementen Method (DEM) werd gebruikt om de bodemstroming tijdens het grondbewerkingsproces te onderzoeken. De modelresultaten en de slijtagesporen uit de praktijk komen goed met elkaar overeen wat betreft het slijtagepatroon. Zoals geconcludeerd uit veldtesten werden naast elkaar bestaande micromechanismen waargenomen, waaronder het microsnijden dat het dominante mechanisme was dat verantwoordelijk is voor materiaalverwijdering. Om de levensduur van de tand te verlengen, werden nieuw ontwikkelde materialen voorgesteld met een verbeterde slijtvastheid tegen microsnijden die getest werden op slijtage.

Staalproducenten ontwikkelen nieuwe staalsoorten met een complexe microstructuur om aan slijtvastheidsproblemen te voldoen. Het slijtagegedrag van verschillende staalsoorten, bedoeld voor het vervangen van tandmateriaal maar ook voor andere slijtage- en erosietoepassingen in de

landbouw en mijnbouw, werden onderzocht met drie abrasieve testsystemen met verschillende complexiteit.

Een van de belangrijkste uitdagingen in de tribologie van landbouwwerktuigen is het leggen van een relatie tussen testen op laboratoriumschaal en de echte toepassingen. In dit onderzoek zijn verschillende testmethoden toegepast: (1) veld testen van landbouwtanden (echte schaal), (2) intermediaire test met aangepaste bodemcontainer (slurrypot test op macroschaal/multi-asperiteitstest) en (3) standaardtests op macroschaal met behulp van ASTM G132 pin-abrasie-tester in multi-asperiteitcontact, evenals enkelvoudige asperiteitstesten met behulp van een krastest (microschaal). Er werd een relatie gelegd tussen verschillende schalen op basis van de kwalitatieve output (vastgestelde slijtage micro-mechanismes) en gevalideerd met behulp van de kwantitatieve gegevens op basis van 3D-profielen van de slijtagesporen.

De drie nieuw ontwikkelde staalsoorten (rein martensitisch, getemperd martensitisch en een meefasig TRIP-staal) werden onderzocht met testen met toenemende schaal, met enkelvoudig en multi-asperiteitscontact. Hun weerstand tegen abrasie werd in relatie gebracht tot hun aan materiaaleigenschappen. Naarmate de schaal dichter bij de werkelijke toepassing ligt, worden meer variabelen en onzekerheden meegenomen. Krastesten werden uitgevoerd met verschillende indenters (verschillende vorm en puntkromtestraal) en verschillende belastingen. Bij de enkelvoudige asperiteitstest werd een bolvormige indenter uit diamant gebruikt bij verschillende normale belastingen. De slijtage-micro-mechanismen werden geanalyseerd met behulp van optische microscopie en 3D-profilometrie. De reine en getemperde martensitische staalsoorten vertoonden een overgang in micromechanisme van microploegen naar microsnijden bij hogere belastingen en bij een kleinere puntradius. Voor het meefasige staal met restausteniet werd, ondanks het Transformation Induced Plasticity (TRIP) effect, microsnijden al bereikt bij lagere belastingen. Het geharde martensitische staal presteerde beter dan het reine martensitische materiaal ondanks de vergelijkbare hardheid en microstructuur.

Het materiaalgedrag werd ook onderzocht in multi-asperiteit contactsystemen. Er werden pen-op-schijftesten uitgevoerd met verschillende belastingen en verschillende abrasieve partikels, evenals slurrypot testen met verschillende nelheden, afmetingen en impacthoeken van de abrasieve media. In de multi-asperiteit-test resulteerde het verhogen van de normale belasting en de abrasieve deeltjesgrootte in een toenemend massaverlies en in de overgang van ploegen naar microsnijden. Martensitische materialen vertoonden betere slijtageprestaties vanwege hun hogere hardheid. Als gevolg van de abrasieve werking werd een nieuw gevormde tribolaag waargenomen in de contactzone van alle monsters.

Testvariabelen zoals deeltjesgeometrie/puntradius (22–200 μm), aanvalshoek (90–120°) en normaalkracht (4.5–24.2 N) werden aangepast om verschillende micromechanismen te bekomen.

Zoals zichtbaar op het werkelijke onderdeel, draagt een Dp-waarde van 0,4, die microsnijden aan de snijkant vertegenwoordigt, aanzienlijk bij tot de verkorting van de levensduur van de tanden. Dp, overeenkomend met microsnijden, kwam veel voor bij de multi-asperiteit pin-abrasietesten en bij krastesten. De slurypot-test reproduceerde alle naast elkaar bestaande slijtagemechanismen die op de werkelijke tand waren geïdentificeerd, inclusief micro-vermoeiing in de vorm van putvorming. De analyse van een matreiaalsectie onthulde de vorming van tribolagen op het oppervlak, voor zowel testen op werkelijke schaal als voor multi-asperiteitstesten. De in-situ optische observaties tijdens enkelevoudige asperiteitstesten verhelderden de overgang tussen de slijtage micromechanismen.

Bij enkelvoudige asperiteitstesten liggen de belasting en de aanvalshoek samen met de vorm van het abrasieve deeltje vast, terwijl bij multi-asperiteitstesten de grootte van de abrasieve deeltjes samen met de aanvalshoek en vorm varieert. Om deze reden was de connectie tussen de drie verschillende testen de Dp van de slijtagesporen. Het overeenkomen van Dp tussen verschillende schalen duidde op eenzelfde slijtage micromechanisme met eenzelfde slijtageproces. De slijtagesnelheid van de drie geteste materialen ragschikte voor de drie testen op dezelfde manier. Om op betrouwbare manier de levensduur van een cultivatortand met schaaltesten te simuleren, moet rekening worden gehouden met het micromechanisme van slijtage en de mate van penetratie van de asperiteiten.

Bij het vergelijken van de testsystemen werden de geteste materialen op weliswaar op dezelfde manier gerangschikt op basis van hun slijtageprestaties, maar in elke configuratie verschilde was een verschillend slijtagemechanisme dominante. De bijdrage van de testparameters, de mechanische eigenschappen van het materiaal ($H, \sigma_M, \sigma_Y, E, \epsilon_M, \epsilon_B, W, \sigma_C, E_C$) en de daaruit gevormde dimensieloze groepen op het slijtagegedrag en de oppervlaktevervorming werd aan de hand van regressiemodellen onderzocht. De gevoeligheid van de geteste materialen voor slijtage werd geëvalueerd rekening houdend met het brede scala aan beïnvloedende parameters. In termen van slijtvastheid presteerde het geharde martensitische staal het beste in alle onderzochte testsystemen en werd het voorgesteld als mogelijk vervangend tandmateriaal. Het meerfasige staal daarentegen ervaarde in het meest ernstige materiaalverlies. Het voorliggende onderzoek, tenslotte, helpt bij het ontwerp van een geoptimaliseerd tribosysteem door de voorspelling van het slijtageproces van staalsoorten in een complexe abrasieve omgeving mogelijk te maken.

ÖSSZEFOGLALÁS

(Hungarian summary)

PhD kutatásom célja, hogy a gyorsan kopó fém talajművelő eszközök kopási élettartamának növelését megalapozó, az abrázíós kopási folyamatokat mélyebben megismerő összefüggéseket és laboratóriumi modellezési lehetőségeket tárjak fel. E tartalmi összefoglaló megértését megkönnyíti annak az ismert jelenségnek az összefoglalása, hogy a talajban dolgozó szerszámok felületét ásványi anyag szemcsék koptatják, erodálják. A jelenség ismert mikro-mechanizmusai, amikor a szemcse a felületet rugalmasan-képlékenyen deformálja vagy forgácsolja. A mikro-mechanizmusok alakulást a szerszám anyaga mellett az abrázíós koptató szemcse alakja, mérete, élgeometriája, sebessége és terhelése, a felületi nyírás hatásszöge (attack angle, továbbiakban AA) nagyban befolyásolja. Nem elhanyagolható a talaj állapota, beleértve a nedvességtartalmat, a talajösszetevőket és azok fizikai tulajdonságait. A fém talajművelő szerszámok felületen visszamaradó abrázíós karcok keresztmetszeti jellemzője a penetrációs fok (degree of penetration, továbbiakban Dp), amely a karcolt felület mikrogeometriai jellemzőiből számítható, és a Dp jellemző száma a domináns felületi mikro-mechanizmusnak.

Kutató munkám során valós szántóföldi műveléssel koptatott kapák részletes felületi és mikroszerkezeti analízisével definiáltam a domináns ható mikro-mechanizmusokat. Ezek alapján laboratóriumi vizsgálati modelleket fejlesztettem, reprodukálva a valóságot jellemző Dp értékeket. A megalkotott gyakorlati és numerikus modellek további gyors kopásvizsgálatokhoz, újabb anyagok tribológiai értékeléséhez szolgálnak.

A szántóföldi referencia méréseket átlagos európai szántóföldi jellemzők mellett (talajtípus, összetétel, vízháztartás), 27MnB5 acélból készült szimmetrikus, ék alakú kultivátor kapák használatával végeztük. A kapák kopásának (tömeg- és lineáris méretcsökkenés), keménység-, és mikroszerkezet változásának vizsgálata azt a célt szolgálta, hogy új laboratóriumi modellek fejlesztésével, egy műszakilag előnyösebb anyagválasztással és konstrukciós módosításokkal meghosszabbítható legyen az alkatrészek élettartama. A kapáknál mért tömegvesztés, geometriai változás alapvetően jól tükrözi a korábbi, szakirodalmakban publikált kopási jellemzőket. A talajművelés során a kopásból származó abszolút tömeg lineáris csökkenése volt megfigyelhető, a méretcsökkenés dominánsan a hegy és az él hosszában, nem pedig a szerszámok vastagságában következett be.

A tesztelt 27MnB5 anyagminőségű kapákon optikailag (3D profilometria) azonosíthatók voltak a domináns kopási mikro-mechanizmusok. A vizsgálati eredmények alapján megállapítható volt a kapák különböző felületi részein a zónaszpecifikus kopási mikro-mechanizmus. A kapák vágóélét egy mikro-forgácsolási, és egy kombinált mikro-forgácsolási/deformációs zónára lehetett elkülöníteni. A csúszófelület keresztmetszetén végzett Vickers-keménységmérés és mikroszerkezeti elemzés is

alátámasztotta azt a következtetést, hogy a koptató igénybevételnek kitett felületen ún. tribo-réteg alakult ki, melynek jellemzői eltérnek az alapanyag jellemzőitől. A kopási mikro-mechanizmusok igazolásához a mikroszkópai adatok alapján, a kopási karcok penetrációs fokának (D_p) kiszámítása szolgált. A talajszemcsék áramlásának leírására, a szemcsék mozgásának megértésére diszkrét elemes numerikus (DEM) modell adott részletes információt. A modell eredményei és a szántóföldi vizsgálatnál tapasztalt kopásnyomok jellemzői jó egyezést mutattak.

A szántóföldi vizsgálatokból eredő kopások részletes tanulmányozása rávilágított arra, hogy jellemzően egy dupla, párhuzamosan ható iker mechanizmus okozta a kapák anyagvesztését. A kettő mikro-mechanizmus közül a talaj kemény szemcséi által okozott mikro-forgácsolás volt a domináns.

További kutatásom során a kapák élettartamának növelése érdekében újonnan kifejlesztett, a mikro-forgácsolással szembeni fokozott kopásállósággal rendelkező anyagok kiválasztása, majd azok részletes laboratóriumi kopásvizsgálata következett.

Az acélgyártó cégek jellemzően új, összetett mikro-szerkezetű acélokat fejlesztenek az abrázíós kopásállósági problémák csökkentésére. A további kutatásaimhoz három olyan acélt választottam, amelyeket jellemzően abrázíós és eróziós kopó anyagnak fejlesztettek főleg mezőgépeszeti és bányipari alkalmazásokhoz. A kiválasztott anyagok tribológiai tulajdonságainak feltárásához három, különböző összetettségű laboratóriumi modellt dolgoztam ki a mikro-mechanizmusok reprodukálhatóságát szem előtt tartva. Ez jelenti a kapcsolatot a valós események és a különböző bonyolultsági szintű modellek között.

Kutatási munkám tehát az alábbi kopásvizsgálati kategóriákat tartalmazta: (1) mezőgazdasági kapák szántóföldi mérése (valós léptékű üzemi vizsgálat, „field testing”), (2) próbapadi kategória (bench testing) talajvályú és „slurry-pot” modellekkel és (3) szabványos vizsgálatok egyszerűsített próbatestekkel és rendszerjellemzőkkel. A makroszintű modellnél „multi-asperity” (továbbiakban MA) azaz több kontaktpontos érintkezési vizsgálatnak ASTM G132 tű-tárcsás (pin-on-disk, továbbiakban PoD) kopásmérést végeztem, valamint mikro szintű vizsgálatához „single-asperity” (továbbiakban SA) azaz egy kontaktpontos modellt alkalmaztam. A különböző szintű modellek között a kopási mikro-mechanizmusok beazonosításával sikerült kapcsolatot teremteni, amelyek validálását a számszerűsített D_p adatok is alátámasztották.

A kutatásba bevont három, újonnan fejlesztett acél (martenzites, hőkezelt martenzites és egy többfázisú acél) abrázíós értékelése SA és MA vizsgálati rendszerekben, a mért jellemzők és az anyagtulajdonságok közötti kapcsolatok feltárásával történt. Az SA méréseket különböző csúcs-sugarú és alakú gömbvégű gyémánt tűvel, különböző terhelési szinteken végeztem el. Az abrázíós karc nyomok értékelését optikai mikroszkóppal és 3D-profilometriával végeztem, majd a jellemző értékek alapján a D_p számítható volt, ami validálta az abrázíós mikro-mechanizmust. A martenzites, és a hőkezelt martenzites acéloknál a mikro-mechanizmusban nagyobb terhelés és kisebb tű csúcscsúgar

esetén volt tapasztalható átmenet a deformáció és a mikro-forgácsolás között. A többfázisú, visszamaradó ausztenittel rendelkező acélnál a TRIP-hatás (Transformation Induced Plasticity) ellenére, a mikro-forgácsolás már kisebb terhelésnél is bekövetkezett. A hőkezelt martenzites anyag a hasonló keménység és mikroszerkezet ellenére, felülmúlta a sima martenzites anyagot.

A több-kontaktpontos (MA) méréseket részben PoD, részben abrazív zagy (slurry-pot, továbbiakban SP) rendszerben végeztem. A PoD vizsgálatoknál az acél anyagminták különböző szabványos abrazív szemcséken csúsztak, eltérő terhelések mellett. Az SP rendszerben változó volt a csúszási sebesség, koptatási úthossz, valamint a szemcsék ütközési orientációja. A MA vizsgálatban a normál terhelés és a csiszolószemcse méret növelése növekvő kopást és a mikro-mechanizmusok átmenetét eredményezte a deformációtól a mikro-forgácsolás irányába. A martenzites anyagok a nagyobb keménységük miatt jobb kopási ellenállást tanúsítottak. A koptató hatás eredményeként valamennyi acélminta érintkezési zónájában újonnan kialakult tribo-réteg volt kimutatható.

A kutatás során a különböző mikro-mechanizmusok meghatározásánál számos rendszerjellemző volt változó: részecske geometria, behatoló tű (indenter) sugara (22-200 μm), a hatásszög (AA) (90° - 120°) és a normál terhelés (4,5-24,2 N). A valódi kapáknál azonosított Dp érték 0.4, amely a vágóélnél lévő mikro-forgácsolást jelenti, jelentősen hozzájárul a kapák élettartamának csökkenéséhez. Ez a mikro-forgácsolásnak megfelelő Dp érték az MA és SA kopásvizsgálatoknál egyaránt jellemző volt. Az SP vizsgálati rendszerben végzett MA méréseknél az iker mikro-mechanizmusok jelenléte volt meghatározó, ugyanúgy, mint azt a kapák egyes zónáinál is tapasztalni lehetett. Az SP modell rendszer sajátossága, hogy az áramló szemcsék ütőhatása miatt felületi kifáradások, azaz pittingek jelentek meg a fémfelületeken. A vizsgálati anyagok keresztmetszeti elemzése kimutatta mind a valós kapáknál, mind a MA méréseknél a felületi tribo-réteg keletkezését. Az SA mérések során használt in-situ optikai értékelések megmutatták a mikro-mechanizmusok között bekövetkező átmenetet.

Amíg az SA vizsgálat során a terhelés, az AA, a karcoló tű alakjával együtt rögzített, addig az MA méréseknél a csiszolószemcsék mérete, a nyírási hatásszög AA és az abrazív szemcse alakja változó. A vizsgálati rendszerek közötti kapcsolatot itt is a kopásnyomok geometriáiból kiszámolt Dp értékek jelentették. Az egyes vizsgálati rendszereknél tapasztalt Dp egyezése igazolta, hogy ugyanaz a kopási mikro-mechanizmus valósult meg, és ugyanazt a kopási folyamatot eredményezte. A különböző szintű vizsgálati rendszerekben a mikro-mechanizmusok egyezése mellett, a kopásállósági sorrend is hasonlóan alakult a mikro-forgácsolási zónán belüli területek esetében. Megállapítottam és igazoltam, hogy a kopás mikro-mechanizmusait és a Dp értékeit figyelembe kell venni a kopásnak kitett talajművelő szerszámok élettartamának kísérleti szimulációja során.

A kopási mikro-mechanizmusok feltárása, reprodukálása különböző bonyolultsági szintű laboratóriumi és próbapadi modellek esetén megalapozta, hogy az egyes anyagok abrazív érzékenységét meghatározzam a különböző vizsgálati rendszerekben, modellekben. Ennek matematikai háttere a

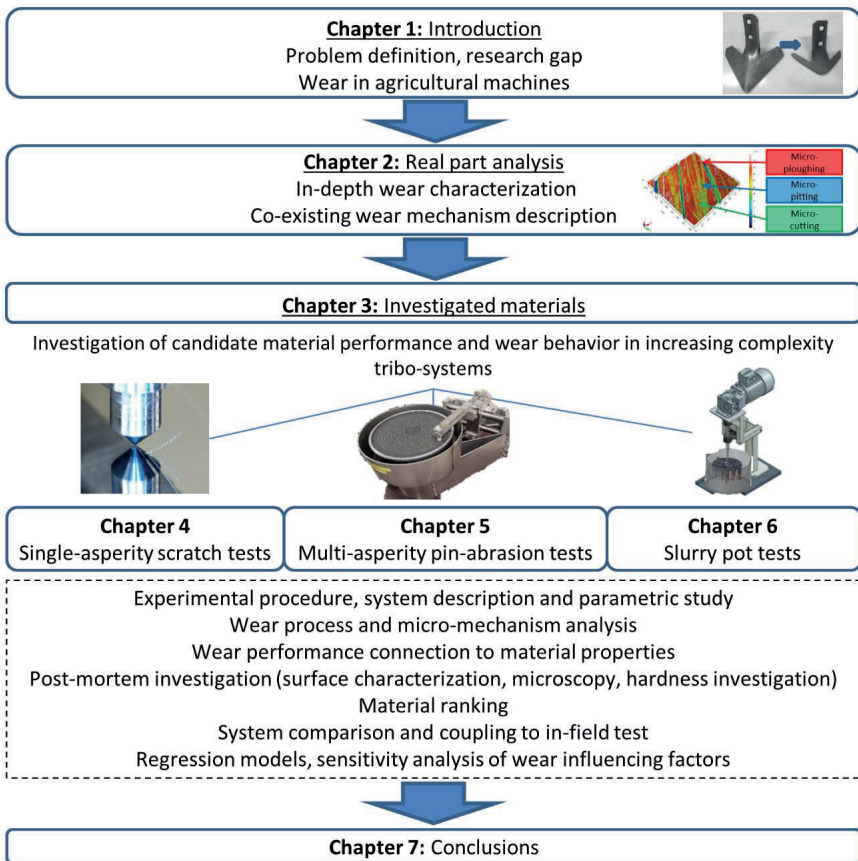
többszörös lineáris regresszió. A tribológiai rendszer eredményei (pl. kopás trendek, felületi érdesség változás) nagyszámú független változó hatásaként értelmezhetők. A regressziós modellek figyelembe veszik a koptatási úthossz, terhelés mellett pl. az anyagok mechanikai jellemzőit (H , σ_M , σ_Y , E , ε_M , ε_B , W , σ_c , E_c), és azokból képzett dimenzió nélküli számok (amik egy-egy anyagi viselkedést jellemeznek, pl. alakváltozási képesség, szívósság) hatását a mért tribológiai jellemzőre. Így komplex módon értékelve az összes vizsgálati eredményt megállapítottam az egyes acélok abrázíós érzékenységét a többszörös lineáris regressziós modellek normalizált együttthatói alapján.

A vizsgált anyagokra megállapított kopásérzékenységi térkép a befolyásoló paraméterek széles skáláját veszi figyelembe. A kopásállóság szempontjából a hőkezelt martenzites acél bizonyult a legjobbnak az összes vizsgálati rendszerben, így javasolható potenciális helyettesítő anyagnak az 27MnB5 helyett. A többfázisú acél esetén volt mérhető a legnagyobb kopás. Kutatási munkám globális eredménye, hogy segíti egy optimalizált tribo-rendszer tervezését, lehetővé teszi a kopási folyamat előrejelzését a vizsgált acélok esetében, komplex koptató környezetben.

1 CHAPTER 1

INTRODUCTION

This chapter introduces the background, the problem definition and the motivation of this research work. After discussing the research questions and gaps, the main investigation goals and the outline of this thesis book are highlighted.



1.1 Background

Tribology as defined by Peter Jost [1] is “the science and technology of interacting surfaces in relative motion - and of associated subjects and practices”. It includes the science of friction, wear and lubrication. Due to the relative motion of interacting surfaces, machine components are influenced by friction and wear, which reduce the lifetime of these components and increase their operation and maintenance costs. Therefore, well-designed tribo-materials and tribo-components have substantial economic importance. Furthermore, less load on the environment, less wear debris generation and lubrication usage means a smaller ecological footprint to achieve a sustainable development. For the development of tribo-materials the designers have to consider that friction and wear are not just material properties; they are system properties, and numerous factors influence their values (material properties, operating parameters, operating environment, contact geometry).

In the following, a general description is given of the wear situation of agricultural equipment and implements due to soil engagement, and various significant wear influencing factors such as soil condition and speed of operation are introduced with their quantitative correlation to wear. Wear mitigation strategies for these metallic parts include material selection and processing, application of coatings as well as design adjustments. In the following sections various wear testing approaches for these equipment and implements are reviewed.

In the case of agricultural machinery and equipment, wear is a particularly important cause of failure [2]. Agricultural equipment is subjected to aggressive wear environment due to contact of machine parts and implements (e.g. ploughs and tillers) with living substances e.g. soil and crop residues, as well as due to the interaction of components with plants such as sugar cane, wheat, rice, cotton, etc.

In agricultural machinery and implements three wear classes are distinguished. The first is machine wear, including various engine, transmission, and hydraulics parts. Wear related to these parts has been extensively studied in the context of automotive and engineering machinery. The second wear group is originated from the crop engagement due to interaction of part-crop/crop residue/soil interaction of the equipment. A good example for this is the wear of cutting and processing parts in a harvester during harvesting of various crops such as sugarcane, rice, wheat, soybean, corn, and cotton. The third wear class involves the ground-engaging implement wear due to soil-implement, crop-implement, and crop residue-implement interactions during land preparation and seeding or planting. Soil tillage is one of the basic activities in most agricultural systems, where ground engagement is provided through implements attached to a tractor and pulled over the fields to perform various land preparation and seeding operations. Figure 1-1 shows the tillage system types.

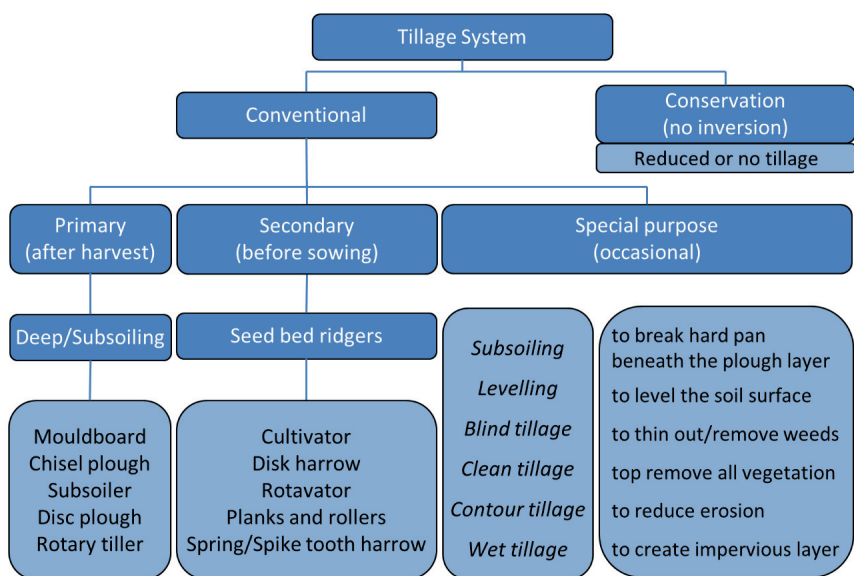


Figure 1-1 Tillage system types [3]

Tillage operation is necessary to ensure an adequate environment for seed germination, root growth, soil erosion and moisture control. Different implements are used for primary tillage, secondary tillage, and seed drills based on soil condition, crop, and farming practices [4]. Primary tillage equipment breaks the soil below the ground and loosens it to prepare a suitable seedbed. Examples of primary tillage implements are moldboards, disk and rotary tillers, and subsoil ploughs or chisels. Secondary tillage equipment includes harrows, pulverizers, cultivators, weeders and other special implements that intervene the soil to shallow depths to conserve moisture, destroy weeds, and level and firm the soil [2]. Examples of primary and secondary tillage equipment are shown in Figure 1-2. Currently, the use of classic tillage method is decreasing and the 'shallow ploughing' is gaining more ground as an effort for better soil conservation and sustainable farming [5]. The reduction in number of tillage operations can be carried out by omitting these operations which do not give more benefits compared to the cost, or by combining some operations (e.g. seeding and fertilising) [3]. Therefore, by eliminating primary and heavy tillage operations to reduce soil compaction and soil erosion, the role of secondary tillage equipment is increasing.



Figure 1-2 Primary (a, b, c) and secondary (d, e, f) tillage equipment [6]

In the present research work secondary tillage equipment: symmetrical skew wedge cultivator tines are investigated.

1.1.1 Wear

The first step in defining the characteristics of the tribo-system is to understand the processes involved in the wear of agricultural components engaging the soil. The input variables (Figure 1-3) play a vital role in the type of wear and the corresponding wear mechanism. The input variables can result in three types of wear, (1) mechanical, (2) chemical and (3) thermal wear [7]. These three types of wear individually or by co-existence cause severe damage to the contacting surface. The wear mechanism is nothing but an ongoing process in the tribo-system contributing to a change of the surface morphology of the contacting bodies. Figure 1-3 shows the complexity of wear mechanisms where multiple factors are contributing to specific wear mechanisms. Mechanical wear or physical separation is most dominant amongst the three wear types. Thermal wear (melting) is manifested by frictional heating and is not the dominant mechanism in the chosen application (agricultural equipment). Likewise, for soil engaging tools the chemical dissolution is a slow process; even before the process attains maturity the physical separation acts vehemently causing severe damage. Thus, in this research the focus will be on the physical separation process. The mechanical wear may be further divided into (1) abrasive wear, (2) adhesive wear, (3) fatigue wear and (4) erosive wear [8]. Very often soil engaging tools are more prone to abrasion, and this is due to the nature of contact and the type of contacting materials

(soil). In general, wear does not take place through one single wear mechanism, so understanding each wear mechanism in each type of wear is important. In many fields of agricultural machinery, abrasion and erosion processes are the dominant wear mechanisms that reduce lifetime of (costly) machine parts.

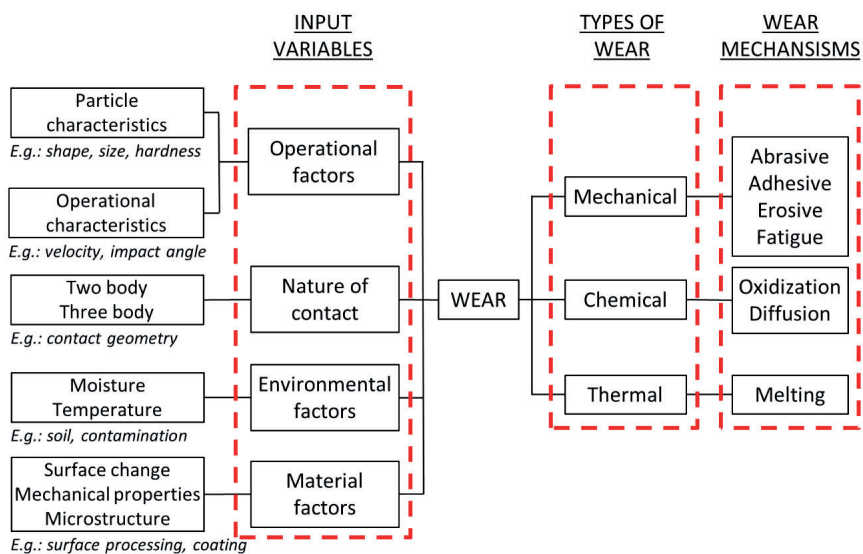


Figure 1-3 Factors influencing wear life

1.1.2 Abrasion

Studies show that the estimated direct cost of wear is 1-2.5% of gross national product (GNP) in developed countries (e.g., England, Germany, USA) [2]. From different wear mechanisms such as abrasion, erosion, corrosion, oxidation, and surface fatigue, abrasion is estimated to account for 50% of total wear losses [9]. Abrasion is defined as a process where a hard indenter or abrasives are forced against a relatively softer material under relative sliding, causing damage on the contacting body [10]. Understanding the process of material damage in abrasion is crucial for mitigating the wear.

Abrasion as a mechanism can be classified by the nature of contact [11] and the microscale mechanism [10]. In this section the classification based on the nature of contact is described. Though there are multiple input variables involved in abrasion, the most influential one is the nature of contact. It is also evident from Figure 1-4 that the nature of contact varies significantly between different applications.

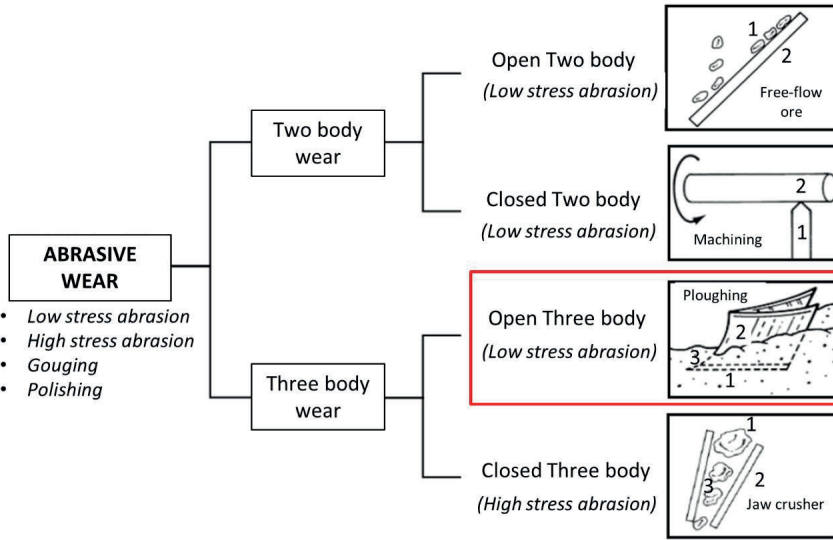


Figure 1-4 Classification of abrasive wear based on the nature of contact [11], [12]

From literature it is widely known that the nature of contact results in two distinctive wear types (two-body wear and three-body wear) [13]. In two-body wear the indenting hard abrasives are in a fixed position, however, in the three-body wear the abrasives are loose particles and are free to roll and slide. The abrasion rate in two-body wear increases with a factor of 10 when compared with the three-body abrasion, because in the three-body situation abrasive grains are free to move, and therefore may not always produce wear [14]. The contact environment determines whether the wear is classified as open or closed. When the surfaces are sufficiently displaced and are independent of one other, an open type of contact is prevalent (Figure 1-4). All these types of abrasive wear are accompanied by a certain degree of mechanical stress which depends on the application. Based on the stress level on the abrasives, low-stress, high-stress, gouging and polishing wear could be differentiated. The difference between low and high stress abrasion is defined based on the damage suffered by the abrasives. In high stress abrasion the abrasives are crushed and tend to fracture; a typical example is the ball mill. However, in low stress abrasion the abrasives remain intact. The agricultural tools are generally considered to experience low stress abrasion [12], [15].

In the following the processes involved in abrasion and their consequences in terms of the distinctive features observed on the contact surface are described. The wear process-tree (Figure 1-5) represents the interrelationship between abrasive wear mechanism and the corresponding surface scars. It has three levels: the influence of contact kinematics, the wear modes, and the distinctive features. In abrasion the contact kinematics is the primary cause for experiencing a particular phenomenon (micro-

mechanism). In the abrasion process, the arising micro-mechanism in the contact zone depends on whether the surface is subjected to plastic or elastoplastic deformation due to the abrasive load. The micro-mechanisms result in different wear scars on the contact surface characterized by features such as scratches, grooves, cracks, etc. It is important to mention that most tribological reports have micrographs representing the surface before and after wear, in order to study data derived from the wear scar and to indicate specific wear mechanisms. A more detailed description of abrasion wear micro-mechanisms is given in Chapter 4.1.1.

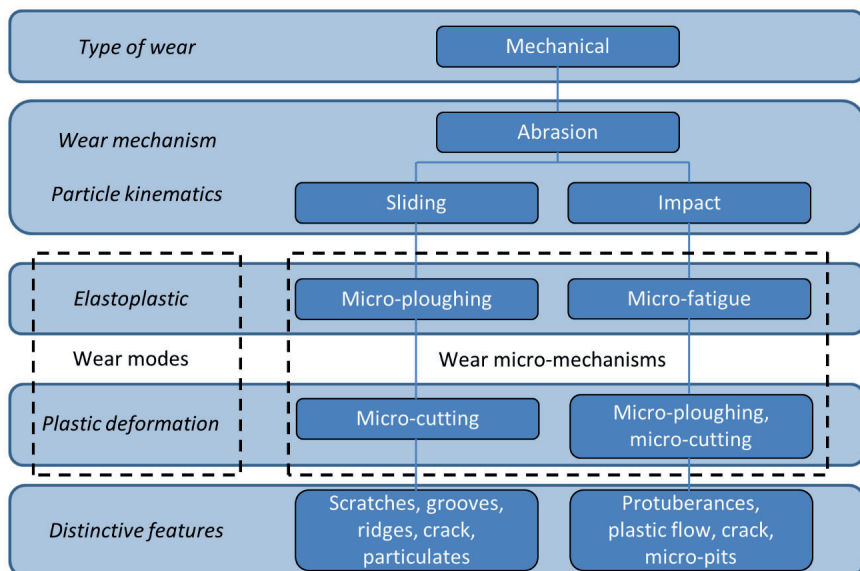


Figure 1-5 Abrasion process tree

1.1.3 Wear in soil engaging agricultural implements

As the productivity of agricultural machines has improved significantly over the years, the ground and crop-engaging components face significantly higher loads and more aggressive wear situations. An example is brought in the publication of Mohapatra [2], where a set of ten sugarcane harvester base cutter blades (approximately 0.3 x 0.1 m with 5-10 mm thickness), which rotate at a speed of 500 rpm and cut the sugarcane crop below the soil, disappear due to extreme wear in less than 24 hours of operation in Brazil, resulting in significant machine downtime and part replacement cost. Only within the agriculture sector, total wear losses are estimated to reach around \$940 million every year in Canada [16] and approximately \$4.4 million in Turkey [17]. The wear behaviour of the components is related to material parameters (composition, processing and micro-structure, properties) [18], component design (geometry and size) in addition to operating conditions (load, sliding speed, environment and temperature) [19].

As in any tribological system, many factors shape the actual wear of agricultural components, e.g. the structural materials, the formed surface and cutting edge geometries, as well as the operating conditions and environment. The specificity of agricultural machines is that they work in a living, biological medium that provides ever-changing conditions for the machine components. Besides the fast changing complex operating environment, the increasing size of agricultural equipment and faster tractors also enhance the stress on the implements. Therefore, it is important that the wear mechanisms resulting from the typical operating conditions (wet and dry soils, organic plant parts, animal manure, stochastically changing temperature and pH) are explored and understood in detail. For tillage implements such as hoes, disks, and ploughs, there are many approaches to reduce wear and to modify friction force. However, the solutions need to be developed based on optimal operating costs and machine productivity. The traction of the implement can be significantly reduced by choosing adequate geometry and arrangement of the tillage tools. Studies have shown that increasing the number of rows of chisels can reduce the traction on machines and result in lower energy consumption. Modelling nature's solutions, called biomimetics, helps here too. Work tool design inspired by dung beetles and black ants (bio-inspired design) has shown promising results in changing the trajectory of soil movement and reducing traction. Studies have also shown that the surface profile of the tillage tool and the rake angle can significantly affect traction. From a material point of view, the material quality of the tool, the surface coatings, and the applied heat treatment can be important, and can help in reducing wear. It is generally accepted that the microstructure of raw materials, coatings and the hardness of the tillage tool play a critical role in the evolution of wear life. Increasing the hardness generally results in an improvement of the abrasion wear resistance. The most common method is the hardening heat treatment of ferrous alloys. It is a versatile process among many alternatives (e.g. mechanical hardening and surface alloying) to increase the life of parts and reduce the cost of replacement. In addition to improving abrasion resistance in aggressive environments, strict cost targets also play a significant role in selecting the right materials and coatings.

Although a number of laboratory test methods exist, they are not sufficient to reproduce the real field wear, mainly due to the uncertainty of the operating field conditions themselves. Many types of model experiments have been performed with custom-made equipment that simulates the traction and wear of different work tools [2]. The main components of the test equipment are in general a soil tank, a tool trolley, a drive system, some measuring instruments and a data acquisition system. Beside different laboratory test models (standard and custom-made soil testers), on-site inspections are also required, which are time-consuming and highly uncertain. The solution is to use the triple testing level (laboratory standard testing, custom-made soil equipment, and field testing) and build a knowledge that connects the test levels. In this way, the number of in-field tests required for evaluation of implement design and optimal operating conditions can be reduced. An accurate description of soil-

tool interaction can help to reduce draft force through the optimization of tool geometry. To further understand the wear process in detail and investigate the wear behaviour of the equipment in different operating conditions coupling the experimental results to modelling and simulation is beneficial. However, the use of digital and statistical methods developed to simulate soil-tool interactions, e.g. computational fluid dynamics (CFD), finite-element analysis (FEA), discrete-element method (DEM), and artificial neural network (ANN) is still limited. On the other hand, the development of algorithms used in the models, and validation and parameterization of the models based on real measurement results, offer the possibility to implement design decisions based on modelling and simulation in combination with a limited number of experiments. Finally, it is very important to choose the right combination of tools and machines to reduce traction and fuel consumption while increasing productivity.

1.2 Problem definition and motivation of the research

Agriculture in the 21st century faces multiple challenges: it has to produce more food to feed a growing population (+2.2 billion forecasted until 2050) with smaller rural labour force and limitations in agricultural land area growth, as highlighted in Figure 1-6 [20]. Agriculture also has to develop more efficient and sustainable production methods and has to adapt to climate change.

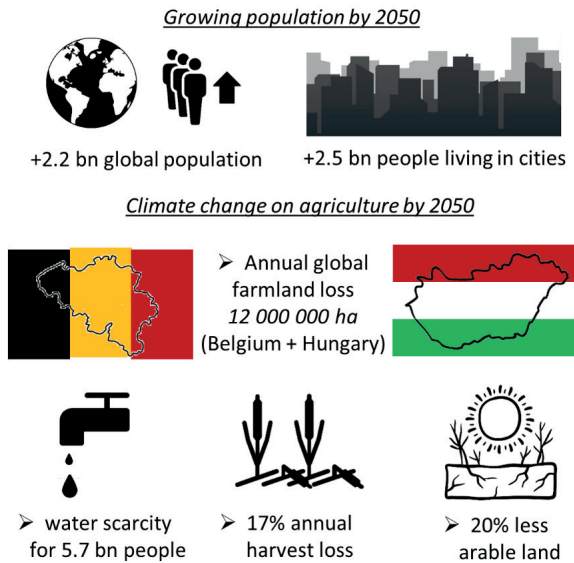


Figure 1-6 Population and agricultural challenges forecasted by 2050

Therefore, the agricultural sector is in need of better performing materials and/or machine design in order to achieve more effective operation, more sustainable farming and also to prevent

contamination of the fields by wear debris. Optimisation of the materials of machine components is necessary. Often weight reduction as well as enhanced wear resistance is targeted for newly developed machine parts. Consequently lighter materials, special alloys and composites are gaining more ground. Severe abrasive wear and impact failure still are a major cause for the premature failure of many agricultural ground tools. For example, ploughshares are extremely vulnerable to abrasive wear in hard fieldwork, especially in stony soils. In these conditions, the equipment design, the operating speed and depth in the soil, and the material quality of the implement determine the fuel consumption of the tractor, the lifetime of the implement, and the frequency of part replacements, therefore influencing the machine uptime. Enhanced wear resistance of the machine parts means a longer lifetime and ensures an operation through a complete agricultural season without the need of changing the part. Due to seasoned crop harvesting or soil cultivating and quickly changing conditions timing is critical, so machine part replacement and downtime is to be minimised.

The tribo-system of interest is complex due to contact with living counter materials (e.g. crops, soil) and constantly changing conditions often resulting in co-existing wear processes. Global warming due to the accompanying extreme weather phenomena also pushes the environmental parameters of the tribo-system to a more radical operating range. Furthermore, one of the key parameters in farming is the economics or benefits of any production technology. The used agricultural implements are not only affected by the soil topographic and texture but also on the financial strength of the farmer. In conclusion, the newly developed agricultural machine elements needs to bear with complex requirements. In case of the engineering development of a new machine, the proper material selection and part design of tribological elements follow the idea of a systematic approach from simplified laboratory testing to the expensive and time-consuming field control. For better machine performance and maintenance, the critical wear parts need continuous development, which is part of the reconstructional design activity of maintenance engineering. However, field tests for new parts are too expensive and time consuming. As the complexity of farm engineering tribology was previously described, the proper modelling of a tribo-system is essential and the acting factors have to be analysed. An optimized development process suggests testing of various materials in lab scale in a simplified tribo-system and only test the best performing ones in real application. The key for a successful development process is finding a representative lab-scale tests which could be scaled for the real part investigation.

1.3 Basics of abrasive wear investigation

In engineering applications with harsh operating conditions such as in mineral industry, soil processing and agriculture, the tribological investigation of the operational variable dependent, location-specific wear and damage mechanisms is particularly important [21], [22]. The demand of extended lifetime for machine elements and an increase in cost efficiency urges to develop new materials. The most cost-effective wear-resistant materials should be identified and applied [23]. In agricultural machinery wear parts are frequently produced from specific steels, e.g. tillage tools, which are exposed to abrasive wear, are made of low alloyed martensitic steel 27MnB5 [21]. Other components such as slurry pumps, extruders, pipes carrying ores, and coal slurry nozzles are exposed to slurry abrasive wear in power plants and mineral processing industries [24], [25]. The equipment and components used in slurry transport experience multiple wear modes and damage mechanisms in the form of abrasion, slurry erosion, and corrosion [26], [27]. Straight pipes exhibit abrasion caused by combination of sliding and rolling particles [23]. These conditions can also be encountered in agricultural applications where crop transport (e.g., wet paddy rice) and cultivation can cause similar problems [28]. The agricultural and mining machine components operate in a wide range of conditions that shape the abrasive wear. The matching of environmental (e.g. energy usage, pollution) and technical requirements (e.g. standards, safety operation) is a complex aspect in the selection and development of the applied materials. Therefore, in abrasive conditions sometimes light and corrosion-resistant polymers [29] or (foamed) aluminium alloys are used [30]. However, where the presence of mass and strength is essential (e.g. in tillage and cultivators), the use of steel is preferred. Generally, alloyed martensitic steels are utilized, often with hard alloy coatings to enhance the wear resistance [31].

Surface damage to a tribological pair is usually caused by consecutive small steps induced by wear micro-mechanisms. At the micro-level, the four different modes of abrasion are micro-ploughing, where the material is plastically deformed and displaced, micro-cutting, defined as micro-machining with chip removal, micro-fatigue, and micro-cracking [32]. The micro-mechanisms generate physical modification at the surface, with or without material removal. The resultant surface damage is the summed outcome of one or more micro-mechanisms and appears in the form of grooves caused by abrasive particles [33]. This macro-wear is the result of a complex tribo-system response influenced by the testing conditions besides the materials in contact [34]. To select the best appropriate candidate material to optimize a tribological system, the tribo-system elements (contacting materials, geometry and surface topography, configuration of contact, relative motion, loading condition, and environment) need to be investigated [32].

The accurate prediction of abrasion behaviour of the materials is difficult because numerous parameters govern the abrasion phenomenon. Researchers concluded that the abrasive wear rate in

steady state conditions is usually inversely proportional to the hardness of the abraded body [10], [33], [35]. Proportional relation was found to the normal load [36]–[39] and the sliding velocity [36], [40]. Effect of size [36], [41]–[43], shape [10], [35] and type [36] of abrasive media on the wear has been studied too. For small particles the wear rate increases with increasing particle size, however, above some critical size the wear rate becomes almost independent of further size increases [42]. A change in shape of abrasive particles from angular to spherical caused a decrease in volume loss, due to lower contact stresses [44]. These findings were also confirmed by pin-on-disk testing of different abrasion-targeted steels with different microstructures, including ferritic stainless steel, medium alloyed ferritic carbon steel, and medium alloyed martensitic carbon steel [22]. The basic relationships between material properties and wear have been investigated in numerous research works. However, the involved material properties are often limited to tensile properties and hardness. Quite a few materials have been considered to be used for abrasive slurry transport [23], but their wear resistance may vary according to the system properties. Furthermore, testing is often done in standardized test set-ups, where direct connection to specific applications is limited. Due to the different abrasion forms that can be present in a wide range, the present investigation is expanded to multiple test systems, which were not connected in the literature previously.

A lot of research has been performed to estimate the abrasion resistance based on well-defined mechanical properties such as Vickers hardness [33], [45], [46], ultimate tensile strength and yield strength [10], [47]–[49], and uniform elongation [50]. Non-linear connections have been found between the abrasive wear resistance and the hardness along with the tensile properties for multiphase low alloyed steels [10], [51], [52]. The contradictory dependencies against basic mechanical properties were attributed to limited data sets, imperfect separation of microstructural and compositional effects, overly simplified statistical analyses, the use of different testing methods, or just the absence of a unique correlation [34]. The abrasive wear resistance of wall lining materials in iron ore mining was investigated [53]. The wear rate was found to have a proportional relationship to the Knoop hardness values; therefore the hardness tests could be used to represent the abrasive wear ranking of these materials. The wear behaviour of 7075 aluminium alloy and 7075/5 wt% Al_2O_3 alloyed composites produced by powder metallurgy was investigated with a focus on microstructure, density, and hardness [54]. Analysis of variance (ANOVA) highlighted the percentage contribution of particle size (11.5%), sliding velocity (0.6%), and applied load (86.9%) on the wear. The experimental data of this work were correlated by reference to dimensional analysis considerations followed by least-squares polynomial regression [55]. In this study, the influence of particle impact velocity, density, concentration, and hardness on the erosion wear was identified, but the effect of the impact angle was neglected. Dry sliding wear behaviour of composites was investigated using a pin-on-disk set-up with different loads, sliding velocity and wt% of hard MoB compound as variables [56]. ANOVA was used to

study the significance and influence of parameters on the material loss, and the correlation between parameters was obtained by a regression equation. MoB content of the composites was observed to be the most dominant factor (57.1%), followed by sliding velocity and load. A broad investigation was performed on low alloyed steels to analyse the connection between abrasion resistance and standard mechanical properties of the materials [34]. ASTM G65 standard abrasion test was used for chemically identical steel samples with different mechanical properties and for samples with similar mechanical properties as the first series, but with different chemical composition and microstructure. A strong linear connection between the wear performance and some mechanical properties was found for the chemically identical samples, however the samples with similar mechanical properties showed weaker correlations. In the recent work of Bustillo *et al.* [57], artificial intelligence models were used to forecast the surface wear based on the surface isotropy levels. For mass loss, the radial basis networks (RBFs) method resulted in the most precise prediction, whereas for surface deformation, the multilayer perceptrons (MLPs) technique brought the best results in terms of indicator Ra. Matuszewski *et al.* [58] developed mathematical models based to describe the connection between the experimentally observed surface wear and the applied test factors (e.g., load, velocity, surface parameters). The output parameters included mass loss, change in geometry, as well as surface roughness parameters. Their study enabled to predict the wear process of kinematic pairs with conformal contact.

Numerous investigations can be found in the literature, where the researchers connect the abrasion resistance of steels to their standard mechanical properties as determined by tensile and hardness testing [34]. However, many unclear or even contradictory correlations have been found, partly due to too small data sets, distinct testing methods, and oversimplified data processing techniques.

A comprehensive evaluation of the abrasion sensitivity of martensitic steels in different wear test systems - taking into account tensile, hardness, impact and compressive mechanical properties and the dimensionless numbers that can be formed from them - is not available in the literature yet, but eventually could support steel (or material) selection and development for a given application.

Understanding the material behaviour under different abrasive wear conditions is important from a design point of view in order to propose better-performing wear-resistant machine parts. To determine the wear performance in a more accurate way, extensive laboratory testing is required covering a wide range of abrasion processes in different tribo-systems.

1.4 Investigation goals and thesis structure

The main goal of this research work is to enhance the operating life of symmetrical skew wedge cultivator tines by proposing a better performing material in terms of wear resistance. Economic limitations are considered as well as possible design adjustments.

The real machine part (agricultural tine) is first investigated in detail in order to understand the specific wear processes and to make experimental laboratory models with different complexity. Chapter 2 – Field investigation contains the in-field analysis of the agricultural tine. Important conclusions are drawn about the wear micro-mechanisms and co-existing wear damage, which could aid future design decisions.

Taking the different abrasion forms into consideration, the investigation in this work is expanded to multiple test systems, which were not connected in the literature previously. Based on the tine analysis, reproducible laboratory test systems are set with different complexity, where the investigated wear-mechanisms are re-created. A connection is set up between the different models with the real part testing (Figure 1-7). A relationship is established between different scales based on the qualitative output (wear micro-mechanism) and validated using the quantitative data extracted from the wear scars (Dp) using post-mortem 3D surface topography profiles and mass loss measurement.

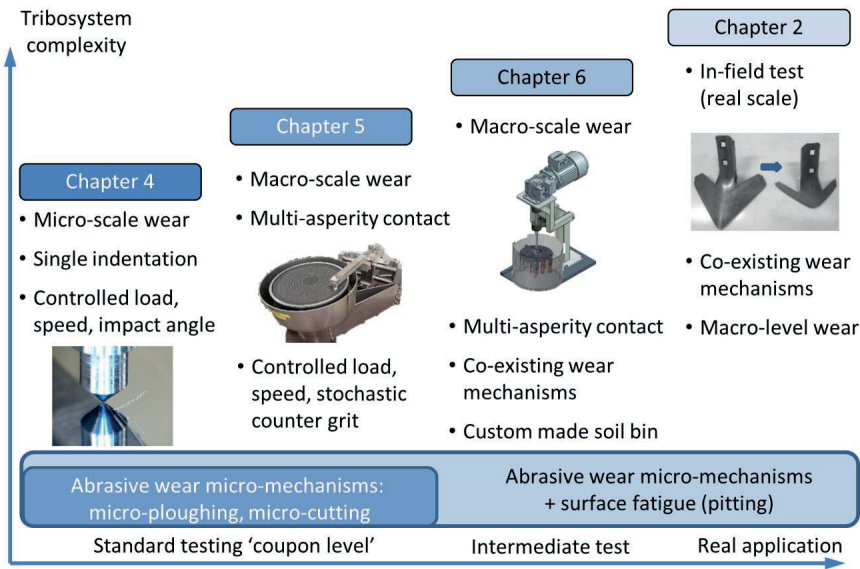


Figure 1-7 Connection and scaling of multi-level wear investigation

To enhance the operating life of the tine, newly developed materials with enhanced wear resistance against micro-cutting were proposed and wear tested in a multi-level investigation. These different materials are tested and compared based on their wear performance.

Identified wear micro-mechanisms are recreated both in micro-level (Chapter 4 – Micro level single-asperity contact abrasion investigation) and on macro-scale (Chapter 5 – Macro level multi-asperity contact abrasion investigation) and the material response to different tribo-parameters is investigated. Single-asperity scratch tests are performed with various loads, indenter tip radii, and attack angles in order to study the abrasive scratch-resistance of the materials. Pin-on-disk tests are used with various loads, sliding distance, and abrasive particles to investigate the material response in a multi-asperity contact abrasion process. The material behaviour is further studied in a slurry-abrasion test system with different sliding velocity, distance, and specimen orientation angle, thus abrasive particle impact angle. This more complex intermediate test method highlights the occurrence of the co-existing wear mechanisms (Chapter 6 – Co-existing wear mode investigation in multi-asperity contact).

The wear is evaluated in each tribo-system as a function of their material properties. The effect of system variables and material properties on the wear performance is investigated with multiple variable linear regression analysis. Correlation analyses are performed to investigate the connection of abrasive wear features with extended mechanical property combinations (hardness H , ultimate tensile strength σ_M , yield strength σ_Y , Young's modulus E , uniform elongation ϵ_M , fracture elongation ϵ_B , Charpy ISO 148-1 W , compressive strength σ_c , compressive modulus E_c) in single- and multi-asperity tests systems and also in a slurry containing system, which can model different abrasive modes on the surfaces. Large amounts of measured tribo-data are processed by multiple linear regression models using IBM SPSS 25 software to determine and evaluate the sensitivity of the abrasive wear and the change of 3D surface topography to material properties and to test system characteristics. In this way, the wear performance of the materials is not only compared in the different test systems, but the significance and contributions of tribo-system parameters on wear behaviour is studied. The sensitivity of the tested materials to abrasion is evaluated taking into account the wide range of influencing parameters. The main research conclusions are summarized in Chapter 7 – Conclusions.

This investigation aids the design of an optimized tribo-system by enabling the prediction of the wear process in complex abrasive environment for the investigated steels. This also helps in future material development to decide what factor has the most impact on the wear and what viewpoints are important to investigate when evaluating the material performance.

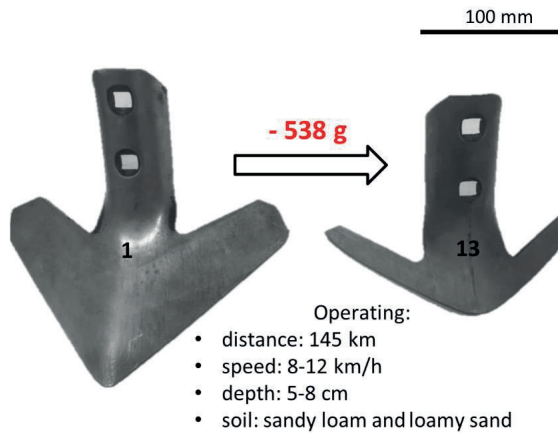
2 CHAPTER 2

FIELD INVESTIGATION OF CULTIVATOR TINES

This chapter summarizes the first step of the lifetime development process: the investigation carried out on the real machine component, a symmetrical skew wedge cultivator tine.

The following article was published based on this chapter:

Á. Kalácska, P. De Baets, D. Fauconnier, F. Schramm, L. Frerichs, and J. Sukumaran, "Abrasive wear behaviour of 27MnB5 steel used in agricultural tines," *Wear*, vol. 442–443, p. 203107, Feb. 2020, doi: 10.1016/j.wear.2019.203107.



2.1 Introduction

2.1.1 Wear process in soil engaging tools

Tillage is defined as the preparation of the soil by mechanical agitation [59]. In the farming process, before planting or seeding a crop, the soil needs to be in a good state. The processes of soil preparation are executed by specially designed agricultural tools. These tools are divided into two categories according to their functionality, which are cutting (primary tillage) and shaping (secondary tillage) of the soil [60]. Soil cutting tools can be further classified according to their shape as being similar to a straight wedge (shares of potato harvesters), a skew wedge (ploughshares, L-hoe blades) or a symmetrical skew wedge (A-hoe blades and double blades, shares of planters and ridgers, subsoilers). Most research has been focused on determining wear resistance and analysis of wear distribution of skew wedge shape ploughshares [61]. In this study symmetrical skew wedge tine is analysed.

Abrasive wear of tillage tools is a major problem for farmers all over the world. The hard mineral particles of different soils can cause severe wear and damage in working machine elements [62]. An example is shown in Figure 2-1.



Figure 2-1 155 mm wide AS 1594 cultivator shares in new condition (left) and in worn condition after 9 km operation in abrasive South Australian soil (right) [63]

In this research primary cutting tools are investigated. In 1986, the National Research Council of Canada estimated of the total cost originating from the wear in the agricultural sector being around \$ 940 million per year [16]. The tines which experience severe wear during operation do not only result into increase in fuel and energy consumption but overall low work quality with the risk of tool loss and thus danger of subsequent processes. Replacement of tines costs not only money but also time, which is critical in the season of seeding and planting crops [63]. From the economic perspective it is clear that research on the wear behaviour of agricultural tools is critical. To increase the wear resistance, the wear process has to be completely understood. Several wear investigations on tillage tools were already performed. They mainly focus on wear rate calculations and parametric influences but do not focus on the wear mechanisms as such [61], [64]–[66].

Tillage wear is commonly classified as open three-body low-stress abrasive wear [12]. Abrasive wear is defined as material removal due to sliding contact with abrasive particles or a rough surface [67]. In three-body wear the particles are loose and may move relative to each other or rotate while sliding across the material. In open three-body abrasion the surfaces are far apart and do not influence the wear of each other [13]. The wear of tillage tools is classified as open three-body low stress abrasion because there is only a small compression load on the particles, which slide and impact on only one wearing surface [68]. Often a dry contact condition is experienced in tillage processes, very high moisture content is to be avoided because it negatively influences the traction. Wear response is based on the properties of the contacting bodies. The second body, which is the abrasive/sand (quartz) particle, plays a significant role in controlling the wear properties of the process itself [63].

2.1.2 Wear influencing parameters

The wear influencing factors can be grouped into material parameters (component material, design, processing, coating), and operating environment. The latter includes the description of the interaction between the tillage and the soil counterface (soil type, moisture content), as well as the operating parameters such as speed, load and working depth.

The wear behaviour of agriculture equipment and implements differs markedly depending on the geographic location. This mostly originates from the variations in soil condition, such as sandy or loam or clay content and hardpan depth, which impact the coefficient of friction as well as abrasive media interactions during the ground engagement. It was found [2] that sugarcane harvester blades that cut the crop below the soil surface have more than double the life in the western India than in the southern part of the country because of the soil composition and hardpan depth differences. For this reason, the nature of the soil also has a significant effect on the reactive draft forces acting on the equipment, significantly influencing the resultant wear rate.

Taylor and Gardner [69] showed that the depth of hardpan soil in northern Mississippi can vary greatly. The shape of the subsoiler has been found to have an influence on its required draft as well as on the implement wear and the energy for soil breakup [70]. This variability suggests that significant savings in tillage energy could be achieved by (manually) adjusting tillage depth periodically throughout the operation. However, the design of tillage tools, in particular subsoilers, may need to be optimized in order to be able to take advantage of these potential savings. The importance of the soil type is further described in the following.

The draft force was studied on the implements in two different soil types: Norfolk sandy loam soil and Decatur clay loam soil [69]. Decatur clay loam soil resulted in significantly higher draft requirement at high depths than Norfolk sandy loam. Clay soils are characterized as more adhesive than loamy and sandy soils. The adhesive force is inversely proportional to the diameter of soil particles. Moreover,

adhesive forces of clay soils vary depending on the type of clay particles, their size and originating material. It was shown [2] that adhesive force increases linearly with the normal pressure. This increase is linear until normal force achieves a threshold value, then the force increases more sharply. The presence or absence of organic matter and its content in the soil has a pronounced effect on adhesive forces. Acidic soils are less adhesive than soil containing fresh rotten materials from previous crop residue. Generally, adhesive force reaches its maximum when the moisture content of the soil is at the liquid limit (between plastic and liquid state). The soil-tillage interaction is complex and is significantly influenced by the moisture content of the soil [71]. Wet soil could provoke non-scouring or sinkage of the implements, breakage and overall high draft and poor tillage performance. In wet soils the fuel consumption of tractors during the tillage process increases sharply compared to dry soil conditions. Fouda *et al.* [72] studied the in the field wear behaviour of carbon-manganese steel ploughshares with different hardness, share position and operating interval in sandy loam soil with varying solid moisture content. They found that a small increase in soil moisture content from 8% to 11% enhanced the wear of all ploughshares with a significant decrease in their expected life. This was explained with the increase in soil packing density due to the rise in moisture content, that also increases the shear strength of the soil.

Soil moisture influences the wear of agriculture implements as well as their friction coefficient and draft force. Higher friction coefficient or draft force on the implements results in escalated fuel consumption of the tractor pulling the equipment [2]. An implement with lower friction coefficient or draft gives the farmers flexibility in terms of using a bigger implement to increase productivity or using a smaller machine with lower horsepower to do the same work.

Abisuwa and Manuwa [73] studied the effect of moisture content of a loamy sand soil on the draft force of various tillage tools using an indoor soil bin equipment. Eight different model tillage tines were used (different width narrow tines, flat and ridged sweeps) in the experiment. It was concluded that equipment operating in wet soil (~14% moisture content) required higher force for operating than in dry soil. Operational parameters such as operational speed and distance, instrument level and working depth have a great effect on the wear of the equipment. Derafshpour [74] investigated the wear of chisel blades with three levels of working depth (15, 20, and 25 cm) and seven levels of functioning area (1.2, 4.35, 6.75, 12, 15 and 18 ha) with an average ploughing speed of 4 km/h. The experimental results verified that working depth, functioning level and their interaction have a significant effect on the material loss from the blade edges and the tip of the blades. Yu and Bhole [12] found a relation between the depth of the plough and the average specific pressure of the soil on the blade as well as the velocity of the blade in the soil. The tip of the blade experienced the highest pressure, but the pressure on different parts of the blade did not increase directly with greater velocity. Al-Suhaibani and Ghaly [75] investigated the effect of operational parameters (depths and speed) on the draft force

of three chisel ploughs running in a sandy and loamy soil. The ploughing depth had a more significant influence on the draft than the ploughing speed. They concluded that in order to reduce the draft force, that ploughing depth should be set based on the crop type (depth of the root system). Novak *et al.* [76] found that the soil quality (sandy or loam) has a more significant effect on the wear than the ploughing velocity. Naderloo *et al.* [77] studied the effect of tillage depth and forward speed on the draft in case of three different primary tillage equipment (moldboard, disk and chisel plough) in clay loam soil. They found that for all the implements the draft force was proportional with the tillage depth and forward speed. Their investigation showed that at the same ploughing depth and operational speed the moldboard plough required greater draft than the disk plough. The phenomenon was explained with the influence of the difference in the geometry, shape and size of the cultivating elements.

The geometry, overall shape and size of the components have a significant influence on the draft force and therefore on wear. Tillage implements designs (size/shape) have evolved over time, mainly by experience, resulting in very conservative designs [2]. In order to optimize the design of the equipment, further information is required about the direction and magnitude of the draft (vertical and horizontal) on tillage implements next to other technical information e.g. horse power of the tractor and matching implement. Appropriate selection of tractor size (hp) and matching implements could minimize operating cost of both tractor and equipment.

Soil engaging implements for tillage operation are most often made of heat treated steels (boron steel and C-Mn, C-Mn-Si steel) due to economic aspects. Bednar *et al.* [5] compared the wear performance of different materials including tool steel (X210Cr12/1.2080), carbon steel (C45/1.0503), austempered ductile iron (ADI), cast iron with globular graphite, and CastoDur Diamond Plates (CDP) (Castolin Eutectic) with weld overlay containing boron and niobium dispersed in a chromium carbide matrix on a mild steel substrate for share cultivator applications using tribological standard test methods according to CSN 01 5084 (Determination of resistance of metallic materials to abrasive wear on abrasive cloth). ADI cast iron was found to have higher wear resistance than C45 carbon steel with ferrite and pearlite microstructure. Among all the materials, tool steel (X210Cr12/1.2080) performed best. However, the economic aspects play a significant role in material selection for the production of these components.

2.1.3 Wear investigation approaches

The most common method to investigate wear rate and compare different materials is based on measurement of the weight loss of the material after a stipulated sliding distance [61], [64], [65]. Ferguson *et al.* [63] measured the mass loss in dry and stony conditions and found a constant mass loss rate over the lifetime of the shares without a running-in phase. Additionally, geometrical dimension is widely used to extract wear data. Natsis *et al.* [64] used the average cutting edge thickness

to investigate the wear on a mouldboard ploughshare. Owsiak [61] measured the thickness of the tine at different locations along the cutting edge. It was evident from his analysis that the dimensional wear decreased with increasing distance of measurement point from the share point and some running-in behaviour was present. The cutting edge of the tine close to the tine tip experienced severe wear. This was explained with the stress concentration which is largest around the tine tip. Owsiak [61] defined three important dimensions next to the thickness measurements, which are tip length, width and edge length. It was found that the losses were not constant, the tip length decreased at a higher pace during the initial sliding and stabilized only after reaching 30% of the total lifetime. It was also observed that part of the cutting edge close to the share point was subjected to the largest wear, while the wear of the edge decreased as the distance from the share point increased. It was explained with the stress concentration in the soil around this zone after blunting of the tip the impact was distributed over a large zone and thus the average stress decreased [61]. This may indicate the presence of different micro-mechanisms on different tine segments. The wear process that affects tillage tools is categorized as open three-body low stress abrasion, composed out of four micro-mechanisms: micro-cutting, micro-ploughing, micro-fatigue and micro-cracking [32].

The wear measurement techniques in previous investigations [61], [64]–[66] are based on mass loss or dimensional changes and the wear micro-mechanisms of the wear process are not characterized. The type of wear mechanism influences the wear rate [78] so understanding the wear micro-mechanisms is necessary for accurate tribological characterization. An important parameter that can give information about the dominant wear mechanism on a surface is the degree of penetration (D_p) of the wear scratch. It is calculated by dividing the depth of the wear scratch with its half width as defined by Hokkirigawa *et al.* [79]. The D_p partly illustrates the severity of wear and the micro-mechanism. It can act as an indicator to distinct the operational regime between mild and severe wear. Low D_p values indicate micro-ploughing with plastic deformation of the material while higher D_p values (>0.3) indicate micro-cutting phenomena with continuous chip formation and material removal. Within a single tine different wear modes can be present, because the different state of stress is exerted on the different segments of the tine. This also influences the flow of the abrasive particles in contact with the tine during the ploughing and the compaction of the soil. In our investigation the flow of abrasive particles was partially analysed with DEM and compared to the results obtained from the field test.

Due to the detrimental effects of tillage tool wear (replacement cost, timing, energy) investigations have already been performed on the determination of the wear influencing factors. These factors are material properties (hardness, toughness and microstructure), soil type (particle hardness, size, angularity and compaction) and also the operational (velocity, working depth) and environmental (moisture, temperature) conditions. The wear measurement techniques in these investigations were often based on mass loss or dimensional changes. Surface characterization for understanding the wear

micro-mechanism has not been done previously. This surface characterization provides information about wear scar morphology, i.e. groove geometry which explicates the particular micro-mechanisms. The wear patterns found on the worn tine have been compared with a DEM model of the soil flow.

2.2 Material and investigation method

The tillage tool that is investigated in this research project is a symmetrical skew wedge tine, which is used for soil cutting and loosening in the first phase of primary tillage. As it is used in the earliest phase of tillage, when the soil has a high compactness, it suffers from severe wear. The tines used in the current investigation were provided by K  ckerling GmbH (Verl, Germany). The investigation took place in a typical European crop production land in loamy sand and sandy loam soils in Germany. The tine is constructed out of an alloyed martensitic steel 27MnB5. The chemical composition of the tine material of base 450 HV hardness (tested with 100 N load) is shown in Table 2-1.

Table 2-1 Chemical composition of investigated agricultural tine [wt%]

C	Si	Mn	S	P	Cu	Cr	Ni	Mo	V	Al	Ti	Nb	B
0.285	0.253	1.125	0.001	0.013	0.015	0.165	0.011	0.028	0.004	0.041	0.035	0.013	0.003

The density of 27MnB5 (1.5529) is 7.86 [kg/dm³], where the tensile strength was measured to be 1575 [MPa] (0.5 mm/s 100 kN on Zwick/Roell Xforce P) and 181 [GPa] Young’s modulus (determination 10 - 20 kN). Thirteen independent agricultural tines corresponding to different sliding distance were investigated for the wear trend, specific wear mechanism and also for its material characteristics (microstructure and hardness). The test conditions of the tines are given in Table 2-2. The total tillage operating distance was 145 km which corresponds to 182 ha. Figure 2-2 shows the cultivator used with the associated tine positions. Tines located in the tractor wheel track were not used for the examination.

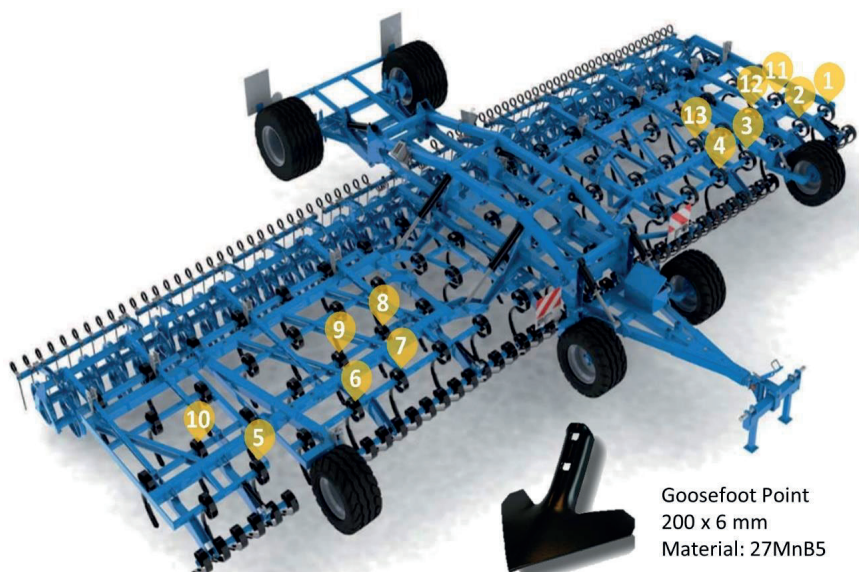


Figure 2-2 Tine positions on the cultivator [21]

Each tine was field tested for a specific distance as mentioned in the below table. The tines were mounted on a cultivator and the influence of the position difference is assumed to be negligible. Tines in the compacted wheel track of the tractor were not used for this investigation. However, it should be noticed that tines could wear asymmetrically when they were positioned at the outside of the cultivator. This is a consequence of the overlap of the work field during tillage. Working speed during the test was in a range between 8 to 12 km/h and the working depth was between 5 and 8 cm. Two different soil types were involved: loamy sand and sandy loam soil. The tines as received from the field were partially corroded and hence the mass for each of the tines were measured after following a special cleaning procedure.

Table 2-2 Tine test conditions [21]

Tine number	0	1	2	3	4	5	6
Distance [km]	0	10.3	21.6	32.8	41.8	53.9	60.7
Soil	-	Loamy sand	Loamy sand	Loamy sand	Loamy sand	Loamy sand	Loamy sand
Mass [g]	1050.00	1022.40	958.95	939.00	842.90	795.20	777.50
Tine number	7	8	9	10	11	12	13
Distance [km]	73.9	82.9	96.4	109.3	119.9	132.7	145.3
Soil	Loamy sand	Loamy sand	Sandy loam	Sandy loam	Loamy sand	Loamy sand	Loamy sand
Mass [g]	748.65	758.65	744.45	734.00	610.10	591.70	483.85

In the first stage the tines were cleaned with vinegar and Loctite SF 7063 to remove the rust and remaining soil particles. Mass loss, linear geometrical and thickness measurements were performed on the cleaned tines with an electronic scale with a resolution of 0.1 g and a caliper with the accuracy of 0.1 mm. To identify the wear micro-mechanism on the tine surfaces, investigation was done using 3D profilometry (Taylor Hobson CCI HD) complemented with macrographic information. Based on this investigation, the regions within the individual tines were segmented geometrically (Figure 2-3) to differentiate for region-specific wear characteristics such as wear mechanism, wear rate, roughness characteristics, microstructure and hardness change. The cross-sectional analysis was made on samples extracted from the different representative regions of the tine (Figure 2-3).

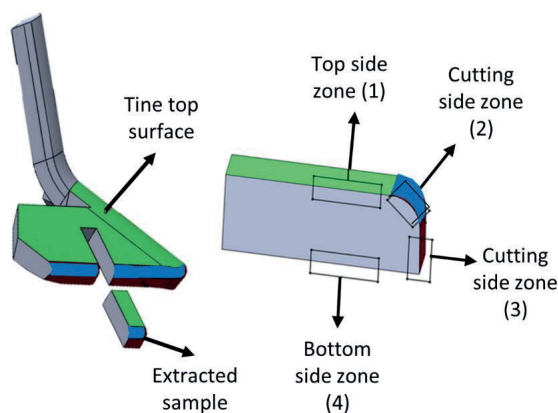


Figure 2-3 Geometric segmentation and sample extraction from tine [21]

Subsequent polishing and etching allowed to investigate the microstructure (Zeiss AxioCam MRc5) at different magnifications (covering the following tine zones: one zone on the top side (green colour), two zones on the cutting side (blue and red colour) and a reference unworn zone (grey color). Scanning electron microscopy (SEM) investigation was also performed for verification and to acquire more detailed information about the differences in surface morphology. Hardness measurements were performed using LECO LV 100AT Vickers hardness tester. Furthermore, the surface was studied in detail for its 3D topography using white light interferometry (Taylor Hobson CCI HD) with 20X lens covering 0.8 mm x 0.8 mm area. The cut-off wavelength for the measurements was set according to the standard ISO 4287. The surface topography data was extracted from the 3D map to calculate the D_p . Hokkirigiwa *et al.* [80] introduced a formula that predicts the degree of penetration in a single-asperity contact scratch test for a certain normal load and an indenter tip radius on a surface with known hardness. The critical value of D_p to set the demarcation between micro-ploughing and micro-cutting is around 0.2 for various attack angles. After a topographic surface characterization measurement it is possible to

calculate the mean Dp of all the grooves that are present on the worn surface. Coronado *et al.* [81] validated the following formula for Dp when comparing two abraded surfaces:

$$D_p = \frac{R_z}{\frac{R_{sm}}{2}} \tag{2.1}$$

where Rz is the ten point height [μm] and Rsm [μm] is the mean spacing at mean line. These are corresponding to the groove depth and the groove width of a single scratch. To investigate the abrasive particles the two soil samples from the field test were characterized. Mineralogy results were obtained with X-ray diffraction (Rigaku Ultima IV). Semi-quantitative and mechanical analysis were performed to obtain soil parameters according to MSZ 20135:1999 4.2 (Determination of the soluble nutrient element content of the soil) and MSZ-08-0206-2: 1978 (Evaluation of some chemical properties of the soil) standards.

2.3 Field investigation results

2.3.1 Mass loss and dimensional change

The geometrical size reduction due to material removal is evident in Figure 2-4.

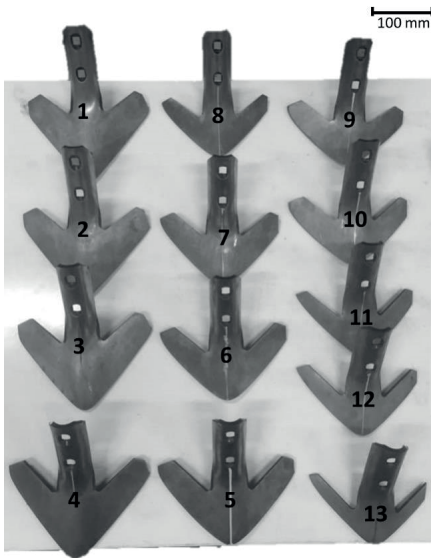


Figure 2-4 Wear of tines (1-13) after different sliding conditions [21]

The present investigation clearly shows the difference between the early stage (10.3 km) and the final stage (145.3 km) of wear. A clear reduction over 55% of the mass loss was observed between a new and a fully tested tine. The mass of each tine is plotted in function of the operating distance (Figure 2-5). A linear trend was observed in the mass loss similar to literature, with an overall wear rate of

3.803 g/km, which corresponds to 190 g/ha from the field investigation. Studies conducted in Turkey indicate that the wear rate is between 90-210 g/hectare in moldboard plough blades, 60-120 g/hectare in cultivator sweeps, and 23-40 g/hectare in chisel plough blades [5]. The difference compared to the field investigation of Ferguson *et al.* [63] (150 mm wide cultivator shares lasted only 9 km in abrasive South Australian soil with 10% gravel content) is due to the aggressive nature of stony soil when compared with the present loamy soil condition. It is clear that the soil type has a significant influence on the wear rate.

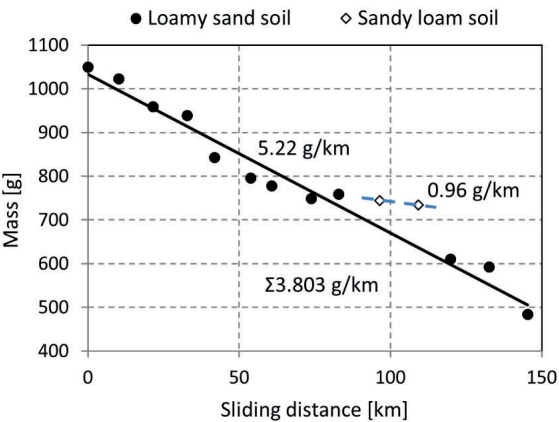


Figure 2-5 Mass of tines in function of sliding distance [21]

Apart from the mass loss a change from a sharp edge of the tines into a rounded geometry is evident. A large decrease in tip and edge length was observed. The shape change in geometry indicates the non-uniform dimensional wear of the tines in function of operating distance. The reason for this is the change in the operating conditions as well as the change in the tribo-system because of the different attack angle of the impacting soil particles and the difference in the contact geometry. As the tine is more worn, the projected frontal area/reference area of the tine is decreasing and the contact with the soil particles shifts more to impact against the front side rather than sliding with a more sharp angle. Based on this information, further investigation on the effect of the attack angle of the soil is to be examined. The defined points for the thickness measurements on the tines, similar to the investigation of Owisak [61], are shown in Figure 2-6-a). The result of the thickness measurements is given in Figure 2-6-b). The wear is more severe closer to the tine tip, probably due to the stress concentration in the soil around this zone.

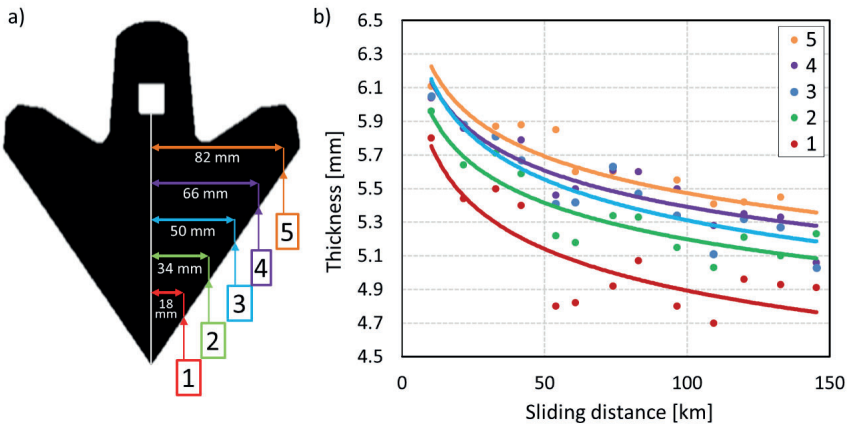


Figure 2-6 a) Defined thickness measurement points on the tine b) Result of thickness measurements in function of operating distance of each tine [21]

The thickness can be described as a power function of the working distance. This means that during the first 50 km of usage the tine shape changes the most. Similar results were also found in the investigation by Owsiak [61]. The first 50 km distance was observed as a running-in period of the wear process. Work hardening is expected in this running-in period which then causes a hardened layer that is continuously removed and recreated by the wear process leading to a steady state wear behaviour. The geometric dimensional loss (tip length, edge length and half width) of each tine is shown in Figure 2-7. The dimensional measurement points marked with x are outliers and considered as false measurements. The rapid increase in the wear of tip length during the initial period was followed by a less severe increasing trend, probably due to the stabilization of the edge shape after some time of operation. The material removal is dominant along the cutting edge (tip and edge reduction) when compared with the loss of thickness and for this reason priority was given to the surface investigation on the cutting edge.

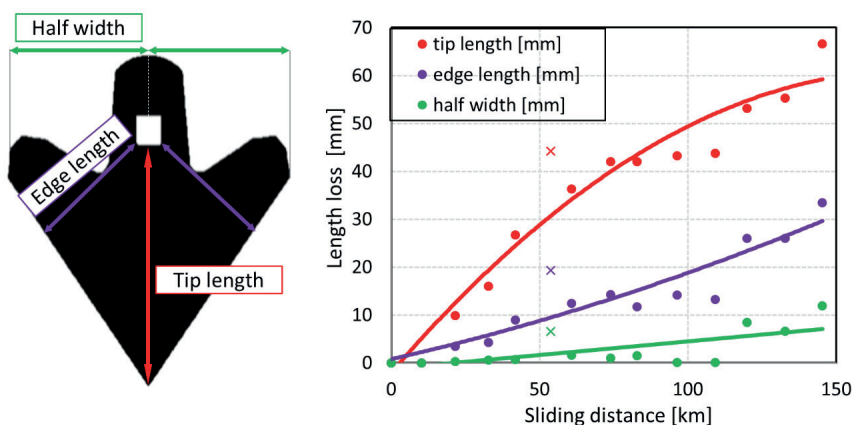


Figure 2-7 Geometrical loss of each tine in function of operating distance [21]

The present in-field investigation shows similar results to that of Ferguson *et al.* [63]. In the initial stage of the wear process the tip length had decreased significantly, but the edge length loss was low. These dimensional changes may be observed as blunting of the tine. The decrease in the width is negligible. When comparing the tip length losses with the thickness reduction it is clear that the wear of the cutting side should be prioritized. The wear of the cutting side caused the largest volume losses of the tine. This confirms the expectations from literature findings introduced earlier, that the wear of the cutting side is more severe than the top surface wear [61], [64].

The tip shape change was also documented. The wing of the tines were cut in their cross section, where the edge length was measured, and thus perpendicular to the cutting edge (Figure 2-8-a). The tines were set in a fixed position with their wing cross-section facing a camera. Macro images recorded their geometric boundaries and together with the results from edge length measurements the shape change is investigated. A sketch of the shape change as a function of the operating distance is presented in Figure 2-8-c) along with the proportional edge length decrease. The shape sketches from tine 1 (10 km), 2 (22 km), 10 (109 km), 13 (145 km) are showing the material loss from the tine top and cutting side as well as the material loss in the edge length. The angle of the tip (τ) with respect to the virtual surface perpendicular to the top surface was plotted in Figure 2-8-b). The tip angle for an unworn tine is 0. Similar to the thickness loss curves, also a running-in and transition to steady state was observed in the τ angle change in function of the operating distance. In the first 20 km the tip angle changed more than in the last 50 km. The angle τ described in the figure has a significant influence on the flow of particles along the cutting edge. To enhance wear resistance either the loss in this angle should be prevented or the material must become less sensitive to micro-cutting mechanism.

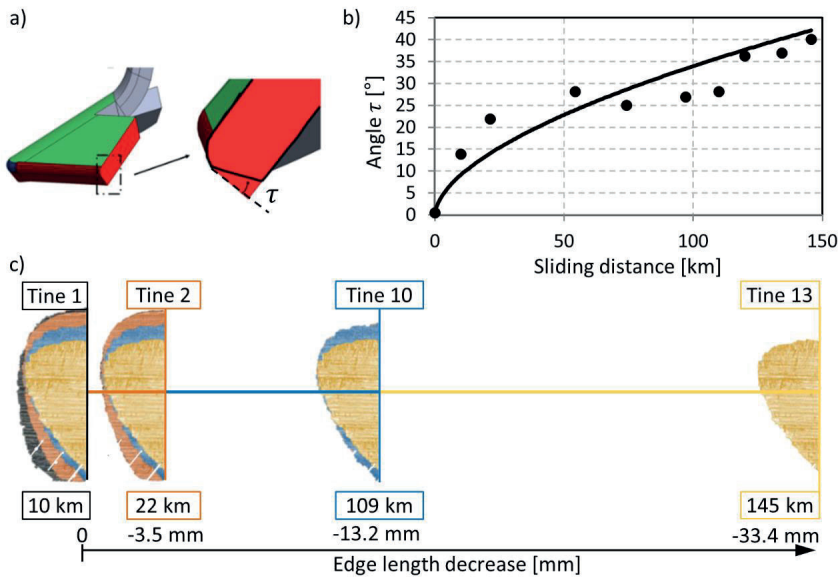


Figure 2-8 a) Defined τ angle in the tine wing cross section b) Tine τ angle change in function of operational distance c) Proportional tine tip shape geometry change with edge length decrease in function of operational distance [21]

2.3.2 Soil investigation

The result of the soil analysis showed that the loamy sand and the sandy loam soil are quite similar. The categorization of the soils is shown in Figure 2-9. The loamy sand soil contains more sand (quartz) fraction and less clay. In the sandy loam a little more humus was measured, which has a positive effect on plants. The particle content of the soils is listed in Table 2-3. The average abrasive particle size with the highest distribution was found to be the coarse sand of >0.25 mm [m/m%] and 0.05-0.25 mm [m/m%] fine sand in case of both soils. The average abrasive particle size with the highest distribution may give indication on the wear track width dimension expected by these quartz abrasive particles to be in the range of 20-500 μm .

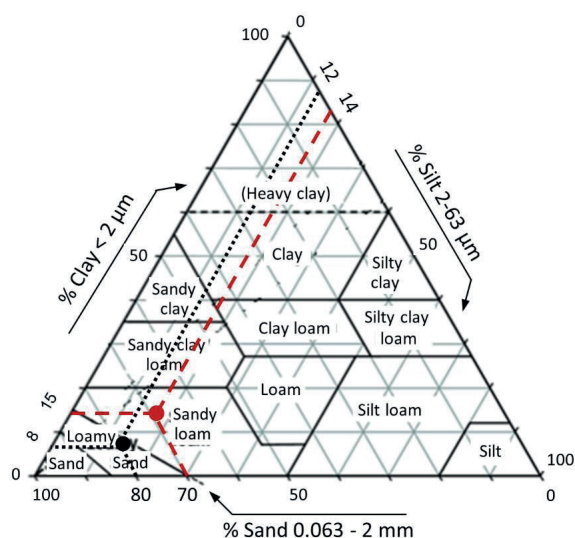


Figure 2-9 Categorization of investigated soils [21]

The difference in wear rate in case of the two different soils was confirmed from the mass measurements of the tines. Tines that run in the loamy sand experienced an average wear rate of 5.22 g/km, while 0.96 g/km in the sandy loam. The abrasive effect of the ~ 10 m/m% more sand content of the sandy loam soil may explain this phenomena. Compared to other soil types (e.g. loam, clay), high sand percentage soils have a significantly higher abrasive effect on tillage tools, however in the soils of this present study no contamination of stones and gravel was found. Other soil parameters such as soil moisture or compaction, but also process parameters such as working depth and speed have a major influence on wear rates according to [61], [63] and prevent a direct comparison of results.

Table 2-3 Particle content of investigated soils [21]

Soil type	Particle content [m/m%]							
	>0.25	0.25-0.05	0.05-0.02	0.02-0.01	0.01-0.005	0.005-0.002	<0.002	<0.02
	mm	mm	mm	mm	mm	mm	mm	mm
	coarse sand	fine sand	sandy silt	silt	silt	silty clay	clay	fine fraction
Sandy loam	35.17	35.29	5.65	4.50	4.19	4.45	10.75	23.89
Loamy sand	32.06	47.91	6.51	4.32	1.30	2.67	5.23	13.52

2.3.3 Surface characterization

Surface topography and morphological investigation was performed to understand the wear process. The different tine regions were investigated separately.

2.3.3.1 Top surface

Beside optical microscopy, white light interferometry was used to understand the transition of surface morphology during wear. The results of 3D topography in Figure 2-10 clearly show a random pattern of the originally painted surface which has been transformed to a directional pattern after the wear process. In addition to micro-cutting and micro-ploughing, micro-pitting was also observed. Material removal through micro-pitting, caused by the repetitive loading by impact and sliding, was observed on the worn tine top surface region close to the tine handle. However, as concluded before the dominant material removal was experienced at the cutting edge of the tines. The orientation of the grooves gives an idea about the relative motion of the soil against the tine. The change from the initial unworn surface topography of average Ra 2-3 μm , Rt 15-20 μm , Rz 8-12 μm , Rsm 120-180 was investigated.

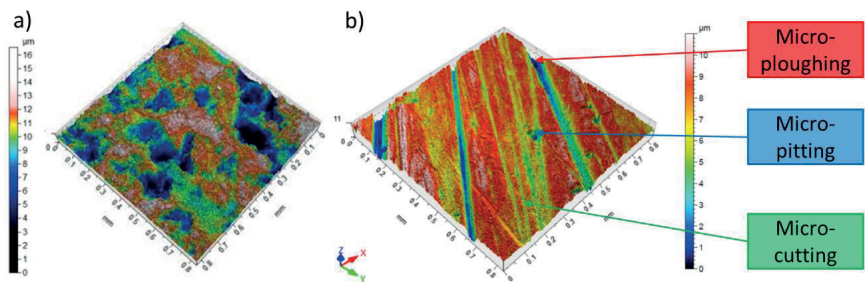


Figure 2-10 3D topography of tine top surface before (a) and after wear (b) (60.7 km operation) [21]

The tine top region surface topography measurement after wear resulted an average Ra 1-2 μm , Rt 10-15 μm , Rz 7-10 μm , Rsm 90-180 μm across all tines with some wider grooves present as seen in Figure 2-11.

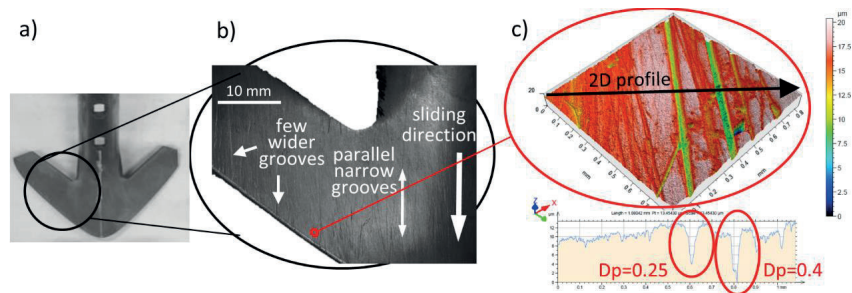


Figure 2-11 a) Tine 6 overview b) macro image of tine 6 top surface c) 3D topography of tine 6 top surface and Dp extraction [21]

Wear micro-mechanisms were characterised with the degree of penetration (D_p) of the abraded grooves. The average degree of penetration from the top surface of the tines are in range of 0.31-0.61 [-], and these values indicate micro-cutting mechanism according to Kayaba *et al.* [82]. The visual inspection also showed oriented, narrow parallel grooves which is in line with the D_p values for validating the micro-cutting mechanism, as seen in Figure 2-11.

2.3.3.2 Cutting side (edge)

Comparing the thickness reduction to the reduction of the edge length and tip length, it is evident that the material removal is dominant along the cutting sides (edges). For this reason, priority was given to the surface investigation on the edges. The arrows in Figure 2-12 show the region of interest (ROI) for macroscopy and topography. From the macroscopic investigation two different wear mechanism were observed on the contact surface of the cutting edge. In the upper region with red arrows large, wide grooves were observed with plastically deformed ridges indicating the local plastic deformation (micro-ploughing). The orientation of the grooves is parallel with the sliding direction of soil against the cutting edge in this upper part. The bottom region with green arrows experienced micro-cutting mechanism with several small narrow grooves and traces of chip formation. The soil motion during the initial contact introduces a local plastic deformation which is mainly visible in the top half area. The direction of the grooves changes due to the flow direction of the soil particles relative to the tine. The particle movement indicates higher contact pressure in the compact regions [83] which promotes micro-cutting mechanism. The surface profilometry and D_p data extraction from the wear grooves confirmed these findings. Macroscopy of the tine cutting side surface and the extracted profile to showcase D_p calculation is shown in Figure 2-12.

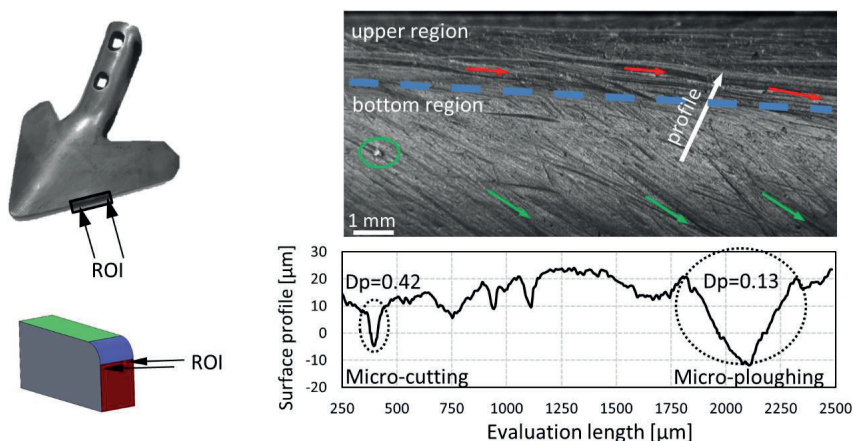


Figure 2-12 Macroscopy of tine cutting side surface and D_p extraction [21]

The lower D_p (compared to the top surface) indicates micro-ploughing and plastically deformed material on the upper part of the cutting edge. The large, wide grooves with plastically deformed ridges, result in an average D_p of 0.09 ± 0.05 [-]. D_p range of 0.24 ± 0.05 [-] was measured at the bottom part indicating a dominant micro-cutting phenomena which results into a more uniform wear pattern with narrow parallel grooves [81]. Traces of continuous chip formation marked in green circle (Figure 2-12) was also observed in this region confirming the micro-cutting mechanism. The co-existence of these two micro-mechanisms observed on the cutting edge with each of them dominant in a specific region could aid future tine designs aiming at prolonging lifetime. A different heat treatment of the upper and lower zones of the cutting edge could be considered. A carefully designed coating on the surface regions which experience more severe wear could be an option too.

Vickers hardness and microstructural analysis were performed on the cross-section of the sliding interface (Figure 2-13). The microscopy covered the following tine zones: one zone on the top side (green colour), two zones on the cutting side (blue and red colour) micro-ploughing and micro-cutting zones, one zone on the bottom (grey colour) side for reference (unworn zone). The microscopic observations show a tribo-layer on the worn surface. This tribo-layer is present in all regions where the sample was in contact with the soil (top side and cutting side). This thin layer is the result of surface hardening, which is a consequence of force interaction between the surfaces and the soil. Due to the local stress rise, the thickness of the tribo-layer is significant in the micro-ploughing zone, where the thickness of this uniform, plastically deformed layer can reach up to $\sim 50 \mu\text{m}$. The local pressure results in compression of the plastically deformed material, where the morphological orientation also changes. In this compressed zone a change in the orientation is clearly observed in the microstructure. On the tine top surface, a thin tribo-layer is observed with traces of uneven material shear-off indicated with red arrows in Figure 2-13. A thin tribo-layer with similar characteristics is observed at the bottom of the tine cutting side. These features give an indication that micro-cutting mechanism is the dominant mechanism in these zones. The unworn bottom tine zone serves as a reference surface without significant changes in its microstructure.

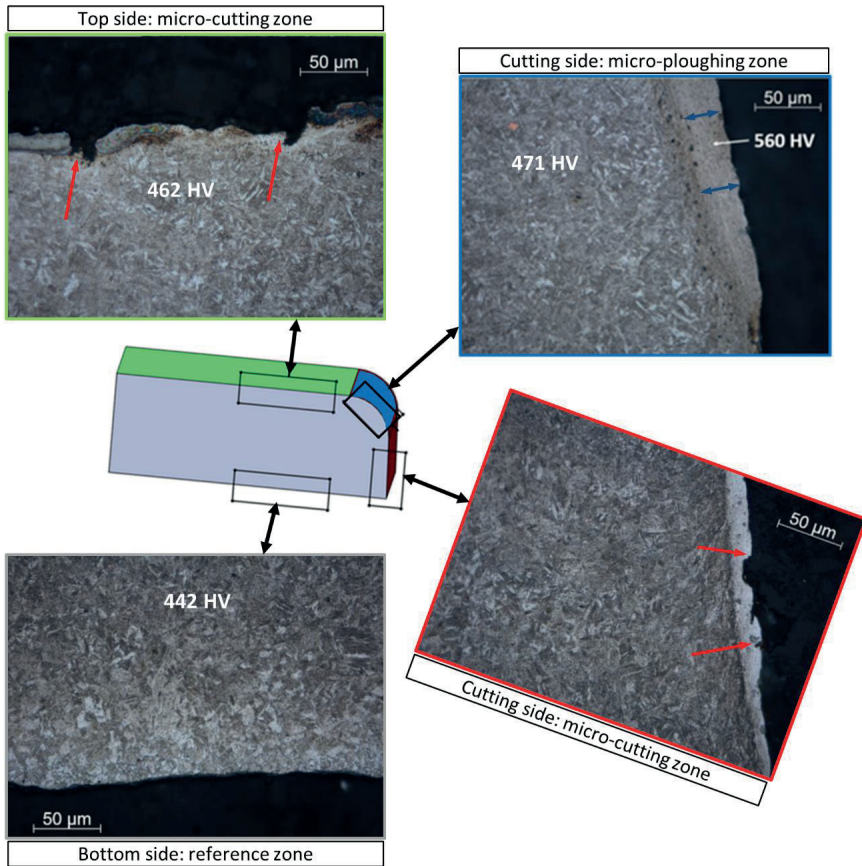


Figure 2-13 Optical microscopy of extracted tine sample 12 (132.7 km operation) [21]

To study the change in morphological orientation and the plastic flow on the contact surface SEM analysis was performed on the extracted tine sample (Figure 2-14). From the SEM images the change in morphological orientation is clear. In the tribo-layer the direction becomes parallel with the sliding direction (blue arrow parallel to the tine zone boundary). In the region where micro-cutting was the dominant micro-mechanism the tribo-layer suffered of material shear resulting in uneven surface boundaries (red arrows indicating material shear in top and micro-cutting zones). Due to the repeated material removal from micro-cutting the tribo-layer is observed to be few (1-2) μm in thickness. The bottom tine surface was considered as a reference because of the unworn condition. In this area no significant change is observed in the microstructure.

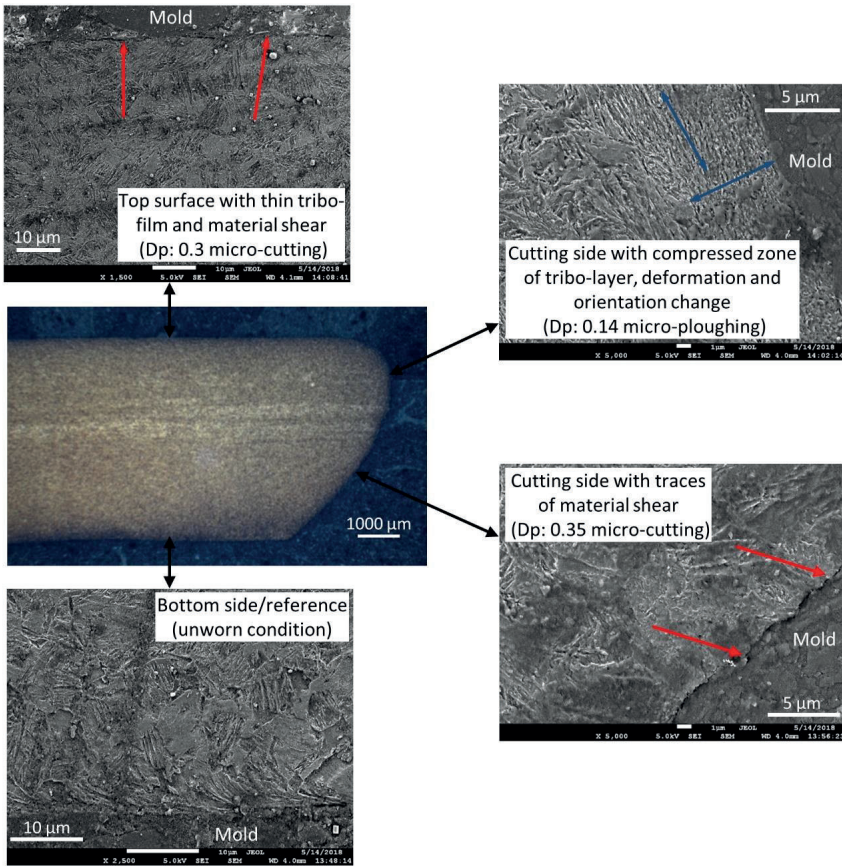


Figure 2-14 SEM on extracted tine sample 12 (132.7 km operation) [21]

2.3.3.3 Surface fatigue

As briefly concluded in 2.3.3.1, in addition to micro-cutting and micro-ploughing, micro-pitting was also observed. Surface fatigue in the form of micro-pitting was initiated by the repetitive stochastic impingement of hard particles (soil contamination, e.g. stones) on the tine top wing surface. The top layer of the soil is described to be less dense and particles could move more freely causing impingements resulting in abrasive erosion. During cultivation the soil particles close to the surface tend to impact and damage the top tine region close to tine handle. This is shown in a blue ellipse in Figure 2-15. The multi-level wear testing approach of this project includes the design of an intermediate laboratory set-up in order to reproduce the observed co-existing wear modes (abrasion and pitting). A more detailed investigation about the complex occurrence of the co-existing wear modes are presented in Chapter 6.

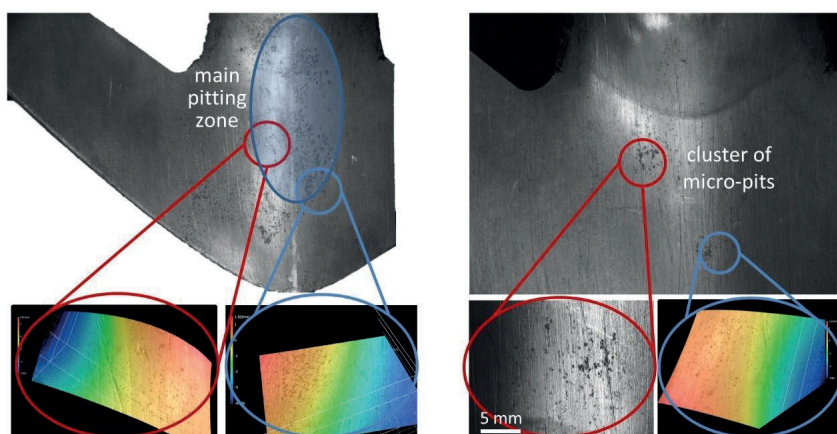


Figure 2-15 Tine wing surface fatigue regions with identified micro-pits

Although beside abrasion, pitting surface damage was identified as a separate wear mechanism on a specific tine region (at the top part of the tine, close to the handle as seen in Figure 2-15), the affected area is limited. Furthermore, the material loss from that tine part is not significant compared to the material removal from the tine wing/cutting edge as concluded from Figure 2-6 and Figure 2-7. Since the severity of pitting is magnitudes behind abrasion, the overall dominant and focused material-removing mechanism is abrasion.

2.3.4 Hardness measurements

Hardness measurements of the relevant areas (top area, micro-ploughing and micro-cutting zone on the cutting side, bottom area) show that the tribo-layer zone has an increased hardness of about 470 HV (increase with ~ 30 HV) (Table 2-4). The change in morphological orientation can be observed from the plastic flow of the material in the direction of relative soil sliding. As a consequence of compressive stresses grain refinement on the top layer is observed, which results in an increased hardness. This increase in hardness was already realized after 10.3 km of sliding distance. The measured hardness of the reference unworn (bottom side) zone remained close to 440 HV.

Table 2-4 Zone specific hardness [HV] change of tines [21]

Tine number	Operation [km]		Tine region	Hardness [HV]	Standard deviation
Tine 1	10.3	Top side	(tine wing surface)	465	7
Tine 1	10.3	Bottom side	(unworn reference)	442	9
Tine 12	132.7	Top side	(tine wing surface)	473	12
Tine 12	132.7	Bottom side	(unworn reference)	439	7

2.3.5 Particle flow investigation with DEM

The Discrete Element Method (DEM) is characterized by the free interaction of individual solids with each other and was originally developed by Cundall and Strack for investigations in rock mechanics [84]. The simulation method has been widely used in various disciplines, especially in recent years. In agricultural engineering, DEM is used to simulate field products such as potatoes or maize, but also for soil cultivation. The subject of wear in agricultural soil tillage has so far only been examined to a limited extent. A study of particle movement with the DEM along critical areas, such as the cutting edge of the tine, was not carried out previously. In frame of the present research project [21], an initial DEM model was developed in order to better understand the test results by linking them with fundamental wear mechanisms. With DEM analysis, the particle movement along the cutting edge of the tine could be identified more precisely. Therefore, only individual particles from the particle bed are monitored at one time step. The motion of the particles is described in the following until they are submerged (Figure 2-16). Particles move perpendicular to the sliding direction of the tines, where the particles slide along the cutting edge (1). The particles move sideways along the cutting edge to the outside as can be seen by their orange trajectory (2). Once the particles are submerged, they move parallel towards the sliding direction of the tine (3). Similarities can be seen in the comparison of the simulation results with the macroscopic image of the cutting edge (Figure 2-16).

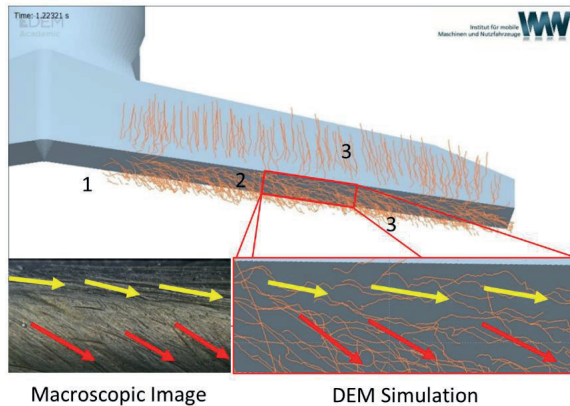


Figure 2-16 Path of soil particles along the cutting edge compared with the scratches observed on the surface [21]

In the upper area of the cutting edge there is also a lateral movement of the particles relative to the cutting edge (yellow vectors), which becomes steeper when leaving the upper third of the cutting edge (red vectors). Tracing the movement of the soil particles gives an indication on the experienced wear pattern of the tine. The used initial DEM is proposed to be developed further as potential future work in Chapter 7.

2.4 Conclusions from field investigation

The wear trends obtained from the in-field tests (mass loss measurements and change in geometrical dimensions) are in good agreement with literature about symmetrical goose foot tines. Rapid increase in the change of tip length during the initial period was followed by a less severe dimensional wear trend. A linear decrease of the absolute mass was observed during the wear process. This is more reflected in the reduction of the tip and edge length than in the thickness reduction. The material removal was concluded to be dominant along the tine cutting edges. Specific wear mechanisms were identified in different regions of an individual tine. Two dominant micro-mechanisms, micro-cutting and micro-ploughing, were observed. Material is removed during micro-cutting, with possible wedge formation. Micro-ploughing results into material flow and plastic deformation with built-up ridges without material removal. The tine geometry was segmented based on the observed micro-mechanisms:

- (1) Top area (tine wing surface) with average D_p for the grooves in the range of 0.46 ± 0.15 [-], these values indicate micro-cutting regime;
- (2) The upper part of the cutting edge was characterized by large, wide grooves with plastically deformed ridges with D_p value 0.09 ± 0.05 [-], which is in the micro-ploughing regime;
- (3) The lower half of the cutting edge showed similar characteristics as the top area with D_p in the range of 0.24 ± 0.05 [-].

DEM simulation of the soil flow in contact with the tine confirmed the observed wear patterns and directions. It was found that the upper part of the cutting edge the particles move along the edge after the initial contact resulting into a plastic deformation of the material. The bottom region which wears off with the described tine tip angle (τ) experienced micro-cutting and gliding of the soil particles in parallel with the sliding direction against the cutting edge.

Future design of tine materials could be focused on enhancing the wear resistance against micro-cutting, which could prolong lifetime of the tines and hence reduce economic losses. An option for this could be the usage of hybrid materials or application of coatings for the cutting edge tine surface. A welded hardcoating layer could contribute to better wear performance. A further possibility to improve the wear resistance is to change the tine geometry. Adjustment of the cutting edge angles would influence the flow of soil particles, which could prove beneficial. The effects of change in cutting edge geometry can be investigated using DEM model and evaluated with regards to the wear risk using the relative movement and the load on the coulter. However, the conclusions derived from the tribological investigation needs to be balanced with economical (e.g. production) and technological (e.g. operation safety) aspects. This means that beside requirements such as e.g. ploughing efficiency cannot be worsened and drag force cannot increase, an overall lifecycle and cost efficiency analysis is required to fulfil decisions made on design according to sustainable development.

3 CHAPTER 3

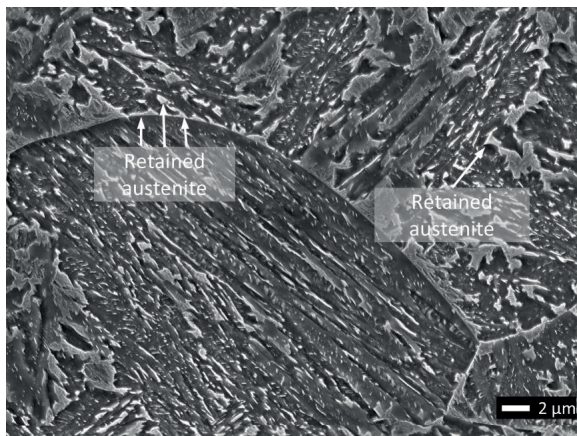
INVESTIGATED MATERIALS

This chapter introduces the investigated materials.

The following articles included the content of this chapter:

Á. Kalácska, P. De Baets, H. Ben Hamouda, K. Theuwissen, and J. Sukumaran, "Tribological investigation of abrasion resistant steels with martensitic and retained austenitic microstructure in single- and multi-asperity contact," *Wear*, vol. 482–483, p. 203980, Oct. 2021, doi: 10.1016/j.wear.2021.203980.

Á. Kalácska, L. Székely, R. Z. Keresztes, A. Gábora, T. Mankovits, and P. De Baets, "Abrasive Sensitivity of Martensitic and a Multi-Phase Steels under Different Abrasive Conditions," *Materials*, vol. 14, no. 6, p. 1343, Mar. 2021, doi: 10.3390/ma14061343.



3.1 Materials

From a material design perspective, increasing both initial hardness and work-hardening capability is a challenge. The hardness of the martensitic structure is often improved by increasing the carbon content, but this also increases the quench sensitivity of the material with a risk of brittleness at room temperature. On the other hand, strain hardening in martensitic Q&T steels is determined by several morphological features in the microstructure such as the prior austenite grain size [85] and martensite packets and blocks [86], which depend on the alloying elements and the hot-rolling process parameters. Increasing hardness to boost material wear resistance is sacrificing toughness, ductility and machinability (cutting and forming). Moreover, reaching higher hardness by increasing carbon content can also be detrimental for weldability. Therefore, a trade-off of materials hardness and in-use properties is required to fulfil industrial requirements.

In addition to martensitic steels, advanced steels such as Transformation Induced Plasticity (TRIP) and Twinning Induced Plasticity (TWIP) are utilised as an alternative for abrasion problems such as mining crushers and bucket loaders. The advantage of such steels is the higher strain hardening capability compared to martensitic steels. Furthermore, it was proved [87] that a combination of ultrahigh strength and good ductility can be achieved by tailoring the volume fraction, morphology, and carbon content of the retained austenite (RA) in a TRIP steel. Strain hardening was reported to be an important mechanical property controlling material response to high-stress abrasion modes [88]. During the wear process, the material develops progressively a deformed layer underneath the contact surface. During this deformation mechanism, the energy applied by the scratching particles on the material surface is partially consumed by the deformation of the material. Retained austenite in the martensitic steel was reported as a solution to increase the strain hardening via transformation-induced plasticity (TRIP) mechanism [89]. In that study, the dry rolling/sliding wear response was obtained for nanostructured bainitic materials with different retained austenite volume fractions and similar hardness. The nanostructured bainitic materials outperformed conventional Q&T grades by a factor of two. The evolution of the TRIP effect was identified as a possible reason for the better wear resistance but the presence of bainitic ferritic structure was another possibility. So far, only a few works were performed on studying the TRIP effect under abrasive conditions. Recently, Saha *et al.* [90] studied the TRIP effect under impact-abrasive and abrasive conditions and suggested that the blocky morphology of the retained austenite could decrease its mechanical stability leading to an early transformation to martensite and eventually premature failure of the steel. On the other hand, for martensitic materials, when the direct quenched structure is already obtained, the tempering process enables further microstructural changes that can increase the strain hardening capability [91]. Krauss [91] reported that at low-temperature-tempering (e.g. heat treatment of the martensite at a temperature around 200°C), the main strengthening mechanism is the strain hardening associated with the dynamic

interactions of dislocations with the fine transition carbides/dislocation substructure of the tempered martensite.

The currently used 27MnB5 tine material is a commercially available, low alloyed manganese boron steel used in agriculture. Due to the experienced wear of this material in the investigated tine application, new standard wear-resistant steels (martensitic quenched and tempered steels) were proposed for a better performing material. Three different abrasion resistant steels have been selected for the present study: fresh martensite (FM), tempered martensite (TM) and multiphase (MP) martensite and bainite with retained austenite. Material compositions are given in Table 3-1.

Table 3-1 Chemical composition [wt%] of the studied materials [92]

Material	%C (max)	%Mn (max)	%Si (max)	%P (max)	%S (max)	%Ti (max)	%Cr (max)	%Ni	%Al (max)	%B (max)	%Mo (max)
FM	0.2	1.9	0.5	0.02	0.005	0.05	0.5			0.004	
TM	0.2	1.9	0.5	0.02	0.005	0.05	0.5			0.004	
MP	0.2	1.6	0.8	0.018	0.005		1.9	~0,20	0.08		0.4

Martensitic grades FM and TM have similar chemical composition and are both hot-rolled down to a thickness of 5 mm. To obtain the fully martensitic structure (Figure 3-1-a)), the material is initially austenitized above 1200°C, hot-rolled and directly water quenched to room temperature in the run-out-table at a cooling rate higher than 10°C/s, followed by coiling. Figure 3-1-a) corresponds to the FM grade.

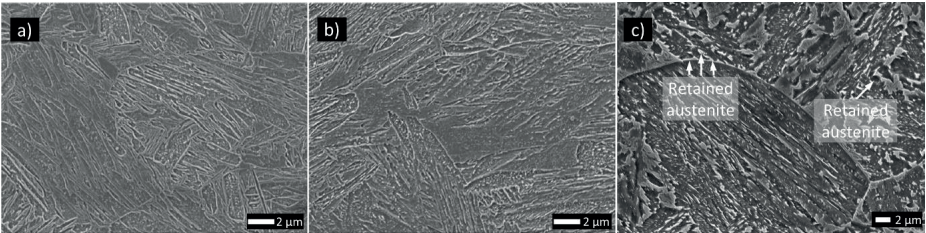


Figure 3-1 SEM of (a) fresh martensite by coiling at room temperature, (b) low-temperature-tempered martensite (2% Nital etched) and (c) MP steel [92]

The fresh martensitic plates followed a subsequent reheating at a temperature of 200°C for 30 mins, followed by air cooling leading to the low-temperature tempered martensitic structure (TM) of Figure 3-1-b). For the MP steel, the material chemistry, hot rolling practice and an adapted cooling strategy enable the formation of a martensitic structure as well as small fractions of retained austenite. A characteristic of the retained austenite structure is its ability to transform into martensitic structure during mechanical or thermal loading. Consequently, the material has an increased work hardening capability due to the TRIP effect.

Mechanical properties of the tested materials are summarized in Table 3-2. The characterization of the materials was carried out in the project RFSR-CT-2015-00010 Research Fund for Coal and Steel (RFCS). For each material, 3 tensile samples were tested, as well as 3 Charpy samples per testing temperature. The results are presented as the average value of the three measurements. The tensile testing was performed on a hydraulic tensile machine from INSTRON with a capacity of 1200kN, according to the EN6892-1 standard. The uniaxial compression test was performed with by a deformation dilatometer machine Bahr DIL-805A/D according to ASTM-E9. The impact tests were performed on a calibrated Zwick/Roell Charpy pendulum, according to the ISO 148-1 standard. The micrographs were obtained with a JEOL SEM equipped with a field emission gun (model JSM 7100F). The retained austenite fraction was determined by X-Ray diffraction, using the D8 Discover setup by Bruker with a Co tube (K α 1), with an accelerating voltage of 35 kV and a current of 40 mA.

Table 3-2 Characteristic features and properties of the used steels [92], [93]

Properties	Notation	Unit	FM	TM	MP
Microstructure	-	-	Fresh martensite	Tempered martensite	Multiphase steel with retained austenite
Retained austenite fraction	RA	m%	<2	<2	12.5
Hardness	H	HV	478	465	367
Ultimate tensile strength	σ_M	MPa	1528	1474	1264
Yield strength	σ_Y	MPa	1314	1413	1031
Young's modulus	E	GPa	217	206	192
Uniform elongation	ε_M	%	3.4	2.8	5.3
Fracture elongation	ε_B	%	8.6	7.4	12.6
Charpy ISO 148-1 (20°C/-40°C)	$W_{(20/-40)}$	J	28/17	38/21	179/32
Compressive strength	σ_c	MPa	1460	1501	1213
Compressive modulus	E_c	GPa	94	96	65

An increase in the yield strength and the toughness of the material was observed after tempering of the martensitic grade. This increase may be attributed to the static strain ageing phenomenon characterized by a relief of the residual stresses at a very small scale (locking of mobile dislocations), as can be expected for a low-temperature-tempering process [94]–[96].

4 CHAPTER 4

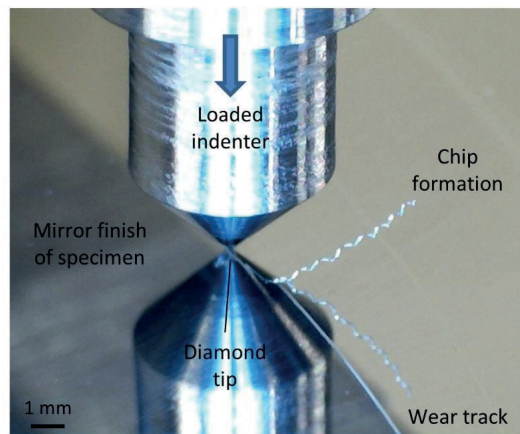
MICRO LEVEL SINGLE-ASPERITY CONTACT ABRASION INVESTIGATION

This chapter summarizes the results obtained from single-asperity scratch tests representing the controlled, micro-level wear investigation.

The following articles were published based on this chapter:

Á. Kalácska, P. De Baets, H. Ben Hamouda, K. Theuwissen, and J. Sukumaran, "Tribological investigation of abrasion resistant steels with martensitic and retained austenitic microstructure in single- and multi-asperity contact," *Wear*, vol. 482–483, p. 203980, Oct. 2021, doi: 10.1016/j.wear.2021.203980.

Á. Kalácska, L. Székely, R. Z. Keresztes, A. Gábora, T. Mankovits, and P. De Baets, "Abrasive Sensitivity of Martensitic and a Multi-Phase Steels under Different Abrasive Conditions," *Materials*, vol. 14, no. 6, p. 1343, Mar. 2021, doi: 10.3390/ma14061343.



4.1 Introduction

Steel making companies are continuously developing new steels with complex microstructure in order to satisfy the demands of applications dealing with abrasion issues in e.g. mining and agricultural industries. This challenge raises an important tribological research need, i.e. the investigation of the abrasion resistance of these new materials.

It is clear that understanding the material response towards a controlled wear loading is an important step to build deeper knowledge on the involved wear mechanisms and to propose recommendations for the design of improved wear-resistant steel grades. In order to determine relative resistance against abrasive wear, reliable laboratory tests are required. Single scratch test is generally used as a benchmark for tribological behaviour of steel surfaces [22]. As reported by Lindroos *et al.* [88] the wear rates determined from single scratch tests, however, are not a proper representation of the true behaviour of the steel in high-stress abrasion conditions, mostly due to the insufficient account of the surface strain hardening behaviour. On the contrary in a multi-asperity test, the specimen experience work hardening at the contact surface due to the multiple contacts with the abrasive. In this work, to study the effect of strain hardening on materials wear resistance, a single and multi-asperity wear test are applied on two martensitic materials: as-quenched and low-temperature-tempered steel and an industrial martensitic-bainitic steel containing retained austenite. This research investigates the material response under single - and multi-asperity conditions and studies the connection of the basic material properties with the abrasive wear behaviour.

4.1.1 Abrasive micro-wear process

Abrasion is one of the dominant wear mechanisms for material removal during the interaction with solid bodies [97]. Surface damage to a tribological pair is often generated by means of successive small steps activated by wear micro-mechanisms. The observed damage is thus the cumulative effect of one or more micro-mechanisms leading to macroscale damage [33]. The abrasion print on the material's surface is mainly demonstrated through the existence of grooves drawn by the hard abrasive particles or protuberances, along the sliding direction. The severity of the abrasion mechanism is often identified from the so-called "grooves", and abrasive wear is therefore also referred to as grooving wear [10]. The four different modes of abrasion are (1) micro-ploughing, (2) micro-cutting, (3) micro-fatigue and (4) micro-cracking [4]. These micro-mechanisms create physical change on the surface with or without progressive material loss. The micro-mechanisms independently operate in plastic or elastoplastic mode. Except micro-cracking the rest of the three micro-mechanisms tend to produce grooves as a wear scar. Under ideal conditions, micro-ploughing in abrasion is the local plastic deformation by material displacement within the solid body, without particle generation. However, due to successive action of abrasives, the repeated contact on the displaced material may finally

generate wear particles (material removal) as a consequence of low cycle fatigue. Micro-cutting is defined as micro-machining process where material removal is evident. Even though grooves are generalized from their morphology and appearance, their distinctive geometrical features can be related to a particular micro-mechanism [32]. The degree of penetration (D_p) is a factor that gives information about the wear groove geometry and can be used to determine the dominant micro-mechanism in a particular application or wear process [80].

4.1.2 Wear investigation approaches

A linear relationship is known between the hardness of steel (pure metal or alloys with identical microstructure) and its wear resistance [33]. For this reason, quenched and tempered (Q&T) martensitic steels are reported to be a suitable solution for abrasive and impact-abrasive applications due to their high strength levels and stable hardness [90], [98]. It was found that in case of steels with different microstructure (quenched, tempered, alloyed) the relative wear resistance is different despite the same hardness. Earlier reports from field tests [61] indicate that, despite the overall hardness, the steel microstructure has a significant influence on the wear resistance. E.g. the volume fraction and size of carbides can be important parameters controlling the wear rate. Although tempered martensitic steel 50S2 is harder than the bainitic material 65G (Q&T), the former experiences severe abrasion due to the smaller volume fraction of carbides [61]. Pin-on-disk testing of different abrasion-targeted steels with different microstructures, including medium alloyed martensitic carbon steel, confirmed that the microstructure has more influence on the wear resistance than the bulk hardness [22]. Nominally similar 400 HB grade quenched wear resistant steels were investigated [99] under heavy abrasive wear conditions. Over 50% difference was recorded in the wear performance and it was found that the surface hardness differences (5–10 HV) do not explain the variations in the mass losses. Microstructural features and hardness profiles seem to affect more the wear performance.

Lindroos *et al.* [88] simulated highly abrasive environments such as mining and crushing by applying single and multiple scratches under high load levels to evaluate wear resistance of several wear grades, including martensitic steels. During the multiple scratching process, a progressive increase in the surface hardness was observed along with a decrease in the wear rate reaching a steady state. At this level, lower wear rates were obtained compared to the single scratch values. The change in the wear rates pointed out the dominant effect of strain hardening on abrasion resistance of steel [100]. Recent researches also proved that hardness is not the only parameter that determines the wear resistance. The three-body abrasive wear behaviour of three ferrous alloys with different microstructures but similar hardness has been investigated using a standard dry-sand rubber wheel test [101]. The transformation-induced-plasticity effect of retained austenite was accounted for the improved wear

resistance. The sensitivity of the wear resistance to microstructure was explained with the different wear mechanisms involved in surface damage. Wear tests were carried out on 35NCD16 steel pins with different heat treatments in a pin-on-plate configuration [102]. A peak of wear rate was observed for a hardness around 430–450 HV, that also reflected the effect of the microstructure and a change of wear mechanisms.

4.2 Experimental procedure

The test protocol for the single asperity scratch test experiments is discussed in the following section. The investigated materials were introduced in Chapter 3. The steel disk specimens were initially prepared (grinding and polishing) in accordance with ASTM G171 – 03(2017) standard for scratch hardness test of materials using a diamond stylus [103]. Before scratch testing, the disk 3D surface characteristics were investigated using a non-contact optical profilometer (Taylor Hobson CCI HD white light interferometer). The processed surface has arithmetic mean deviation (S_a) ranged between 0.002 to 0.005 μm , an S_z value (ten point height) from 0.02 to 0.5 μm and root mean square mean deviation (S_q) of 0.002 to 0.01 μm . The scratches were made using Rockwell-type diamond indenters with various tip sizes mounted on a static arm (similar to a phonograph) under different loading conditions (Figure 4-1-b)). The sequence of events involved in the material removal process during the single-asperity test was monitored on-line using Dino-Lite AM4113ZT4 USB camera with 430-470x optical magnification. The processing of the images and videos was carried out with DinoCapture 2.0 program. The in-situ monitoring is facilitated by the static positioning of the pin and the damaged surface being open to the optical train of the microscope. Figure 4-1-a) shows the single-asperity test set-up.

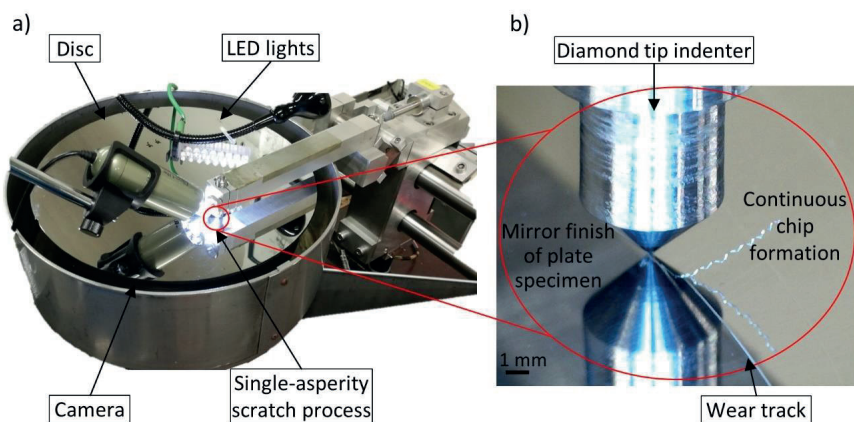


Figure 4-1 a) Single-asperity test set-up, b) scratch testing (MP steel with 25 μm tip radius, cone angle 90° diamond tip indenter under 10.8 N load) [92]

In the design of experiments for the single-asperity testing, three sets of variables were used based on (1) plate materials, (2) pin geometry (indenter cone angle and tip radius) and (3) operational parameters (load). Three repetitions were made for extreme and intermediate test conditions, which covered the highest and lowest load as well as the smallest and largest tip radius (Table 4-1). The sliding speed was set to 0.45 mm/s and the total sliding distance to 30 mm. Environmental parameters were measured during scratch testing: 21.4-22.8 °C temperature and 48-54% relative humidity.

Table 4-1 Characteristics of indenters for single-asperity test and test matrix with number of repetitions

Indenter				Load [N]			
Cone angle γ	Tip radius r	Apex angle δ	Attack angle α	0.9	1.3	5.8	10.8
90°/120°	25 μm	90°/120°	45°/30°	3	1	1	3
90°/120°	50 μm	90°/120°	45°/30°	1	3	1	1
90°/120°	100 μm	90°/120°	45°/30°	1	1	3	1
90°/120°	200 μm	90°/120°	45°/30°	3	1	1	3

4.3 Parameters influencing wear micro-mechanisms in single-asperity scratch testing

In the single-asperity scratch test the wear micro-mechanisms were evaluated using the degree of penetration (D_p) of the wear groove, which was calculated from the 3D surface topography after the scratch tests. D_p gives information about the groove geometry and is defined as the ratio of the groove depth on half the groove width [82]. Hokkirigawa [80] introduced a formula that predicts the degree of penetration in a scratch test for a certain normal load F_N and indenter tip radius r on a surface with hardness H . Groove depth [μm] is h , while the full groove width in the surface level is $2w$ [μm].

$$D_p = \frac{h}{w} = r \left(\frac{\pi H}{2F_N} \right)^{\frac{1}{2}} - \left(\frac{\pi H r^2}{2F_N} - 1 \right)^{\frac{1}{2}} \quad (3.1)$$

Different D_p value ranges are associated with each wear micro-mechanism. The material hardness has an influence on these ranges. The transition in micro-mechanism from micro-ploughing to micro-cutting is induced by increasing the attack angle of the abrading particle, hence increase of D_p [10], [79]. D_p also partly illustrates the severity of wear, and the micro-mechanism by itself can act as an indicator to decide the operational regime being mild or severe wear. In single asperity testing, the topographic data and wear micro-mechanism experienced by individual scratches of each groove were analysed. The 3D topographic data is extracted with TalyMap software. In the process to obtain the D_p of the wear scar, the cross-section profiles of the scratch (600 in total) at several defined locations across the groove were extracted. The investigated area covered 300 μm x 300 μm after 5 mm, 15 mm and 25 mm from the beginning of the scratch. To study the wear characteristics, the extracted data were averaged and merged into one average cross-section profile (Figure 4-2). The groove depth, which is calculated from the levelled surface, is divided by the half-width of the profile at the surface

level to obtain D_p . The groove area (A_g) is shown in dark, while the shoulder/ridge areas ($A_{s1}+A_{s2}$) are highlighted in light grey. Multiplying these areas with the scratch length results in the volume of the groove and of the ridges/shoulders respectively. The wear volume is calculated by extracting the shoulder volume (V_s) from the groove volume (V_g). Low D_p (<0.1) and similar area ratio between shoulders/ridges (light grey area) and the groove (dark grey area) indicates micro-ploughing.

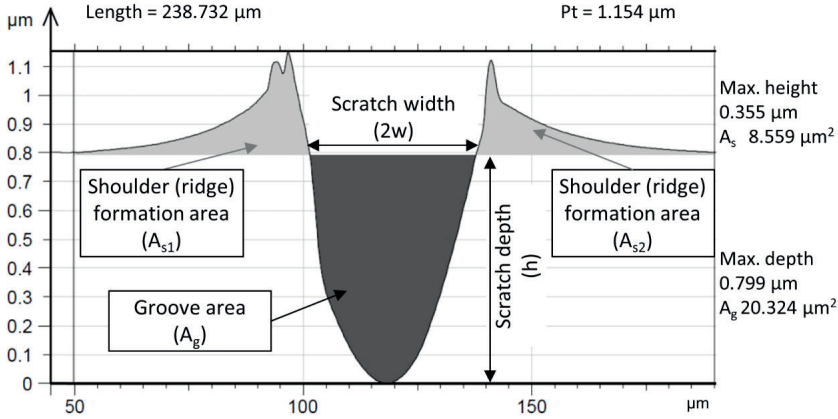


Figure 4-2 Extraction of groove data for scratch made on TM with 5.8 N load, 120° cone angle, 200 μm tip radius diamond indenter [92]

The groove volume and the shoulder/ridge volume were calculated for a scratch length (L) of 30 mm.

$$V_g = A_g \cdot L \text{ [mm}^3\text{]} \quad (3.2)$$

$$V_s = A_s \cdot L \text{ [mm}^3\text{]} \quad (3.3)$$

The degree of wear β [-] was calculated with the method introduced in the literature [104]:

$$\beta = \frac{V_g - V_s}{V_g} \quad (3.4)$$

Where V_g is the groove volume [mm^3] and V_s is the shoulder volume [mm^3]. $\beta=1$ indicates the ideal material removal with pure cutting mechanism. If $\beta=0$ there is no material removal, hence pure ploughing mechanism. To obtain the specific wear rate k [mm^3/Nm], the following formula was used [104]:

$$k = \beta \frac{V_g}{F_N \cdot L} \quad (3.5)$$

Where F_N is the normal load [N], L is the scratch length (sliding distance) [m].

The test conditions for the single asperity testing were designed to study the influence of normal load, attack angle and indenter tip radius for all three different steel grades.

4.4 Results of scratch testing

4.4.1 Wear modes

In the following section, single-asperity test results are discussed in detail. With regards to the micro-mechanisms, the 3D topography measurements are in good agreement with the visual inspection. 3D surface topography of two extreme conditions is shown in Figure 4-3. The groove with a 0.68 Dp value was characterized as micro-cutting caused by a high load (Figure 4-3-a). Nevertheless, irrespective of the high attack angle, the low load condition produced micro-ploughing where the Dp value is 0.07 and the groove depth is below 1 μm . This also confirms the findings of Zambrano [38], that the load has significant influence and is dominating the wear mechanism.

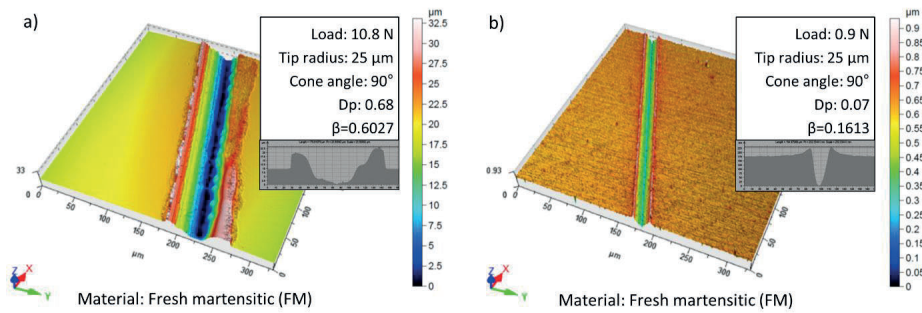


Figure 4-3 Scratches made on material FM (a) 10.8 N test resulting Dp 0.68 micro-cutting and (b) 0.9 N test resulting Dp 0.07 micro-ploughing [92]

Using the on-line monitoring module in the scratch tester, the wear micro-mechanisms were optically identified. Microscopic images of the wear track and generated debris were used to validate the dominant wear micro-mechanism. The test conditions (load, indenter cone angle, indenter tip radius, material) influenced the transition between the micro-mechanisms. Some examples for these micro-mechanisms and wear tracks are shown in Figure 4-4. During micro-ploughing, the material is plastically deformed with only ridge formation instead of material removal resulting in shallow, narrow wear track without debris (Figure 4-4-a, e). Wedge formation was observed (Figure 4-4-b, c) as an intermediate mechanism transitioning to micro-cutting with occasionally discontinuous, separate flake-like chip formation resulting in the wear track of Figure 4-4-f, g. Material removal with continuous long debris forming the chip along the scratch ridges evidences micro-cutting (Figure 4-4-d, h). All of these characteristics were clearly observed from the on-line monitoring. For micro-ploughing mostly FM and TM material produced a clear recording, and for micro-cutting it was the MP and FM steel. (Figure 4-4).

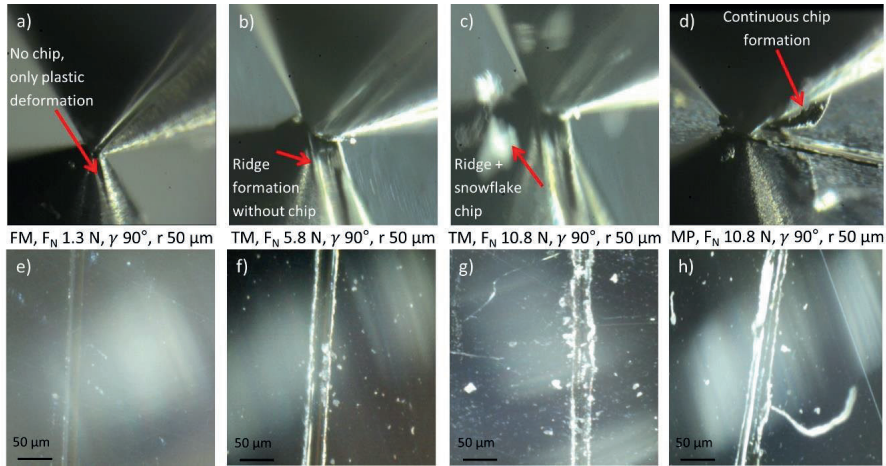


Figure 4-4 In-situ images acquired using video microscope for single-asperity tests,
a) Micro-ploughing – FM: load F_N 1.3 N, tip radius r 50 μm , cone angle γ 90°, and its wear track (e)
b) Wedge formation – TM: F_N 5.8 N, r 50 μm , γ 90°, and its wear track (f)
c) Wedge formation – TM: F_N 10.8 N, r 50 μm , γ 90°, and its wear track (g)
d) Micro-cutting – MP: F_N 10.8 N, r 25 μm , γ 90°, and its wear track (h)

4.4.2 Groove depth

In the following, the groove depth is analysed. Figure 4-5 shows for all 3 tested materials the summary of wear track groove depth change as a function of load and indenter tip radius for both cone angle 90° and 120°. According to the research work of Sin *et al.* [43], the decrease in D_p introduces the creation of ridges due to plastic deformation; the same remark has also been reported [105]. It shows that as the attack angle decreases, it indicates a transition in the predominant micro-mechanism.

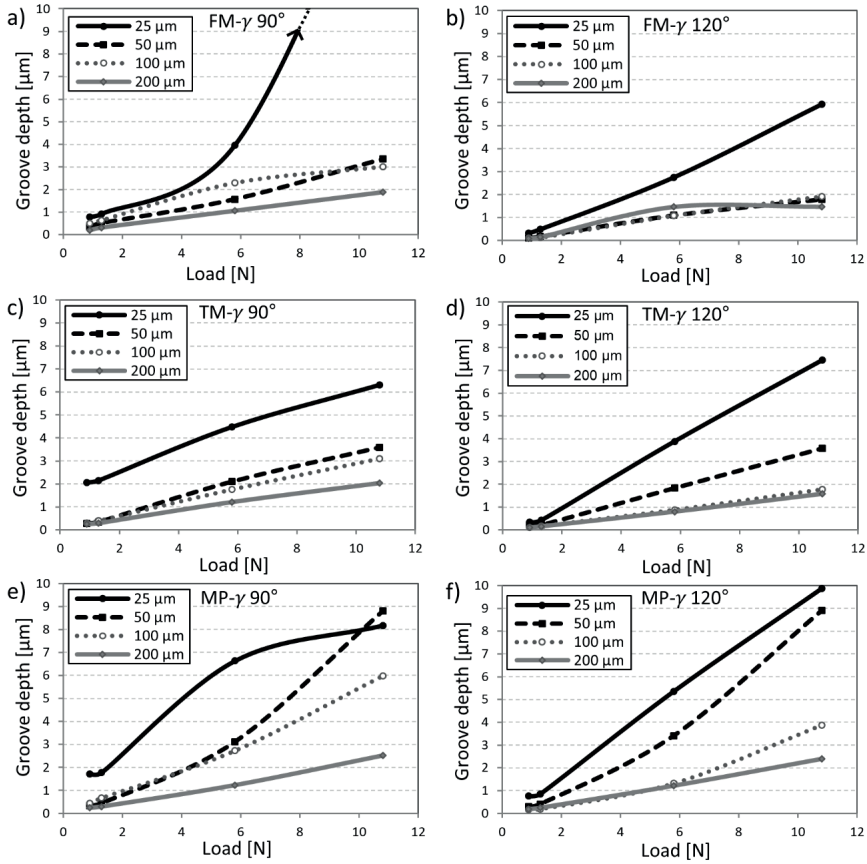


Figure 4-5 Groove depth [μm] as a function of the load (0.9 N, 1.3 N, 5.8 N, 10.8 N) and indenter tip radius (25 μm, 50 μm, 100 μm, 200 μm) in case of FM with cone angle 90° (a) and 120° (b), for TM with cone angle 90° (c) and 120° (d), and in case of MP with cone angle 90° (e) and 120° (f)

The occurring micro-mechanisms were associated with the hardness of the materials. From the investigation of Muttan and Watson [46], it is expected that the material with the lowest hardness (MP - 367 HV) may experience deeper scratches and hence a higher D_p , resulting in lower wear resistance. This phenomenon was evidenced in the present single-asperity test results. Increasing the cone angle of the indenter created deeper grooves, except for the fresh martensitic material. The deepest groove was made with the 25 μm tip radius indenter loaded with 10.8 N. MP steel resulted into the deepest scratches, which indicates higher D_p in case of same groove width.

4.4.3 Degree of penetration (Dp)

Dp was analysed for understanding the effect of operational parameters on the micro-mechanisms (Figure 4-6) during single asperity scratch test. According to literature [80] the region of the plots below $D_p \sim 0.1$ means that no material is removed, only plastic deformation of the material occurs. The zone between $D_p \sim 0.1 - 0.2$ represents wedge formation and transition zone to micro-cutting. Plot region above $D_p \sim 0.2$ indicates micro-cutting, with chip formation and wear of the material.

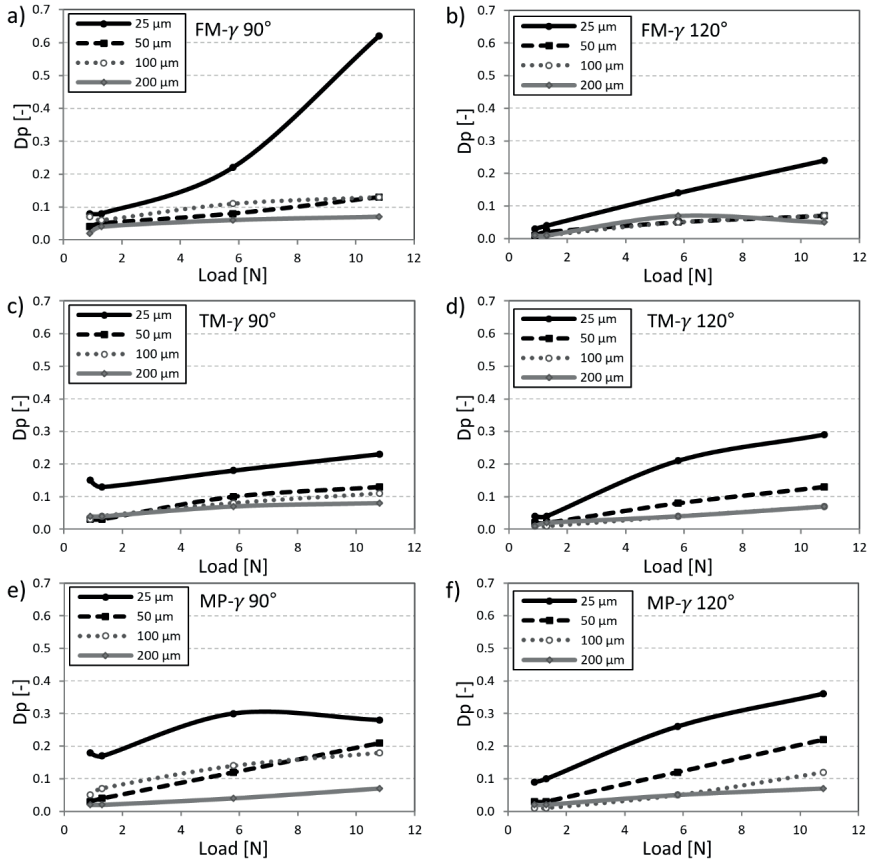


Figure 4-6 Dp [-] as a function of the load (0.9 N, 1.3 N, 5.8 N, 10.8 N) and indenter tip radius (25 μm , 50 μm , 100 μm , 200 μm) in case of FM with cone angle 90° (a) and 120° (b), for TM with cone angle 90° (c) and 120° (d), and in case of MP with cone angle 90° (e) and 120° (f)

The MP steel resulted into the highest Dp values, except for the test using 90° cone angle and 10.8 N load on the fresh martensitic material. Micro-cutting was observed in these cases (Dp higher than 0.2), verified with the on-line vision monitoring of chip formation. Testing with the same conditions and only increase in the cone angle did not always result into shallower scratches.

The low load test conditions (0.9 N, 1.3 N) with 25 μm tip radius resulted into Dp in the range of 0.03-0.18 [-], indicating micro-ploughing as micro-mechanism in case of all three steel grades. It is evident, that micro-ploughing regime was achieved using low loads: the material is plastically deformed and not removed. In case of lower load testing conditions (0.9 N, 1.3 N) and high indenter tip radius (100 μm , 200 μm), only the nose radius comes into effect because the wear depth is not sufficient for the cone angle to play a role due to the indenter geometry. Increasing the load to 5.8 N was followed by Dp transitioning into the range of 0.14-0.3 [-]. These values are in the transition zone of wedge-formation (edging) to micro-cutting. On increased load, the indenter engages deeper into the material and will introduce the formation of micro-cut grooves with higher Dp values. This can be seen in Figure 4-6 from the difference in Dp between tests made on all materials with 50 μm indenter tip radius with 1.3 N load and 10.8 N load, respectively. 10.8 N load tests with 25 μm tip radius resulted in micro-cutting in the Dp range of 0.24-0.62 [-]. Tests made with 25 μm tip radius and different loads conditions covered all three Dp regimes and micro-mechanisms by itself, which was not the case for tests performed with larger tip radius (50-100-200 μm). The tests performed with larger tip radius fell short of reaching the micro-cutting regime. The MP steel was prone to micro-cutting and hence showed the highest wear rate.

4.4.4 Parametric study, specific wear rate

The calculated specific wear rate for the tested materials during the single-asperity tests is shown in Table 4-2 and Table 4-3. The calculated standard deviation is less than 10%, larger standard deviation ($\sim 15\%$) was only found in some cases with 25 μm tip radius, where the high local stress concentration resulted in differences in the wear track dimensions. The values are shown for the largest and smallest tip radius with the highest and lowest load. With respect to the wear rate, the best performing material according to the single-asperity tests was the TM – tempered martensitic material, followed by FM – fresh martensitic and the least performing material is the MP – retained austenitic material. The wear rate difference between the martensitic and MP steel materials could be partly explained by the difference in hardness (Table 3-2). However, in case of FM and TM, the initial hardness difference of 13 HV is not explaining the inferior performance of FM compared to the TM material. This difference may be attributed to the tempering effect on the martensitic microstructure. In fact, when tempering is applied to the martensitic material, the density of fine transition carbides ($\sim 2\text{ nm}$) is typically increased and might contribute to the strengthening mechanisms [91]. Consequently, the material has an improved toughness while maintaining hardness and strength at a high level. According to a study from Chintha *et al.* [106], when comparing the behaviour of materials having the same hardness and microstructure but different toughness, the less tough will detach more materials due to abrasive

action. In Table 4-2 and Table 4-3, the colour shading indicates the wear performance: green is the best and red is the least performing material in the given conditions.

Table 4-2 Specific wear rate k [mm³/Nm] *10⁻³ of FM, TM and MP steel from single-asperity testing with 90° cone angle indenter [92]

Load [N]	Tip radius [μm]					
	25			200		
	FM	TM	MP	FM	TM	MP
0.9	1.95±0.230	1.51±0.248	2.73±0.496	1.03±0.009	0.85±0.007	1.31±0.010
10.8	33.4±2.820	19.2±1.752	30.1±3.921	5.42±0.623	4.52±0.764	13.3±1.226

Table 4-3 Specific wear rate k [mm³/Nm] *10⁻³ of FM, TM and MP steel from single-asperity testing with 120° cone angle indenter [92]

Load [N]	Tip radius [μm]					
	25			200		
	FM	TM	MP	FM	TM	MP
0.9	0.38±0.006	0.25±0.005	1.90±0.057	0.59±0.003	0.45±0.004	2.35±0.004
10.8	9.16±0.925	9.65±0.351	14.6±0.685	5.17±0.727	2.77±0.215	7.88±0.056

4.4.5 Multiple linear regression models and sensitivity analysis

This section describes the significance and contributions of test parameters, the material’s mechanical properties (hardness H , ultimate tensile strength σ_M , yield strength σ_Y , Young’s modulus E , uniform elongation ϵ_M , fracture elongation ϵ_B , Charpy ISO 148-1 W , compressive strength σ_c , compressive modulus E_c) and the dimensionless numbers formed from them for the wear behaviour and the surface deformation. Large amounts of measured tribo data were processed by multiple linear regression models using IBM SPSS 25 software. The abrasive sensitivity of wear performance and the change of 3D surface topography to material properties and to test system characteristics was investigated. The sensitivity of the tested materials to abrasion was evaluated taking into account the wide range of influencing parameters, such as the properties of the examined steels (Table 3-2) and some dimensionless numbers formed from these properties (Table 4-4).

Table 4-4 Dimensionless numbers formed from material properties [93]

$\frac{H}{E}$	ratio between hardness and elasticity modulus
$\frac{\sigma_M}{\sigma_Y}$	ratio between ultimate tensile strength/yield strength
$\frac{\varepsilon_B}{\varepsilon_M}$	ratio between fracture elongation/elongation at maximum tensile load
$\frac{W_{(20)}}{W_{(-40)}} = W$	ratio between Charpy impact strength at 20 °C/Charpy impact strength at -40 °C
$\frac{\sigma_Y E}{\sigma_M H}$	ratio between combined tensile performance/combined bulk-surface stiffness
$\frac{E_c}{\sigma_c}$	ratio between compression modulus/compression strength
$\frac{H \varepsilon_B}{\sigma_Y}$	ratio between combined Hardness-strain capability/yield strength
$\frac{\sigma_Y}{\sigma_c \varepsilon_B}$	ratio between yield strength/combined compression—strain capability
$\frac{WEH}{\sigma_M \sigma_Y}$	ratio between combined Charpy ratio and strain capability/combined tensile strength
$\frac{W}{\varepsilon_B}$	ratio between Charpy impact strength ratio/fracture elongation
$\frac{W \sigma_Y}{E}$	multiplication of combined Charpy impact strength ratio and elastic tensile behaviour

The statistical analysis relies on multiple linear regression models. Such models are useful if one examines how a dependent variable depends on several independent variables simultaneously, assuming that the dependence is (approximately) linear. Let n be the number of independent variables then the formulation of such model is

$$Y = a_0 + a_1 X_1 + a_2 X_2 + \dots + a_n X_n, \quad (3.6)$$

where Y is the dependent variable and X_1, X_2, \dots, X_n are the independent variables. The method of least squares is the most common way to fit such a model to the measured data. First, an F test was always carried out to see whether the corresponding model was relevant. If the p-value was less than 0.05, that is, it was significant, then the model was relevant. Usually, the R^2 value measures the goodness-of-fit of such a linear model, i.e., it shows how much of the variance of the dependent variable may be explained by the independent variables. If $p < 0.05$ holds for coefficient a_k ($k \in \{0, 1, \dots, n\}$), then it is statistically different from 0, and thus, the corresponding independent variable X_k plays a role in describing the dependence of Y . In the discussed models, only the explanatory variables are included for which their associated coefficient turned out to be significant. To see which independent variable had the greatest effect on Y , one must consider the absolute value of the standardized (or beta) coefficients of the significant independent variables; the higher this value is, the greater the effect.

Among the possible methods of entering variables into a linear regression model, the stepwise method was used. This means that at each step of the model building algorithm, among the possible, significant independent variables, the one which caused the highest change in R^2 was entered. The algorithm ended when there were no new independent variables to enter. In some cases of the below presented models, not all significant variables were included; e.g., those causing very low change in R^2 were neglected. It is important to mention that one of the assumptions of the applicability of multiple linear regression is that the independent variables are not collinear. Since many of the parameters of the studied materials have high correlation coefficients with another parameter, not all of them were used in the models at the same time. A more detailed description of such models in material science can be found [29]. The statistical evaluation of the models was carried out by using IBM SPSS 25, using the stepwise method to enter a new variable into a specific linear regression model.

The test conditions (load, indenter cone angle, indenter tip radius, material) influenced the transition between the different micro-mechanisms. In order to investigate the dependence of scratch characteristics on the material properties and test system characteristics, multiple linear regression models were constructed. In these models, the independent variables coming from test systems were the cone angle γ , the load F_N , and the tip radius r . Further independent variables were the material properties and the dimensionless indicators formed from them. In equation (3.6) the dependent variable Y is the scratch width, and the independent variables X_1, X_2, \dots are the previously mentioned ones. According to this, the best fitting of all models (using the method of least squares) for the scratch width was

$$2w = a_0 + a_1 F_N + a_2 \frac{W \cdot \sigma_y}{E} \quad (3.7)$$

The model turned out to be statistically relevant, that is, it significantly differs from a constant function, since the F-value was 377 and $p < 0.001$. The obtained coefficients a_0 , a_1 and a_2 of the respective independent variables are presented in Table 4-5 (see the second column).

Table 4-5 Coefficients of the regression model for scratch width in single-asperity test [93]

Model	Coefficient	Standardized Regression Coefficient, Beta	t	p
Constant	11.019	-	7.594	<0.001
F_N	3.898	0.922	26.829	<0.001
$\frac{W\sigma_y}{E}$	383	0.202	5.871	<0.001

The model with the specific coefficients takes the form

$$2w = 11.019 + 3.898 F_N + 383 \frac{W \cdot \sigma_y}{E}. \quad (3.8)$$

For this model, the goodness-of-fit is $R^2 = 0.89$. The load has the highest effect on the scratch width, while among the material parameters e.g., $(W\sigma_y/E)$ has some effect, this can be seen from the extent and the ranking of the absolute value of the Beta-coefficients.

The best fitting model of the possible ones for the scratch depth was

$$h = a_0 + a_1F_N + a_2r + a_3\sigma_c \tag{3.9}$$

The model is relevant ($F = 43$ and $p < 0.001$). Table 4-6 summarizes the coefficients of the model.

Table 4-6 Coefficients of the regression model for scratch depth in single-asperity test [93]

Model	Coefficient	Standardized Regression Coefficient, Beta	t	p
Constant	5.951	-	2.932	<0.001
F_N	0.448	0.662	9.867	<0.001
r	-0.014	-0.350	-5.215	<0.001
σ_c	-0.003	-0.157	-2.344	<0.001

For this model, the goodness-of-fit is $R^2 = 0.572$. The load has the highest effect on the scratch depth, followed by the tip radius, while among the material parameters e.g., σ_c has some effect.

The best fitting model of the possible ones for the Dp was

$$Dp = a_0 + a_1F_N + a_2r + a_3\gamma, \tag{3.10}$$

which turned out to be relevant ($F = 35$ and $p < 0.001$). The coefficients of the model are summarized in Table 4-7.

Table 4-7 Coefficients of the regression model for Dp in single-asperity scratch test [93]

Model	Coefficient	Standardized Regression Coefficient, Beta	t	p
Constant	0.213	-	4.384	<0.001
F_N	0.013	0.545	7.647	<0.001
r	-0.001	-0.448	-6.289	<0.001
γ	-0.001	-0.188	-2.633	<0.001

For this model, the goodness-of-fit is $R^2 = 0.533$. The load has the highest effect on the Dp, followed by the tip radius and the cone angle. This confirms the results from Figure 4-6.

The best fitting model of the possible ones for the groove area (A_g) was

$$A_g = a_0 + a_1F_N + a_2r + a_3E_c, \tag{3.11}$$

the model is relevant since $F = 51$ and $p < 0.001$. The coefficients of model (3.11) are presented in Table 4-8.

Table 4-8 Coefficients of the regression model for groove area for single-asperity scratch test [93]

Model	Coefficient	Standardized Regression Coefficient, Beta	t	p
Constant	185.217	-	3.961	<0.001
F_N	19.837	0.693	10.813	<0.001
r	-0.513	-0.300	-4.675	<0.001
E_c	-0.002	-0.229	-3.575	<0.001

For this model, the goodness-of-fit is $R^2 = 0.622$. The normal load has the highest effect on the groove area, followed by the tip radius. Among the material parameters E_c has some effect.

For the resulting wear, multiple linear regression models were constructed to see the sensitivity of material properties and test system characteristics on it. In the test systems, the sliding distance s , the load F_N , the tip radius r , and the cone angle γ were considered as independent variables, as well as the material properties and the indicators formed from them. According to this, the best fitting model of the possible ones for the wear volume was

$$V_g - V_s = a_0 + a_1 F_N + a_2 s + a_3 \frac{WEH}{\sigma_M \sigma_Y} + a_4 r \quad (3.12)$$

The model is relevant (the F-value was 57 and $p < 0.001$). The coefficients of the model are presented in Table 4-9.

Table 4-9 Coefficients of the regression model for groove volume in single-asperity scratch test [93]

Model	Coefficient	Standardized Regression Coefficient, Beta	t	p
Constant	-90251.994		-5.305	<0.001
F_N	16474.646	0.459	11.292	<0.001
s	38.693	0.300	7.389	<0.001
$\frac{WEH}{\sigma_M \sigma_Y}$	30.409	0.213	5.248	<0.001
r	-361.825	-0.168	-4.142	<0.001

For this model, the goodness-of-fit is $R^2 = 0.374$. The load has the highest effect on the wear volume, followed by the sliding distance. In this case, the dominant influence of the load on the material loss confirms previous literature findings [38]. Among the material parameters the $(WEH/\sigma_M \sigma_Y)$ has some effect.

Figure 4-7 shows the wear values obtained with the highest load and indenter tip radius (10.8 N with 200 μm) as a function of dimensionless numbers composed from material property parameters. This offers an indication of the effect of the derived factors on the wear trend for each material. Proportional relations were found between the wear and $(WEH/\sigma_M \sigma_Y)$, as well as $(W\sigma_M/E)$. Increased material loss was observed by rising these dimensionless number values. In the case of $(\sigma_c \varepsilon_B/\sigma_M)$ and $(H\varepsilon_B/\sigma_Y)$ a similar trend was found. Inverse relations were established between values (H/E) , $(\sigma_Y/\sigma_c \varepsilon_B)$, $(\varepsilon_B/\varepsilon_M)$, (E_c/σ_c) and the wear of the tested steels.

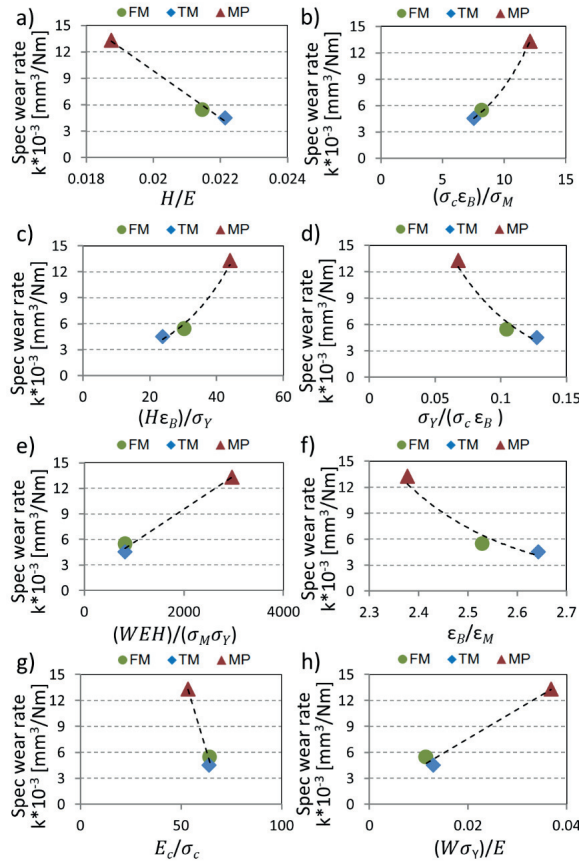



Figure 4-7 Wear obtained with highest load and indenter tip radius (10.8 N with 200 μm) in the function of dimensionless features: (a) $\frac{H}{E}$, (b) $\frac{\sigma_c \epsilon_B}{\sigma_M}$, (c) $\frac{H \epsilon_B}{\sigma_Y}$, (d) $\frac{\sigma_Y}{\sigma_c \epsilon_B}$, (e) $\frac{WEH}{\sigma_M \sigma_Y}$, (f) $\frac{\epsilon_B}{\epsilon_M}$, (g) $\frac{E_c}{\sigma_c}$, (h) $\frac{W \sigma_M}{E}$ derived from the mechanical properties

Based on the above discussed linear models, Table 4-10 summarizes the abrasive sensitivity for the resulted scratch characteristics (width, depth, degree of penetration, groove area, and volume). The factors are in increasing order of effect. The abrasive sensitivity is the extent how the independent variables (test variables and material properties and indicators formed from them) affect a dependent variable (e.g., wear) which is related to the standardized regression coefficients. Therefore, the higher the absolute value of the corresponding standardized regression coefficient is, the higher the abrasive sensitivity of the dependent variable is (wear, groove characteristics) with respect to the independent variable.

Table 4-10 Abrasive sensitivity ranking to single-asperity scratch system variables [93]

Effect of influencing factors 	F_N	F_N	F_N	F_N	F_N
		r	r	r	s
	$\frac{W\sigma_y}{E}$	σ_c	γ	E_c	$\frac{WEH}{\sigma_M\sigma_Y}$
					R
Independent variable	$2w$	h	Dp	A_g	V_g-V_s

4.4.6 Coupling to material properties

The MP steel was prone to micro-cutting and hence showed the highest wear rate (Table 4-11).

Table 4-11 Connection of material properties with wear characteristics from single-asperity testing [92]

Material	Specific wear rate, k [mm ³ /N m]	Hardness [HV]	Retained austenite fraction (m%)	Grain area with highest relative volume [μm ²]	Yield strength [MPa]
FM	0.003866	478	< 2	4	1290
TM	0.002955	465	< 2	15	1413
MP	0.004884	367	12.5	19	791

In this case, the austenite-to-martensite transformation does not seem to enhance the material's wear resistance. At this single contact condition, wear seems to be predominantly driven by the initial hardness and TRIP effect may not be high enough to enable the material to resist better to the shearing load resulting in micro-cutting. On the other hand, the low-temperature-tempered material (TM) exhibits higher wear resistance than the fresh martensite grade (FM), although the hardness level is slightly lower. The TM material has clearly higher toughness than the FM grade leading to an improved crack-resistance during the chipping mechanism while scratching [107], [108]. According to Chintha [109], as the hardness of the base steel increases, or loading conditions change, the wear damage mechanism changes from ductile to brittle. Increasing the base hardness perhaps reduces the ability to dissipate penetration energy, and the depth of deformation also decreases. Hence, the improved surface hardness limits the indentation resulting in less energy dissipation into the material. In case of materials with same hardness but different toughness (strain/deformation capability), the less tough tends to suffer micro-cutting wear with minimal deformation due to abrasive action. This results in higher wear because the deformation of the indentation environment is minimal and high portion of the energy is consumed in crack initiation. This means, an ability to spread deformation to a greater depth can increase the wear resistance at a given hardness. Hence, toughness should play a role by delaying microscopic fracture events. Retained austenite may help in increasing toughness so further

studies should compare fully martensitic and retained austenite containing microstructures with similar hardness levels.

4.5 Conclusions from single-asperity scratch testing

The wear micro-mechanisms were replicated in the micro-level (single asperity) wear testing. The increase of the load resulted in a transition from micro-ploughing to micro-cutting in case of single-asperity test. Using smaller tip radius (abrasive size) resulted in a similar effect. The highest wear rate was obtained with the highest testing load (10.8 N) using a 25 μm tip radius indenter resulting in the highest local stress state. The martensitic materials with higher hardness reached micro-cutting regime in a more narrow range of testing conditions. Despite the similar microstructure and hardness, based on the abrasion wear rate value k , the tempered martensitic TM material structure enabled smaller micro-cutting wear due to a good combination of initial hardness/strength and toughness, while the fresh martensitic structure resulted in 30% higher wear. Micro-cutting was observed at 90/120° cone angle and 25 μm particle size with 10.8 N load. It was confirmed that toughness/ductility does play a role in wear resistance (e.g. FM vs TM) but it has to be combined with sufficient hardness depending on the wear mechanism. Proportional relations between the wear values of the materials and the dimensionless numbers of $(WEH/\sigma_M\sigma_Y)$, as well as $(W\sigma_M/E)$ were established in case of testing with the highest load and indenter tip radius (10.8 N with 200 μm). There are reciprocal relations between the values of ratio between hardness and elasticity modulus (H/E), the ratio between yield strength/combined compression—strain capability ($\sigma_Y/\sigma_C\epsilon_B$), ratio between fracture elongation/elongation at maximum tensile load (ϵ_B/ϵ_M), and the ratio between compression modulus/compression strength (E_C/σ_C) and the wear of materials. Increasing these dimensionless number values resulted in lower wear.

5 CHAPTER 5

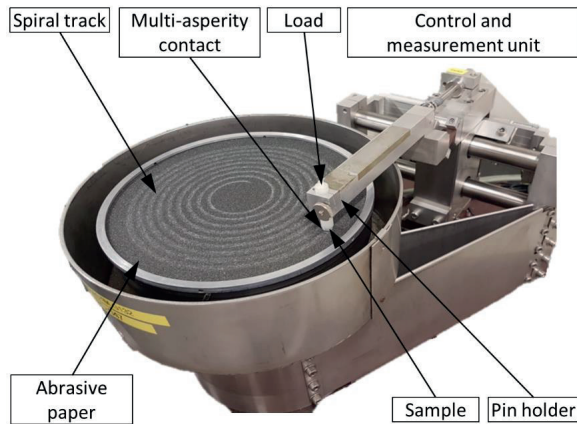
MACRO LEVEL MULTI-ASPERITY CONTACT ABRASION INVESTIGATION

This chapter summarizes the results obtained from multi-asperity pin abrasion tests representing the macro-level wear investigation.

The following articles were published based on this chapter:

Á. Kalácska, P. De Baets, H. Ben Hamouda, K. Theuwissen, and J. Sukumaran, "Tribological investigation of abrasion resistant steels with martensitic and retained austenitic microstructure in single- and multi-asperity contact," *Wear*, vol. 482–483, p. 203980, Oct. 2021, doi: 10.1016/j.wear.2021.203980.

Á. Kalácska, L. Székely, R. Z. Keresztes, A. Gábora, T. Mankovits, and P. De Baets, "Abrasive Sensitivity of Martensitic and a Multi-Phase Steels under Different Abrasive Conditions," *Materials*, vol. 14, no. 6, p. 1343, Mar. 2021, doi: 10.3390/ma14061343.



5.1 Introduction

Abouei [110] investigated the percentage of martensite following intercritical annealing of dual-phase steel at 780°C for 6.5, 7.5, 9, and 20 minutes followed by water quenching. Dry sliding wear tests using pin-on-disk apparatus showed that for various applied loads increasing the martensite volume percentage decreased the wear rate. Generally, the wear performance is correlated to the hardness of the material. Nevertheless, a large number of wear mechanisms are determined by material properties other than hardness. It was concluded, that from a material and microstructural perspective, abrasive wear performance can be improved by enhancing fatigue strength and heterogeneous microstructure apart from hardness [111]. For that reason, in order to control them, it is important to understand the properties and microstructure of materials contributing to wear resistance.

It is evident from the literature review that there are multiple input variables contributing to alter the wear micro-mechanism. From the view point of soil tillage application, the nature of contact (three-body abrasion) is pre-defined and in the tillage application a low stress abrasion test is most appropriate. Existing standards, e.g. ASTM G132, on low stress open three body abrasion provide a guideline for limiting the other input variables for operational, environmental and material characteristics.

Standard wear tests are primarily designed to rank the materials based on their wear resistance. The wear mechanisms and the corresponding micro-mechanisms derived from these tests acts as additional information to study the wear process and to understand the fundamentals of material loss. Different types of wear testers are used for experimentally simulating the low stress open three body abrasion [11], [13], [112]. The classical ASTM G65 'Standard test method for measuring abrasion using the dry sand/rubber wheel apparatus' is widely used [12], [113]–[118]. Considering the unsatisfactory results from the lab-scale testing, wear tests are also performed in real scale components [61], [66], [119], [120] but also at intermediate scale [61], [121]. The latter are rather expensive and may have uncertainties from the inhomogeneity of soil compaction and environmental conditions. Though ASTM G65 standard is widely used, unsatisfactory results were reported for experimental simulation of the abrasive wear of tillage tools [12]. Some factors considered for unsatisfactory performance are the (1) poor repeatability, (2) unreliable results and (3) poor representativeness for the real application. It is also possible that there is a difference in micro-mechanism between the real application and the corresponding lab scale test, leading to unsatisfactory test results. Tillage tools subjected to low stress abrasive wear are usually made of carbon steel or low-alloy steel. Since their abrasive wear resistance is dependent on the tribological system, it also depends on the soil conditions and not only on the intrinsic conditions of the material. The influential factors are the chemical composition, production history, mechanical properties and microstructure of the material; the particle shape, size, the soil strength, density and moisture, and rock and gravel content; the relative velocity and impact angle

between soil and the tool. Thus, there is no simple relationship between the abrasive wear resistance and the material's common mechanical properties alone. For the same reason, the ASTM dry sand/rubber wheel test, the most commonly used test for abrasive wear, is not entirely satisfactory for determining the abrasive wear characteristics experienced by tillage tools [12]. The worn surface features of the specimen subjected to a pin-on-abrasive disk test are more representative for field tests, as concluded by Swanson [68].

5.2 Experimental procedure

The same materials as introduced in Chapter 3 have been used for this investigation. ASTM G132 tests were used for multi-asperity testing. The test rig set-up is shown in Figure 5-1.

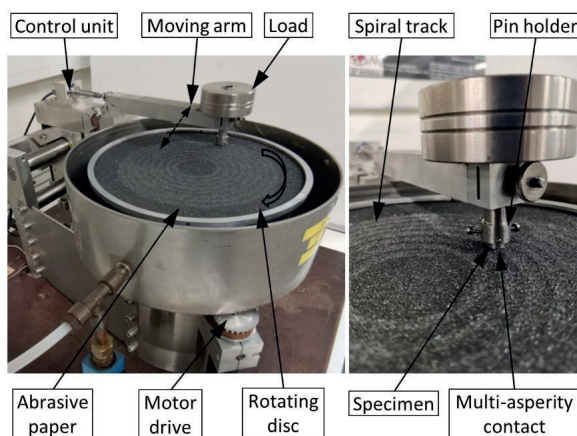


Figure 5-1 Abrasive pin-on-disk testing set-up [93]

The cylindrical pin specimens (5 mm length and 8 mm diameter) for ASTM G132 multi-asperity tests were laser cut from steel sheets. The contact surface of the samples was pre-grounded and subsequently polished. Pre-grinding was performed using P80 abrasive paper for a sliding distance of 3 m at a load of 11.4 N. The same procedure was then repeated with a P800 abrasive paper for polishing. The procedure resulted in a unidirectional polished surface. After an ultrasonic cleaning and drying of the samples at room temperature, 2D surface roughness measurements were performed using a diamond stylus profilometer (Hommel Somicronic Surfacan) with a 2 μm tip radius perpendicular to the polished surface pattern. The investigation confirmed that an adequate surface roughness for the wear testing of R_a 0.3 μm was achieved, next to an average R_z 2.8 μm and R_q 0.5 μm and R_t 3.2 μm . An electronic scale with an accuracy of 0.1 mg was used to weigh the samples before and after wear testing. The specimen height dimension was also measured using a digital calliper with 0.01 mm accuracy. All measurements were performed 5 times per specimen and subsequently averaged.

The surface morphology of the specimen was investigated before and after the experiment. After the wear test, the 3D contact surface topography was extracted using a non-contact optical (white light) profilometer (Keyence VR 5200 microscope). A magnification lens of 20x resulted in a sample area of 0.8 mm x 0.8 mm. Microscopic and macroscopic images of the contact surface of the specimen were made. After the investigation of the worn surface, the samples (pins) were cut in half for cross-sectional studies. The half samples were warm embedded in epoxy and the cross-section surface was polished prior to SEM analyses and micro-hardness measurements. The Vickers hardness was measured on a LECO LV 100AT device with a diamond indenter using 2.94 N applied normal force in the cross-section at 20 different locations starting from the contact surface and moving into the subsurface direction. In the multi-asperity testing, a constant relative sliding velocity of 100 mm/s was used for a sliding distance of 9 m. A spiral wear track ensured that the contact surface always interacts with fresh abrasives. These parameters meet the requirements of the ASTM G132 – 96(2013) standard test method for pin abrasion testing apart from the load [122], where the suggested contact pressure is ~1 MPa higher. The pins were mounted in the test rig in such a way that the same rolling direction (from the manufacturing of sheets) was ensured for the contact with the abrasive. Three repetitions were made for extreme and intermediate test conditions, which covered the highest and lowest load as well as the smallest and largest abrasive particle sizes (Table 5-1). Four levels of loading were used leading to a contact pressure of 0.09 to 0.48 MPa on different abrasive papers. Environmental parameters measured during the testing: 21.4-22.8 °C temperature and 48-54% relative humidity.

Table 5-1 Multi-asperity test matrix and number of repetitions [92]

Counterface		Load [N]			
Abrasive paper	Grit size [μm]	4.5	11.4	17.3	24.2
P800	22 μm	3	1	1	3
P180	82 μm	1	3	1	1
P120	125 μm	1	1	3	1
P80	200 μm	3	1	1	3

5.3 Parameters influencing wear micro-mechanisms in multi-asperity contact testing

For the multi-asperity contact investigation, two parameters were changed during the testing: normal load and abrasive paper type (particle size). The effect of the abrasive particle size and attack angle was already published [42], [123]. A parameter that combines the effect of the overall size and sharpness of an abrasive particle and quantifies this effect is the ‘spike value’ [124]. This value refers to both the sharpness and the size of the particle. Different abrasive papers are used to represent different attack angle. Four different types of SiC abrasive papers were used [125]; their characteristics are shown in Table 5-2.

Table 5-2 Characteristics of abrasive papers used for multi-asperity tests [92] [126]

Abrasive paper	P800	P180	P120	P80
Abrasive particle size [μm]	22	82	125	200
Average apex angle δ [$^\circ$]	90	111	117	125
Average attack angle α [$^\circ$]	45	35	32	28

Two variables which can influence the wear micro-mechanisms are the load and the attack angle. The influence of the attack angle on the wear behaviour is shown in Figure 5-2. Particles from P800 abrasive sheet have smaller tip radius and apex angle than P80 particles. A higher attack angle promotes micro-cutting as a mechanism. The P80 particle has a larger apex angle (hence lower attack angle) and tip radius, thus promoting micro-ploughing. Larger tip size evidences sufficient free space between the abrasives and allows the test material to plastically flow around the abrasives. It was concluded [38] that the load has a significant influence on the predominant wear mechanism. In the present research the test conditions for the multi-asperity testing are set in order to study the influence of load, attack angle and abrasive particle size for all the three different steel grades.

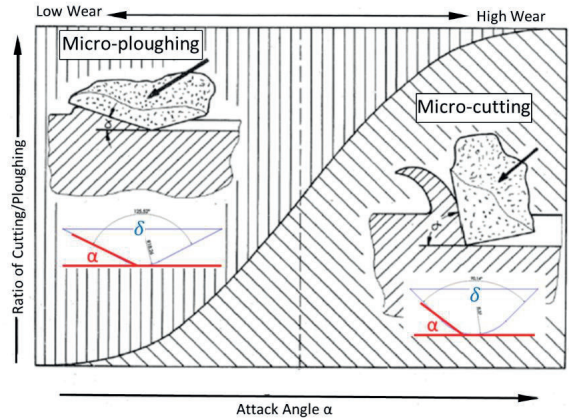


Figure 5-2 Influence of attack angle on wear behavior [10][92]

5.4 Results of pin-on-disk testing

5.4.1 Surface characterization and wear modes

During the multi-asperity test the specimen does not rotate around its axis and hence the scratch marks are oriented in one direction as seen in Figure 5-3. The worn surfaces of all specimens appear to be less shiny than the original surface due to the roughening of the surface. The images show a clear difference in the surface roughness for specimen subjected to lower and higher load and increasing abrasive grit size during the wear testing. The above observations are also in good agreement with the microscopy investigation.

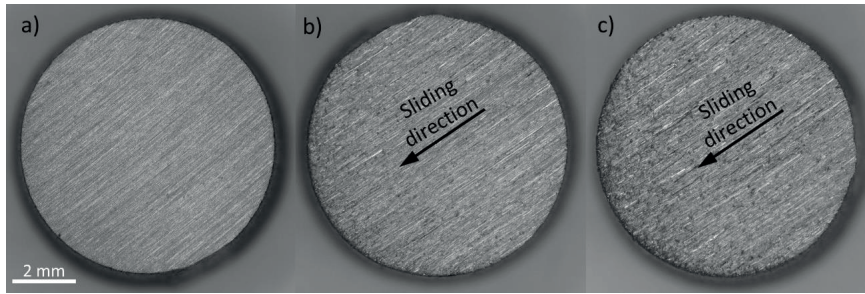


Figure 5-3 Macroscopic images from material FM samples a) polished surface before wear testing, after test with 11.4 N, P120 (b) and with 17.3 N load and P80 abrasive paper (c)

Investigating the contact surface with microscopy revealed the differences between samples tested at low (4.6 N) and high load (24.2 N) conditions (Figure 5-4). Higher load testing resulted in more significant surface deformation of the materials. Traces of local plastic deformation, less uniform scratches with wedge formation may be observed as characteristic features of micro-ploughing as a predominant wear micro-mechanism. However, more severe grooves were also identified with leftover/embedded chip covering the contact surface. In the case of lower loads, a more uniform worn surface is observed with clearly oriented shallow grooves. Especially the FM and MP materials show clear characteristics of micro-cutting. In case of the tempered martensitic material, the traces are not so predominant (Figure 5-4).

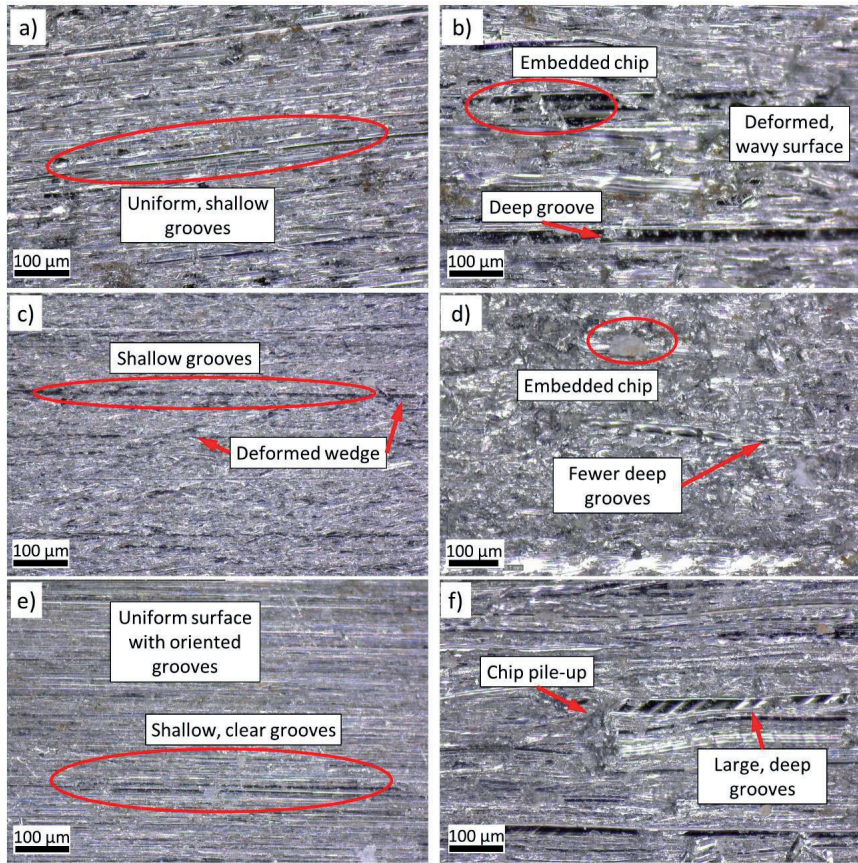


Figure 5-4 Worn surface microscopic images of multi-asperity tested samples a) FM 4.6 N, P800 b) FM 24.2 N, P80 c) TM 4.6 N, P800, d) TM 24.2 N P80, e) MP 4.6 N P800, f) MP 24.2 N, P80

5.4.2 Mass loss

The mass loss [mg] as a function of the sliding distance for the tested materials during the multi-asperity tests is shown in Figure 5-5. Increasing the load and the abrading particle size resulted in more severe wear. As reported in the literature [81], [127], the slope of the wear curves increases with the abrasive size up to a critical particle size (CPS). Upon entering this critical size range, the wear behaviour may change [42]. This was confirmed in the tests with MP material, where a shift in wear rate was evident above 82 μm abrasive particle size (Figure 5-5i–l). The wear rate stabilized for the MP material in case of these conditions. The effect of the load was found to be more straightforward. Testing with higher load was always followed by more severe material loss. The role of particle size and attack angle was already reported in [123]. “Spike value” was introduced as a quantitative feature that takes the sharpness and size of the particle into consideration [124]. With the smaller average particle size of

the P800 a lower material removal than on a P80 paper would be expected. However, the higher attack angle of the embedded P800 particles due to their smaller tip radius mitigates this effect. Generally, higher attack angles enhance the micro-cutting process.

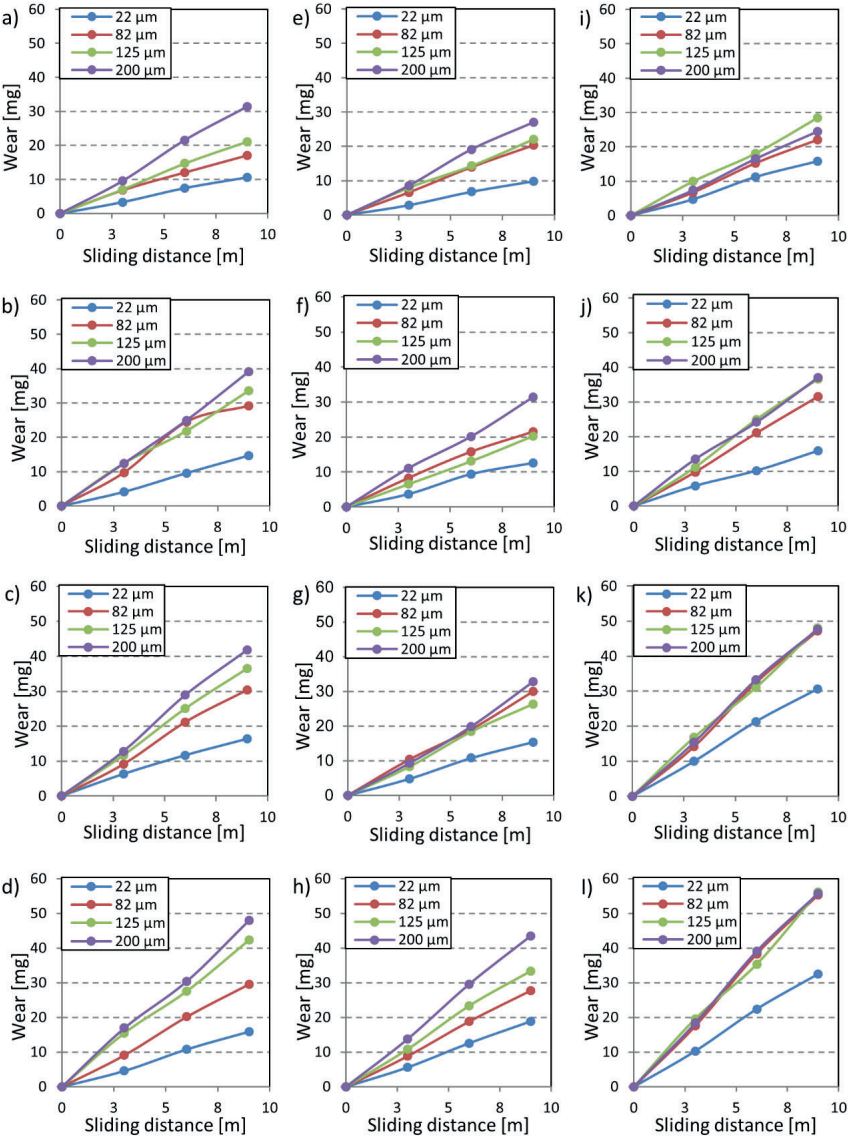


Figure 5-5 Wear [mg] in function of sliding distance for different abrasive particle sizes (P800 - 22 μm, P180 - 82 μm, P120 - 125 μm, P80 - 200 μm) and increasing load (4.5 N, 11.2 N, 17.4 N, 24.2 N) for material FM (a–d), material TM (e–h), and MP steel (i–l) [93]

Figure 5-6 shows the most severe wear condition values as a function of dimensionless numbers composed from material property parameters. This offers an indication of the effect of the derived factors on the wear trend for each material. Proportional relations were found between the material loss and (σ_M/σ_Y) , as well as $(H\varepsilon_B/\sigma_Y)$. Increased wear was observed by rising these dimensionless number values. In the case of and $(WEH/\sigma_M\sigma_Y)$ and $(W\sigma_Y/E)$ a similar trend was found. Inverse relations were established between values (H/E) , $(\sigma_Y/\sigma_c\varepsilon_B)$, $(\varepsilon_B/\varepsilon_M)$, (E_c/σ_c) and the wear of the tested steels.

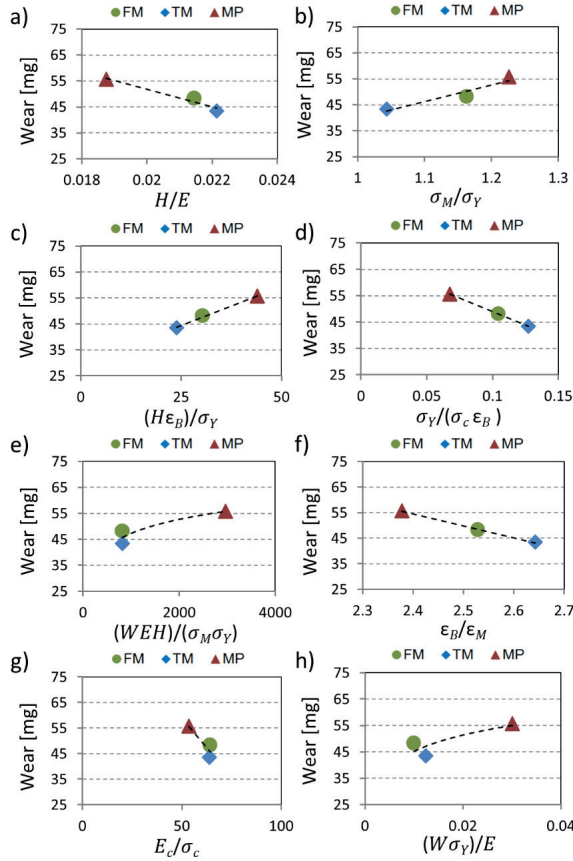


Figure 5-6 Wear of the most severe test condition (P80, 24.2 N) in the function of dimensionless features: (a) $\frac{H}{E}$, (b) $\frac{\sigma_M}{\sigma_Y}$, (c) $\frac{H\varepsilon_B}{\sigma_Y}$, (d) $\frac{\sigma_Y}{\sigma_c\varepsilon_B}$, (e) $\frac{WEH}{\sigma_M\sigma_Y}$, (f) $\frac{\varepsilon_B}{\varepsilon_M}$, (g) $\frac{E_c}{\sigma_c}$, (h) $\frac{W\sigma_Y}{E}$ derived from the mechanical properties [93]

5.4.3 Parametric study and wear rate

The wear rate was calculated by normalizing the mass loss with load and sliding distance. In the present investigation, the trend in wear rate is in good agreement with the literature [127] (Figure 5-7-a). For small abrasives, the wear rate increases proportionally with the increase in the abrasive particle size until it reaches the critical particle size (CPS). Beyond the CPS, the tendency of wear rate may change, and the wear rate can increase at a lower rate (curve 1), it can also become constant, independent of further abrasive size increases (curve 2), or it can exhibit a decreasing rate (curve 3). Though this behaviour has been previously explained by many hypotheses [37], [42], [128]–[131] there is no generalized explanation for all abrasive wear settings.

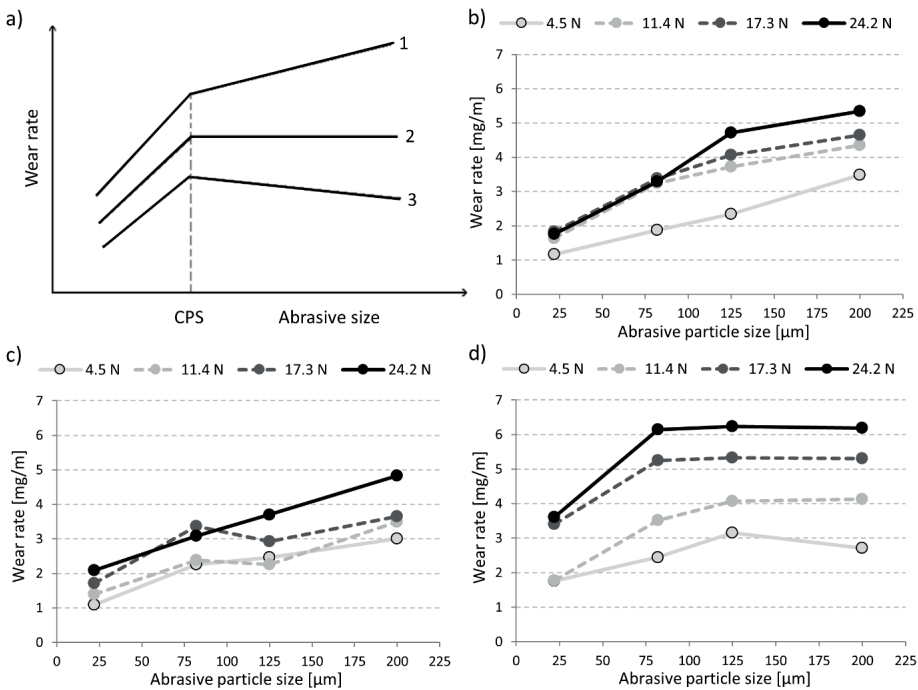


Figure 5-7 Schematic representation showing the typical curves of wear vs abrasive grain size [81] b) Wear rate [mg/m] of FM steel in function of grit size [μm] c) Wear rate [mg/m] of TM steel in function of grit size d) Wear rate [mg/m] of MP steel in the function of grit size [92]

The effect of abrasive size on metallic materials was investigated using two-body configuration on quenched and tempered cast irons with different percentages of retained austenite, aluminium and AISI 1045 steel [81]. It was found that for small abrasive particles, the wear mass loss increased linearly with the increase of particle size. For higher abrasive sizes, the mass loss increased much more slowly. It was concluded that the critical abrasive size is related to the wear micro-mechanisms and the microchip morphology. Figure 5-7-b-c-d shows the wear rate as a function of the abrasive particle size

for all three materials. The standard deviation shows less than 10% for all the tests. The average CPS values in literature are around 100 μm [43] for SiC abrasive, however, the value depends on the material grade. In case of our tests, the CPS value is around 80 μm for all investigated materials, as seen from the trend change after 75 μm .

This was further confirmed from the Dp investigation. The different micro-mechanism regimes –shown with Dp- obtained during the tests for all materials in function of counterface abrasive size are presented in Figure 5-8. The Dp was calculated as described in equation 2.1. The chart serves as an indicator to quantify the dominant wear micro-mechanisms identified from the worn surfaces.

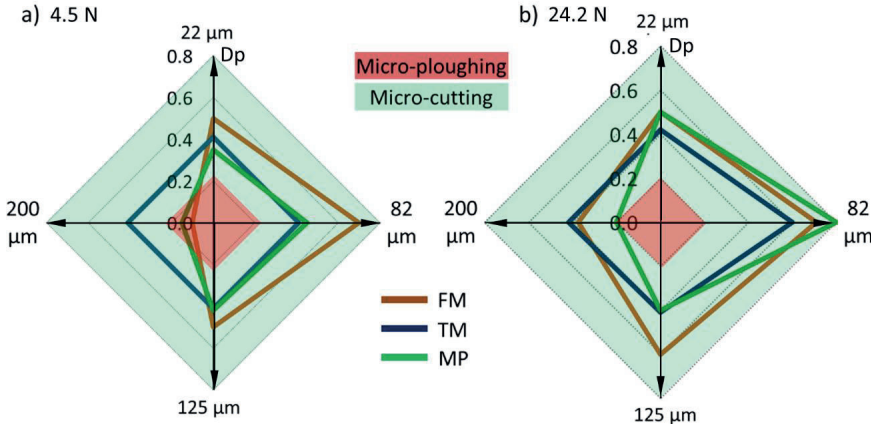


Figure 5-8 Dp and micro-mechanism regimes of FM, TM, MP materials obtained from multi-asperity testing in function of abrasive particle size

It is evident, that micro-ploughing regime was achieved using low loads and 200 μm abrasive size and hence material is plastically deformed and not removed in this case. At low contact pressures, the spherical part of the tip comes into contact with the worn surface. This results in low attack angles, leading to the micro-ploughing regime. P180 tests (82 μm abrasive particle size) resulted with highest Dp in both load condition, where the critical particle size threshold is reached. Increasing the load resulted in bit higher micro-cut Dp values in all cases. The wear severity is influenced by the load condition, hence the specific wear rate was calculated by normalizing the mass loss with the sliding distance and the load. It offers another option for evaluating the test results to understand the influence of the load. Comparing with the wear rate [mg/m] it is clear that specific wear is highest with low load (4.5 N) condition tests. Increased load results in decrease of the specific wear rate. However, the absolute wear results differ and in the following the wear rate will be used for comparison between the materials.

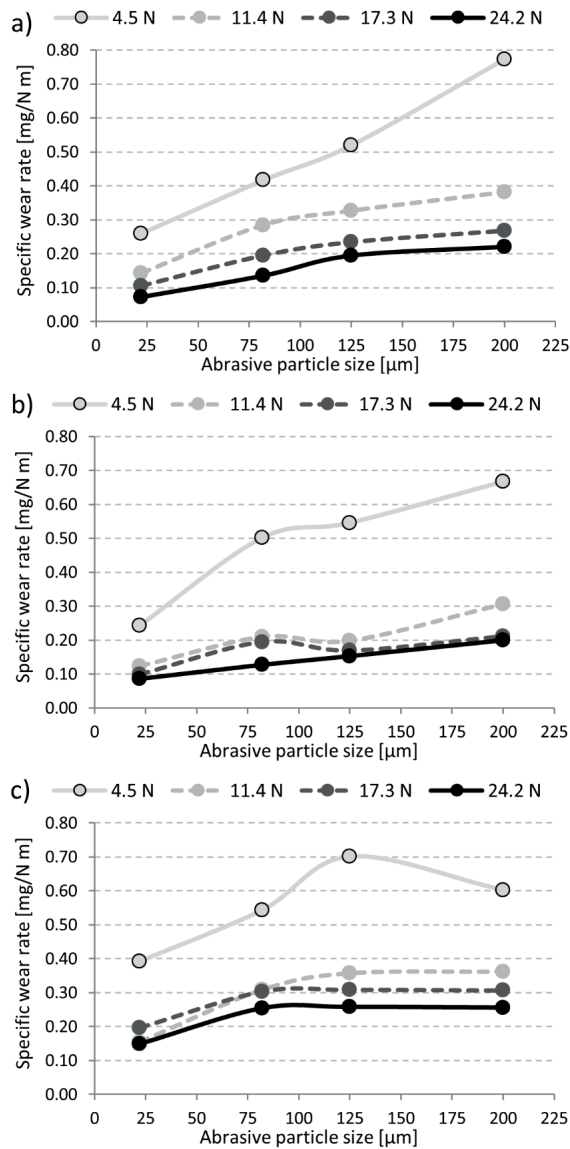


Figure 5-9 Specific wear rate [mg/N m] of tested materials in function of abrasive grit size a) FM, b) TM, c) MP

The wear rate of the investigated materials is shown in a 3D plot in Figure 5-10, as a function of normal load and average grit size. From the plots, TM material has the lowest wear rate and, thus, the highest wear resistance, followed by the FM material. The MP material was the least performing.

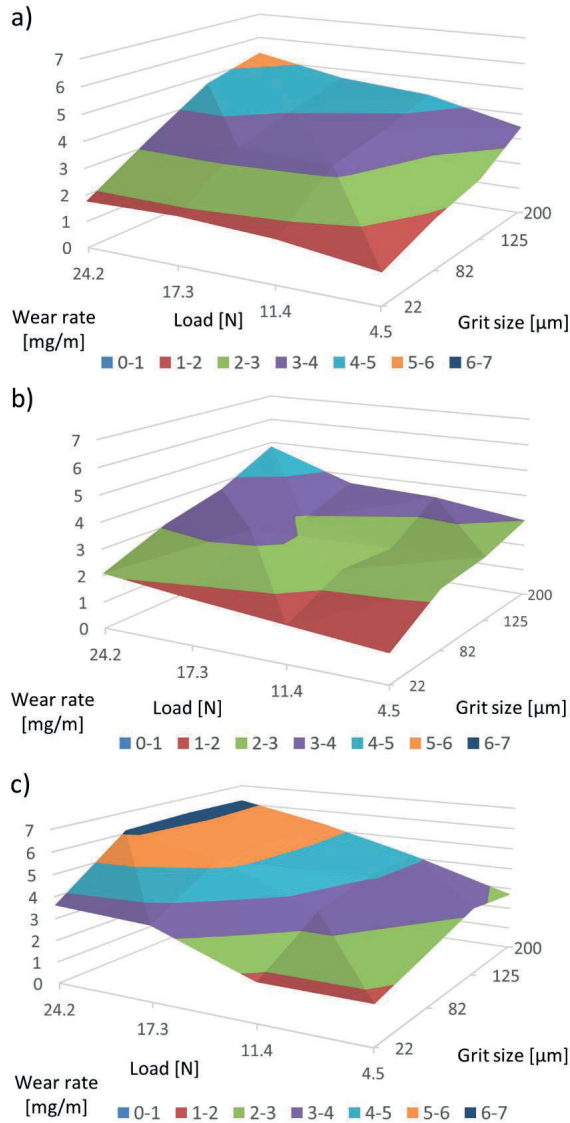


Figure 5-10 Wear rate [mg/m] (Z-axis) of FM (a), TM (b), MP (c) materials from the multi-asperity test as a function of the load (24.2 N, 17.3 N, 11.4 N, 4.5 N) (X-axis) and the grit size (22 μm, 82 μm, 125 μm, 200 μm) (Y-axis) [92]

The calculated wear rate [g/km] for the tested materials during the multi-asperity tests is introduced in Table 5-3. The values are shown for the largest and smallest abrasive particle size with the highest and lowest load. The best wear resistant material according to the multi-asperity tests was the TM, followed by FM and the least performing material is the MP. The wear rate differences can be partly

explained by the difference in initial hardness amongst the martensitic and MP steel structure. However, similar to the single-asperity test results, the 13 HV higher hardness of FM does not explain the inferior performance of FM compared to the TM material.

Table 5-3 Comparison of average wear rate [g/km] of materials during multi-asperity testing [92]

Load [N]	Abrasive particle size [μm]					
	22			200		
	FM	TM	MP	FM	TM	MP
4.5	1.17±0.11	1.09±0.08	1.76±0.13	3.48±0.06	3.00±0.14	2.71±0.07
24.2	1.76±0.15	2.09±0.22	3.61±0.06	5.34±0.12	4.83±0.17	6.19±0.17

5.4.4 Hardness investigation

Surface hardness measurements on the material samples after multi-asperity testing at the lowest and highest load condition are shown in Figure 5-11. Due to the test configuration, the contact surface of the specimen experiences multiple passes with fresh abrasive resulting in work hardening. Average values are shown with a deviation below ~5%. The hardness was measured in a profile of two rows with 10 measurement points, one row ~15 μm beneath the contact surface, and the second 250 μm deep. The hardening effect is evident for all tests. The hardness growth was higher with increasing load. FM experienced the highest hardening with an increase of 26 HV, followed by TM with an increase of 23 HV on average. MP steel has only experienced a minor hardness increase of 9 HV on average.

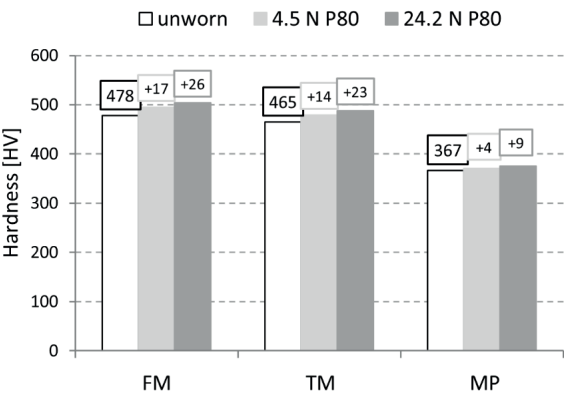


Figure 5-11 Hardness test results on multi-asperity samples compared to reference (unworn) condition for all 3 materials [92]

To investigate the effect of work hardening on the wear performance, the strain hardening ratio (ultimate tensile strength (σ_M)/yield strength (σ_Y) was plotted in Figure 5-12. This ratio clearly shows a higher value for the MP material compared to the two martensitic materials. The high ratio indicates the higher work hardening capability of the MP material upon tensile loading. On the other side, the

tempered martensitic material showed a smaller work-hardening ratio compared to the fresh martensitic material. The decrease of the work hardening behaviour of the martensitic material can be attributed to the low-temperature tempering process. During the tempering steps, dislocation annihilation, internal stress relaxation and/or the precipitation of small transition carbides take place leading to a slight decrease in the tensile strength and an increase in the yield strength, causing the change in the hardening ratio.

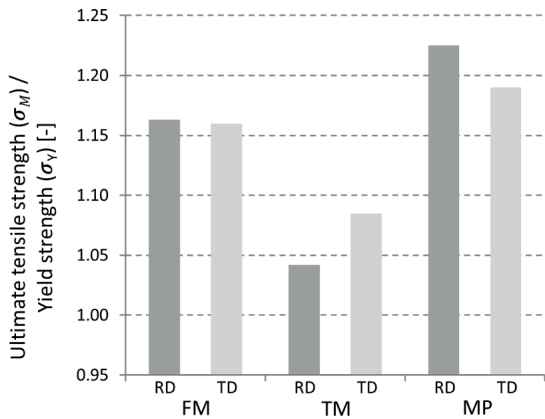


Figure 5-12 Variation of the ratio (Ultimate tensile strength σ_M /Yield strength σ_Y) in the rolling direction (RD) and transverse direction (TD) for the three materials: FM, TM and MP [92]

Although the MP steel exhibits the highest strain hardening ratio according to the stress-strain tensile curve (Figure 5-12), the worn surface hardness measured in Figure 5-11 does not show a significant increase. This could be linked to the stability of the retained austenite during the hardening process. To understand this behaviour, an X-ray diffraction experiment was applied on the surface and subsurface exposed to wear enabling the evaluation of the retained austenite phase fraction after wear and at different load levels. Results are given in Table 5-4. In this table, the retained austenite fraction decreases when increasing the normal load until it is completely transformed into martensite at a load level of 24.2 N.

Table 5-4 Evolution of the retained austenite before and after multi-asperity wear tests at different load levels [92]

Condition	Before wear	Worn P180, 4.5 N	Worn P120, 17.3 N	Worn P80, 24.2 N
Fraction of retained austenite	12.5	4.0	3.4	<2.0

5.4.5 Microstructure investigation

Besides the hardness, the microstructure of the sliding interface was investigated with SEM. Figure 5-13 shows a cross-sectional view across the sliding direction for the three tested materials used in the current investigation. The extracted material samples were embedded in an epoxy mould and polished before the investigation. All three materials evidenced a tribo-layer on the contact surface. In case of the low load (4.5 N) test, the samples experienced less severe deformation. Close to the contact surface (1-5 μm) a deformed layer was observed, where the grains seem to be plastically deformed in the direction parallel to the material surface due to the shearing force during scratching. In case of the 24.2 N load, the cross-sectional SEM analyses show more severe traces of plastic deformation in the material (compressed and deformed grains) and a less clearly distinguishable wavy contact surface.

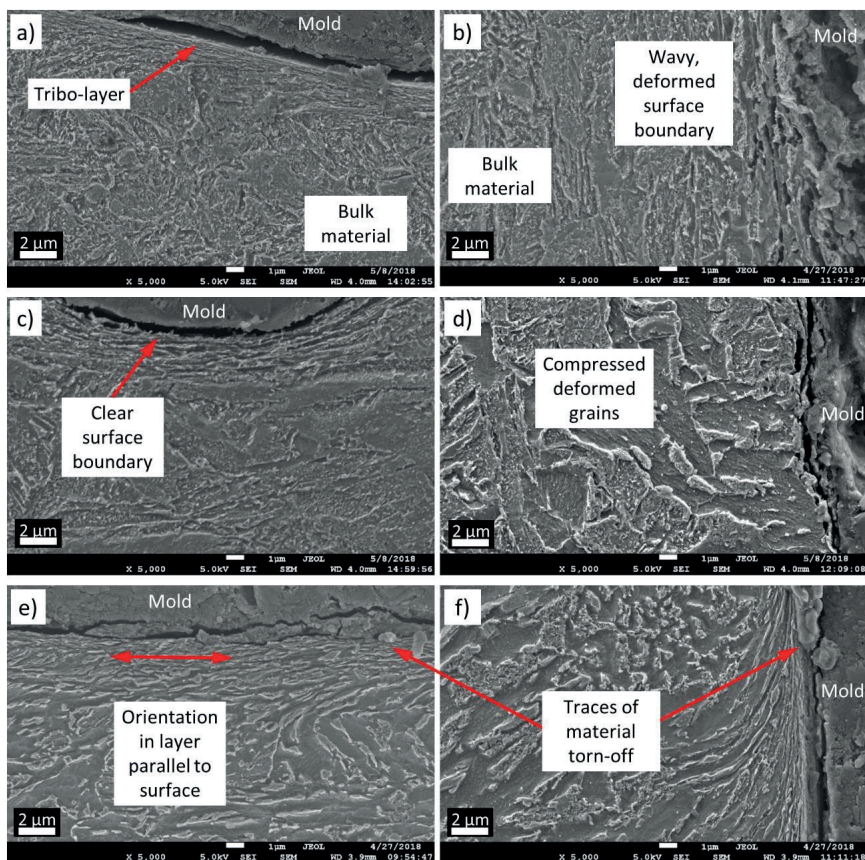


Figure 5-13 Cross-sectional SEM investigation of multi-asperity test samples perpendicular to sliding direction a) FM 4.5 N, P800 (22 μm), b) FM 24.2 N, P80 (200 μm), c) TM 4.5 N, P800 (22 μm), d) TM 24.2 N, P80 (200 μm), e) MP 4.5 N, P800 (22 μm), f) MP 24.2 N, P80 (200 μm) [92]

The characteristic features of the wear micro-mechanisms observed in the microscopy images of the contact surface of the worn samples could also be identified in the SEM images. These two investigations are in good agreement. SEM surface micrographs indicate the dominant micro-mechanism and the surface topography of the samples. P800 tests shown in Figure 5-13 resulted in uniform wear tracks with clear-cut shallow grooves and less surface deformation indicating the dominance of micro-cutting. P80 tests resulted in more severe grooves, however, traces of material shear (embedded chip) could be observed beside the deformed surface. These features could indicate presence of both micro-ploughing and transition to micro-cutting. This is confirmed by the Dp charts (Figure 5-8). Although the wear rate is highest in case of 24.2 N and P80 tests, the specific material removal is more severe for low load test condition (4.5 N).

5.4.6 Multiple linear regression models and sensitivity analysis

Similar to the method described in 3.5.5, again multiple linear regression models are investigated to see how the wear results depend on the material properties as well as the testing variables. The independent variables were the sliding distance s , load F_N , and abrasive particle size d , together with the material properties and the dimensionless parameters derived from them. According to this, the best fitting model of the possible ones was

$$\Delta m = a_0 + a_1 s + a_2 d + a_3 F_N + a_4 \frac{\sigma_y}{\sigma_c \epsilon_B} \quad (4.1)$$

The F-value of the model was 261 and $p < 0.001$, which means that the model is relevant. Table 5-5 summarizes the coefficients of the model.

Table 5-5 Coefficients of the regression model for multi-asperity test [93]

Model	Coefficient	Standardized Regression Coefficient, Beta	t	p
Constant	-0.002		-1.209	<0.001
s	0.003	0.827	29.031	<0.001
d	0.0001	0.268	9.404	<0.001
F_N	0.0005	0.241	8.450	<0.001
$\frac{\sigma_y}{\sigma_c \epsilon_B}$	-0.101	-0.184	-6.468	<0.001

For this model, the goodness-of-fit is $R^2 = 0.848$. On the wear of the test sample the time of the experiment (sliding distance) has the highest effect, furthermore, the material related parameter ($\sigma_y / \sigma_c \epsilon_B$) has some effect.

The best fitting model of the possible ones for the change of the contact surface hardness was

$$\Delta H = a_0 + a_1 \frac{W \sigma_y}{E} + a_2 s \quad (4.2)$$

The model is relevant ($F = 699$ and $p < 0.001$). In Table 5-6, the coefficients of the model are presented.

Table 5-6 Coefficients of the regression model for multi-asperity test [93]

Model	Coefficient	Standardized Regression Coefficient, Beta	t	p
Constant	539.836		156.937	<0.001
$\frac{W\sigma_Y}{E}$	-5904.081	-0.986	-37.018	<0.001
s	1.722	0.145	5.436	0.001

For this model, the goodness-of-fit is $R^2 = 0.994$. The material parameter ($W\sigma_Y/E$) has a dominant effect on the hardness change, while the sliding distance also plays a role.

The change in surface roughness parameters after wear testing with the most severe conditions (P80 tests with 24.2 N) was studied. To investigate the change of the surface topography, white light optical microscopy was used. Figure 5-14 shows the original 3D surface characteristics and their worn condition, and Table 5-7 summarizes the roughness values.

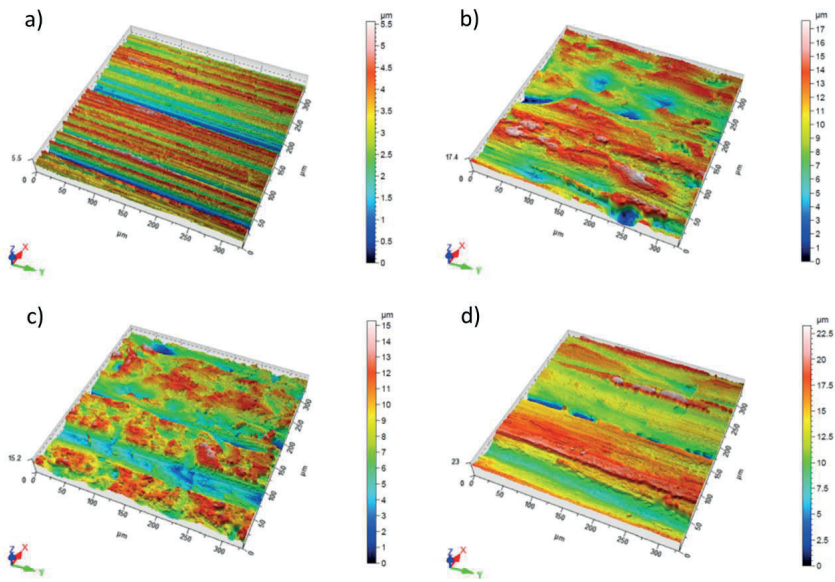


Figure 5-14 3D surface roughness of the tested materials with P80 abrasives and 24.2 N load (a) unworn, (b) FM, (c) TM, (d) MP [93]

All the materials suffered surface deformation, with material deposition to form new hills and valleys. The clearest grooves were identified on the MP material indicating a dominant micro-cutting effect with continuous chip generation and material removal. The groove depth values from Figure 5-14 are in line with the measured wear from Figure 5-5.

Table 5-7 Surface characteristics after the wear tests (P80 with 24.2 N) and the change in % [93]

Parameter	Name	Unit	FM	%	TM	%	MP	%
Ra	Arithmetical mean height	[μm]	2.65	+111	2.45	+94	2.76	+104
Rz	Max. height	[μm]	14.26	+66	14.72	+80	16.08	+88
Rp	Highest peak	[μm]	6.52	+43	6.32	+45	7.51	+78
Rv	Lowest valley	[μm]	7.74	+91	8.40	+120	8.57	+98
Rt	Total height	[μm]	19.58	+63	20.68	+91	22.42	+91
Rc	Average height of profile element	[μm]	9.61	+79	9.51	+91	10.75	+109
Rq	Root mean square height	[μm]	3.26	+98	3.10	+91	3.49	+103
Rsm	Mean width of profile elements	[μm]	201.84	+16	215.63	+42	245.87	+68
Rsk	Skewness	-	-0.22	-173	-0.35	-155	-0.28	+190
Rku	Kurtosis	-	2.74	-70	3.41	0	3.30	-1

For the surface roughness parameters as dependent variables, multiple linear regression models were built, where the independent variables were sliding distance s , load F_N , and abrasive particle size d , besides the material properties and the indicators formed from them. According to this, the best fitting model for the change in Ra among the possible ones was

$$\Delta Ra = a_0 + a_1 d + a_2 s \quad (4.3)$$

where the F-value of the model was 43 and $p < 0.001$, which means the model is relevant. The coefficients of the model are summarized in Table 5-8.

Table 5-8 Coefficients of the regression model for multi-asperity test [93]

Model	Coefficient	Standardized Regression Coefficient, Beta	t	p
Constant	0.715		6.642	<0.001
d	0.005	0.527	6.981	<0.001
s	0.067	0.453	6.000	<0.001

For this model, the goodness-of-fit is $R^2 = 0.493$. The size of the abrasive in the experiment has the highest effect on the change in Ra of the worn surface, followed by the sliding distance. The effect of material parameters is negligible. Change in the Rz, Rt, Rp, Rv Rc, and Rq parameters follow the same trend, where the size of the abrasive particles has the highest effect on the change of the roughness parameter, followed by the sliding distance. However, the following surface roughness parameters showed different dominant dependence.

The best fitting model of the possible ones for the change in Rsm was

$$\Delta Rsm = a_0 + a_1 d + a_2 \frac{\sigma_y E}{\sigma_M H} + a_3 s \quad (4.4)$$

The model is relevant ($F = 30$ and $p < 0.001$). The coefficients of the model are presented in detail in Table 5-9.

Table 5-9 Coefficients of the regression model for multi-asperity test [93]

Model	Coefficient	Standardized Regression Coefficient, Beta	t	p
Constant	373.585		8.320	<0.001
d	0.152	0.450	5.982	<0.001
$\frac{\sigma_y E}{\sigma_M H}$	-5.497	-0.391	-5.202	<0.001
s	1.816	0.370	4.922	<0.001

For this model, the goodness-of-fit is $R^2 = 0.431$. The size of the abrasive in the experiment has the highest effect on the change in Rsm of the worn surface, while the only material parameter with some effect is $(\sigma_y E / \sigma_M H)$.

The best fitting model of the possible ones for the change in Rsk was

$$\Delta Rsk = a_0 + a_1 s + a_2 W_{(20)} + a_3 d \quad (4.5)$$

The model is relevant since the F-value was 53 and $p < 0.001$. In Table 5-10, the coefficients of the model are presented.

Table 5-10 Coefficients of the regression model for multi-asperity test [93]

Model	Coefficient	Standardized Regression Coefficient, Beta	t	p
Constant	0.334		10.381	<0.001
s	-0.029	-0.640	-10.0682	<0.001
$W_{(20)}$	-0.001	-0.423	-6.659	<0.001
d	-0.001	-0.247	-3.891	<0.001

For this model, the goodness-of-fit is $R^2 = 0.645$. In this case, the sliding distance in the experiment has the highest effect on the change of Rsk, among the material parameters the Charpy strength $W_{(20)}$ has notable effect. The size of the abrasive particle resulted in a minor effect.

The best fitting model among the possible ones for the change in Rku was

$$\Delta Rku = a_0 + a_1 s + a_2 \frac{\sigma_y E}{\sigma_M H} \quad (4.6)$$

which is relevant ($F = 86$ and $p < 0.001$). Table 5-11 summarizes the coefficients of the model.

Table 5-11 Coefficients of the regression model for multi-asperity test [93]

Model	Coefficient	Standardized Regression Coefficient, Beta	t	p
Constant	7.164		11.926	<0.001
s	-0.057	-0.715	-11.527	<0.001
$\frac{\sigma_y E}{\sigma_M H}$	-0.085	-0.373	-6.022	<0.001


For this model, the goodness-of-fit is $R^2 = 0.658$. The sliding distance in the experiment has the highest effect on the Rku of the worn surface and $(\sigma_y E / \sigma_M H)$ is the only material parameter with a significant, but moderate effect.

According to the above-presented results it can be seen that besides the initial hardness and the Charpy impact strength the elasticity modulus and the tensile parameters play role in the change of surface parameters. These results are in line with the influence of applied loads on the micro-geometry. The micro-geometry of the moving steel surfaces under normal load suffers shear, bending, and compressive effects mainly, resulting in the appearance of plastic deformation, wedge formation, and micro-cutting [97], [111].

Since the roughness parameters of the examined materials have a high deviation, most of the models which investigated a change of a parameter connected to surface roughness, the goodness-of-fit varied to a large extent. For the evaluation of the sliding process the linear approach was used, however, some researchers may prefer polynomials. Power functions or even higher order polynomials may offer better approximation (greater R^2) in case of large number of data. On the other hand, by using higher-order polynomials, the mixed parameters of the second or higher power models could cause physical information loss. Also, a global linear model which is fitted for the data of all examined materials might provide less goodness-of-fit because of the relatively high differences in some material properties. Here, the main focus was to detect the parameters and material properties which affect the surface roughness parameters, furthermore to see a ranking of these affecting factors, that is which has the highest effect of all, etc.

Table 5-12 summarizes the findings on the discussed linear models with respect to the abrasive sensitivity for wear and the resulted surface roughness parameters. The factors that play role are presented in increasing order of effect.

Table 5-12 Abrasive sensitivity ranking to pin-on-disk test system features [93]

<div> <div>Effect of influencing factors</div> <div>  </div> </div>	s	$\frac{W\sigma_y}{E}$				
	d			d	s	s
	F_N	s	d	$\frac{\sigma_y E}{\sigma_M H}$	$W_{(20)}$	
	$\frac{\sigma_y}{\sigma_c \epsilon_B}$		s	s	d	$\frac{\sigma_y E}{\sigma_M H}$
Independent variable	Δm	ΔH	$Ra, Rz, Rp, Rv, Rt, Rc, Rq$	Rsm	Rsk	Rku

5.4.7 Coupling to material properties

The most ductile MP steel resulted in the highest wear rate. Comparing the martensitic materials the FM material performed worse in abrasion scratch resistance despite having 13 HV higher hardness than the TM material. This confirms that the relative wear rate is more microstructure than hardness dependent. Though the MP material showed higher strain hardening upon tensile testing (higher tensile to yield strength ratio), and transformation of retained austenite occurred upon wear testing, the worn subsurface only showed limited hardening. This may be due to a relatively low C content in the austenite which would lead to a martensite with a relatively low hardness.

The explanation for the difference in wear resistance, despite the similar microstructure and hardness of fully martensitic and tempered martensitic materials, is connected to the difference in yield strength and ultimate tensile strength. The tempered martensitic material has higher yield strength and lower tensile strength. The ratio is 1.16 for the fresh martensitic material and 1.1 for the tempered material. The mechanical properties such as yield strength and toughness after the tempering have been improved despite the lower strain-hardening and ductility, resulting in a more cutting-resistant material.

5.5 Conclusions from multi-asperity pin abrasion testing

In the case of multi-asperity testing, the load increase resulted in higher D_p values indicating more severe wear. Multi-asperity tests with the biggest particle size resulted in lower D_p values. With increasing abrasive particle size, the wear rate increased in case of all materials until a critical particle size ($\sim 80 \mu\text{m}$), where the wear rate became independent of further size increase. The most severe wear was obtained with the highest used load (24.2 N) and highest abrasive grit size (200 μm) during multi-asperity tests. Subsurface work-hardening was confirmed by hardness measurements and SEM. Plastic deformation observed (underneath the contact surface) indicated the predominant ploughing wear micro-mechanism. In the case of 24.2 N tests, traces of material shear were observed (on the boundary of the contact surface) indicating a dominant micro-cutting mechanism. Despite the higher toughness and the retained austenite fraction (and transformation thereof) the MP material showed the worst wear performance in both test configurations. The higher toughness/ductility might provide some advantage in lower load test conditions (e.g. multi-asperity tests with 4.5 N). The much harder martensitic materials outperform the MP, probably due to low initial hardness and limited hardening of the latter.

The results of this study are in line with the conclusions of Chintha [109], who state that thermomechanical processed medium carbon steels in quenched and low temperature tempered conditions achieve good hardness and (fracture) toughness, which may be beneficial for the wear resistance. The MP steel in this application did not give the highest wear performance despite its higher

toughness and retained austenite fraction. Initial low hardness/strength, even after surface hardening produced by wear, could be the origin for such performance. The transformation of retained austenite and its (limited) contribution to the hardening and wear performance is to be further investigated. As possible future work should comprise determining of the carbon content in the austenite to see whether that could have played a role. Also (nano) indentation measurements on the martensitic matrix and on retained austenite before (and after) wear testing could be considered.

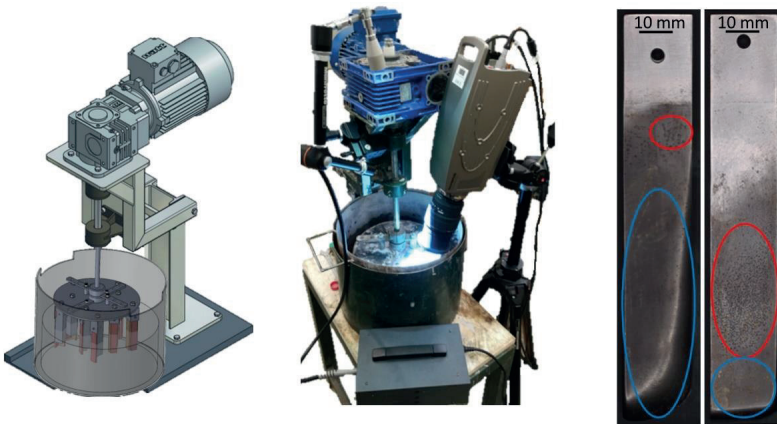
6 CHAPTER 6

CO-EXISTING WEAR MODE INVESTIGATION IN MULTI-ASPERITY CONTACT

This chapter summarizes the results obtained from multi-asperity slurry-pot wear tests representing a more complex macro-level wear investigation.

The following article was published based on this chapter:

Á. Kalácska, L. Székely, R. Z. Keresztes, A. Gábora, T. Mankovits, and P. De Baets, "Abrasive Sensitivity of Martensitic and a Multi-Phase Steels under Different Abrasive Conditions," *Materials*, vol. 14, no. 6, p. 1343, Mar. 2021, doi: 10.3390/ma14061343.



6.1 Introduction

Through the years many laboratory wear tests have been developed to simulate a range of wear conditions, from two and three-body abrasion to sliding friction and solid particle impingement. However, their relevance and usefulness are often questioned with regards to the extent to which they simulate real industrial tribological systems. This is especially true for the evaluation of coatings and surface treatments that are intended to reduce wear and improve the lifetimes of industrial components. A comparison of a simulated 'in-service' rig test with a standardized laboratory abrasion test was made by Whittaker *et al.* [132]. The results demonstrate that the laboratory test has some validity within certain operating parts of the industrial system, but for a meaningful indication of likely wear life, full 'in-service' test conditions are needed, due to the complexity of real tribological systems. Significant attempts have been made at quantifying abrasive soil wear and at understanding the underlying wear mechanisms. The main goal of simulating the in-field wear with standard and customized tests and equipment is to reduce costly field trials. There are several standard and nonstandard tests used for quantifying abrasive wear [2]. E.g. ASTM G65 standard is developed to quantify abrasive wear of materials and coatings for construction and farm equipment. Although this method can be used to evaluate relative wear resistance of materials, it is not entirely satisfactory for determining the abrasive wear characteristics experienced by implement tools in real applications. Therefore, to quantify wear of farm implements, special soil bins have been developed to create soil-tool interaction that is closer to actual field conditions. Custom built soil bin facilities are used to investigate and simulate the implement draft force, wear, and failure experienced in the field. A typical soil bin facility consists of the soil bin, tool carriage, drive system, instrumentation, and data acquisition system. However, typical soil bin testers do not reproduce the observed pitting mechanism on the tine top region. Therefore, to be able to investigate the micro-pits as well as to speed up the testing, a modified test system in the present study was used.

Specimens are tested in multi-asperity contact immersed in an abrasive slurry. This multi-asperity contact test configuration was designed to experimentally simulate the wear of components that experiences abrasion as well as fatigue (erosive) wear mechanisms. This set-up enables to test in a more complex environment that is closer to the real application, and where co-existing wear mechanism occur [21]. Although more uncertainties are involved in the slurry-contact mechanism, the effects of the wear-influencing parameters are investigated. The method also provides a quick and efficient ranking of materials in terms of abrasion wear rate.

6.2 Slurry abrasion-erosion

Solid particle erosion refers to the wear originated from a series of particles striking and rebounding from the surface, while abrasion results from sliding of abrasive particles across the surface under the action of an externally applied force [133]. The clearest distinction is that in case of solid particle erosion the force exerted by the particles on the material is due to their deceleration (impact), while in abrasion the externally applied normal force is often constant. Erosion involves a transfer of kinetic energy from the impinging particle to the target surface, and the contact time between the erodent and the eroded surface is much shorter than in abrasion [134]. In case of solid particle erosion thinning of the component, surface roughening, and possibly formation of ripple patterns is expected [133]. In this case, a clear cut distinction is difficult between erosion and abrasion, because of the very dense particle distribution in the liquid, where the pack of particles tend to slide across the surface resulting in abrasion. Slurry erosion is a process of surface degradation due to repeating impacts of solid particles carried in a liquid medium [135]. It usually occurs under turbulent flow conditions when the moving slurry interacts with a surface of a solid body. The accurate prediction of erosion behaviour of materials is difficult as numerous parameters govern the erosion phenomenon. All these parameters can be broadly classified as impinging variables, particle variables and material variables [136].

The impact velocity and the size of the solid particle affect the kinetic impact energy of a single particle. In a heavy-duty slurry pump or tillage in stony soil, the particle size can be up to several centimetres, while in fine particle mineral processes the particle sizes are typically between 100-250 μm . The increase of particle concentration in a liquid further influences the total impact energy. Erosion rate increases with increasing impact velocity and particle size [136]–[138]. Depending on impact velocity, slurry erosion is divided on high- and low-velocity erosion. If velocity increases above 6-9 m/s, high-velocity erosion is formed, while below this velocity, slurry erosion is called low-velocity erosion [139], [140]. Furthermore, the impact angle influences the wear severity, so a variation of specimen angle and orientation to the slurry flow was included in the testing. In addition, tribo-corrosion plays a role in the wear damage in some operations [23]. This material degradation process is the combined effect of corrosion and wear, which will not be addressed in this study. It has been earlier reported that the role of corrosion is smaller [141]. Mainly due to corrosion, quenched wear resistant steels are not widely used in piping. However, due to their good mechanical wear resistance, it may result in a greater effect on the pipe lifetime than their relatively poor corrosion resistance when dealing with highly abrasive slurries [142].

Slurry erosion is a complex phenomenon and not yet fully understood [134], but recently the topic has gained interest. Although the most commonly used materials for slurry transport were tested, and their wear data is reported [23], detailed investigation on the wear mechanisms and possible newly

developed materials has not been performed, yet. Quite a few materials have been considered to be used for slurry transport [23], but their wear resistance may vary according to the system properties. Only few studies rank potential materials in custom made test configuration, where the wear resistance, as well as the involved wear mechanisms, are investigated in detail. In the developed configuration, both slurry abrasion and erosion are studied in the same test run, highlighting the boundary conditions for the aforementioned mechanisms.

In the current research, a slurry-pot tester was developed for experimentally simulating abrasion and slurry erosive wear of martensitic steels for agricultural and mineral processing applications. The designed test set-up offers an efficient and simple method to compare wear rate and investigate the dominant wear mechanism of candidate materials under both abrasion and slurry erosion. The study deals with a short term mechanical wear mechanism investigation caused by relatively large particles (2-2.5 mm) at relatively low speed ~ 1 m/s through slurry abrasion and erosion. The focus is on highlighting the appearance of different wear mechanisms and on investigating the operational parameters that influence these mechanisms.

6.3 Experimental procedure

The same materials as introduced in Chapter 3 have been used here. The used abrasive medium was corundum (Korund EKF-10, MOTIM, Mosonmagyaróvár, Hungary). This is a crystalline form of Al_2O_3 , a rock-forming mineral. The average size of a new corundum particle is in the range of 2000–2360 μm , with 3.87 kg/dm^3 density and 9.0 Mohs hardness (2050 Knoop kN/mm^2). The effectiveness of an abrasive depends on its hardness, shape, grain density, and grain size. The smaller the grains, the slower their effect, but the angular shape results in increased abrasion [143].

The concept of the test rig is shown in Figure 6-1-a. The test set-up was developed and manufactured in MATE, Gödöllő, Hungary. The rotating disk is driven by a three-phase induction motor on a vertical shaft through a 1:10 worm drive. The shaft is supported by ball bearings in order to minimize friction. The disk is eccentrically placed in a cylindrical container (Figure 6-1-b) to provide better mixing. The medium in the container is composed of abrasive media and water in a 4:1 ratio (16 kg corundum and 4 kg water). Preliminary tests proved that this ratio avoids too dry conditions in which the specimen would create a clear furrow in the abrasive particle bed and inhibit further contact. The water is needed to support the flow back of the abrasive particles after the contact and it also acts as a lubricant to prevent high friction and local overheating of test samples. On the other hand, more water to abrasive media was to be avoided because of the lack of significant wear. On the disk, vertically mounted specimen holder columns are placed on two different radii (75, 115 mm), five pieces on each radius. Figure 6-1-c shows the bottom view of the disk with the mounted holders and specimens in different configurations. On each specimen holder column, two specimens (120x20x5 mm) are mounted

perpendicular to each other. These holders could be rotated around their axis in order to set the orientation angle of the specimen with respect to the slurry flow direction. Due to the geometry of the specimen holders, the centre of the specimens was placed on four different radii (65, 85, 105, and 125 mm). The samples on radius 65 mm and 105 mm were facing the centre of rotation (centre shaft), and the samples on radius 85 mm and 125 mm were facing the pot wall. With a radius drawn from the centre of rotation to the edge of the specimen holders, the specimens facing the centre of rotation (R65 and R105, marked orange) close at 45° and the specimen facing the pot wall (R85 and R125, marked green) close at 135°, as it is shown in Figure 6-1-c). The top 20 mm of the specimens, where they are mounted to the specimen holder, is protected with an extra plate to keep a reference, unworn zone on each sample. In static position, the specimens were covered in the slurry to a depth of 60 mm depth (half of the specimen height).

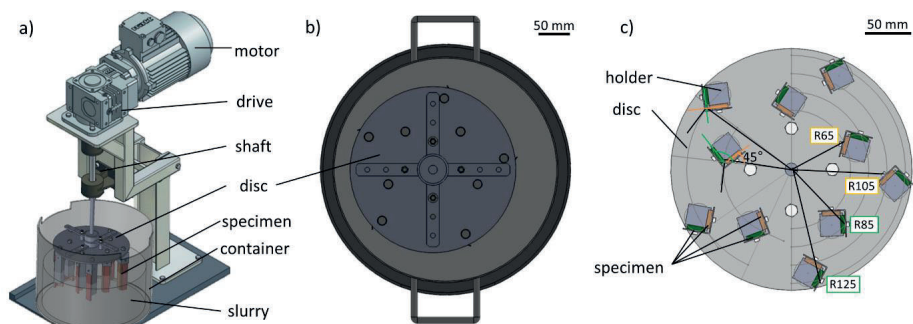


Figure 6-1 (a) Test rig concept; (b) top view of the eccentric placed disk in pot; (c) bottom view of the disk with the mounted specimen on radii 65, 85, 105, 125 mm in different angle configuration [93]

During operation, the rotation of the shaft agitates the slurry and causes the moving specimen to slide and impact against the abrasive in the slurry. Depending on the location of the samples on the holder, collisions occur with different mean impact velocity values and at different angles. Tests were performed at a rotational speed of 140 rpm and a room temperature of 21 ± 1 °C. The slurry pot was placed inside a container with a continuous flow of cooling water, providing the cooling through the pot walls.

In the developed abrasive slurry test configuration, the effect of the circumferential distance travelled by specimen (sliding distance), sliding velocity, and specimen orientation angle (indirect method obtaining different collision and tangential sliding in a chaotic 3D flow of slurry) on the material loss was investigated. The change in surface topography and hardness was also monitored. Slurry pot testing of 20 specimens was carried out for 180h (9 × 20 h) of operation. All three materials were tested with the same conditions, and the cycle was repeated to ensure three repetitions for each material. The testing parameters and conditions are shown in Table 6-1.

Table 6-1 Slurry pot test parameters [93]

Radius	[mm]	125	105	85	65
Surface velocity	[m/s]	1.885	1.583	1.282	0.98
Orientation angle	[°]	135	45	135	45
Wear area	[%]	55	75	25	20
Sliding distance	[m/20h]	13,572	11,400	9229	7057

At every 20 hours the test was briefly paused, the slurry was replaced with fresh abrasives, and the samples were investigated for their weight and hardness of the worn zone. Based on pre-tests the 20 hours period was found to be sufficient to prevent significant fragmentation and breakage of the corundum particles as well as to prevent drying out of the slurry. After cleaning the specimens, the surface roughness was monitored with Mitutoyo Surftest SJ 211 (Kawasaki, Japan) stylus 2D profilometry. The hardness was measured with Zwick (Ulm, Germany) Roell Indentec 81,875 A/B tester using a diamond tip indenter and 30 kg (~300 N) indentation force. On all specimens, 10 indents were made in the worn zone and 10 in the unworn reference zone. After 180 hours of testing the specimen were investigated with Keyence (Osaka, Japan) VR-5200 wide-area 3D microscopy to analyse the worn specimen surface topography change caused by wear.

6.4 Results of slurry pot testing

6.4.1 Wear rate

In the slurry-pot system, the material samples move in a slurry medium at four circumferential mean speeds and two angles of orientation and suffer abrasive erosion on the surface. The different specimen positions resulted into different contact areas with the slurry due to the centrifugal action on the slurry flow. Due to centrifugal force the slurry level is higher at higher radius. For adequate comparison of the wear for different radii, the contact area (specimen area exposed to wear) has been taken into account, and the wear values were normalized accordingly. Verification with the help of image processing tools (OpenCV and Scikit-Image), the specimen surface area affected by wear (colour change) was detected and calculated from pixel values. These were averaged for all radii resulting into estimated contact areas of 20%, 25%, 75%, 55% for radii of 65, 85, 105, 125 mm respectively. Figure 6-2 shows the relative mass loss [%] as a function of sliding distance, where the initial mass was normalized with the specimen area exposed to wear. For a better comparison of the relative mass loss values, an extra vertical line is drawn at 60 km sliding distance for all radii. The standard deviation in the mass loss [%], including the repetitions, was below 0.1%. All materials showed a similar trend with a linear increase in wear. The relative wear of the specimen placed on radius 105 mm is an order of magnitude higher than the rest of the samples. Similarly, specimen mounted on radius 65 mm suffered severe wear, hence the effect of specimen orientation (angle of attack) had a more significant role on

the wear severity than the difference in the radius (higher circumferential speed). This phenomenon could be explained by the effect of the centrifugal force on the slurry. The centrifugal force pushes the abrasive particles in a radial direction to the 45° oriented specimen surfaces, resulting in more severe material removal. In the swirly, chaotic movements of the suspension the orientation of the surfaces will determine the complex load on the surfaces. The internal side (specimen facing the centre shaft of rotation) differs from the external (specimen facing the pot wall) concerning the speed of the particle, the impact angle and the impact energy.

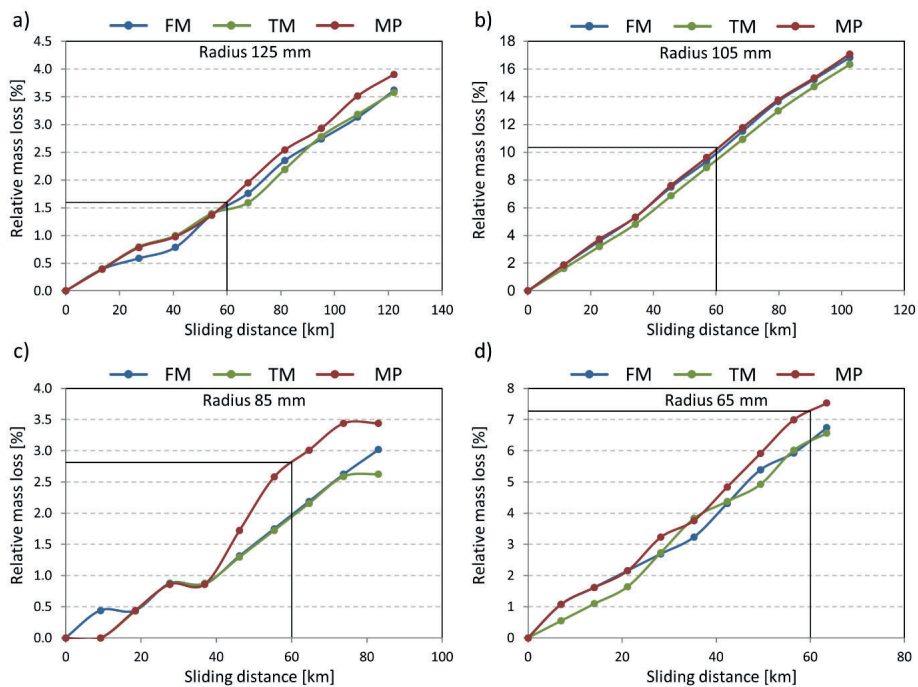


Figure 6-2 The relative mass loss [%] of the tested materials (FM, TM, MP) in the function of sliding distance in different positions; (a) radius 125 mm, (b) radius 105 mm, (c) radius 85 mm, (d) radius 65 mm [93]

Despite the higher circumferential velocity of the slurry abrasive particles on radius 125 mm, less wear was recognized on these samples than on samples mounted on radius 85 mm (for the same orientation). On specimen mounted on radius 125 mm significant pitting was also observed, except on the multiphase steel. Due to the design configuration of the slurry pot tester, both abrasion and erosion were co-existing. The material properties, the specimen radius, and orientation affected the wear mechanisms and the severity of the wear. In erosion literature, materials are classified as ductile or brittle based on the dependence of their erosion rate on the angle of impingement. Ductile materials have a maximum erosion rate at low angles (~15–30°), while brittle materials experience a peak

erosion rate close to 90° [133]. The tested materials are considered more brittle than ductile, except the retained austenitic multiphase steel due to its microstructure and lower hardness [144]. The tests confirmed that the MP steel performed better against surface erosion, however suffered severe abrasion. As Figure 6-2 shows, the mass loss curves of the MP steel are clearly over the mass loss of the martensitic materials in most cases. TM was the best performing in most of the cases, closely followed by FM material.

Overall, TM resulted in an average mass loss of 0.0753 [%/100 km], while FM experienced more severe wear [0.0815%/100 km]. The least wear-resistant multiphase steel averaged 0.0881 [%/100 km] mass loss during the slurry pot tests.

6.4.2 Surface characterization and wear modes

The wear mechanisms identified from the post-mortem analysis (Figure 6-3) validates the explanation of wear severity. Figure 6-3 shows the images of the tested specimens from material FM (a, b, c, d) on different radii and their corresponding height map. Abrasion was observed mostly on samples mounted on radius 105 mm and pitting was observed to be the most severe on samples mounted on radius 125 mm.

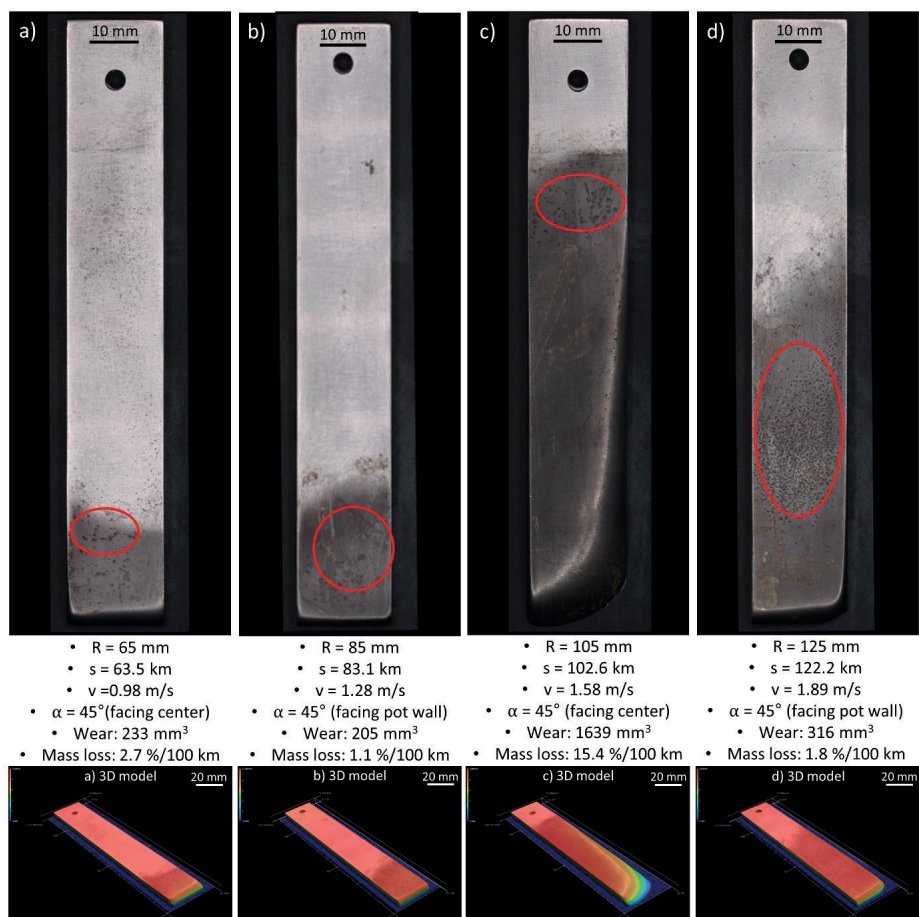


Figure 6-3 Slurry pot test specimen of FM material after 180 hours run and their corresponding 3D height map analyzed with white light interferometer

The significant pitting present on samples mounted on radius 125 mm could be explained with the particle movement in the media. As a result of the collision contact with the test specimen, these particles were found to glide/fly away and bounce back from the pot wall. In general, severe pits appeared on the specimen surface area close to or above the media level, where the contact was impact rather than sliding. Here, the damping effect of the water was less significant. After the impact, backflow effect of the abrasive particles (media equilibrium) within the water was prevalent. To validate this explanation, high-speed camera video recordings gave an insight to this phenomena. In Figure 6-3 the red circles indicate the areas observed to be exposed to severe pitting. As concluded, the specimen orientated towards pot wall suffered severe pitting, but less overall wear. This was observed in case of all of the tested materials.

Figure 6-4 shows an image comparison of worn slurry pot specimens after 180 hours of operation for all materials on radius 105 and 125 mm as these samples had the largest worn areas.

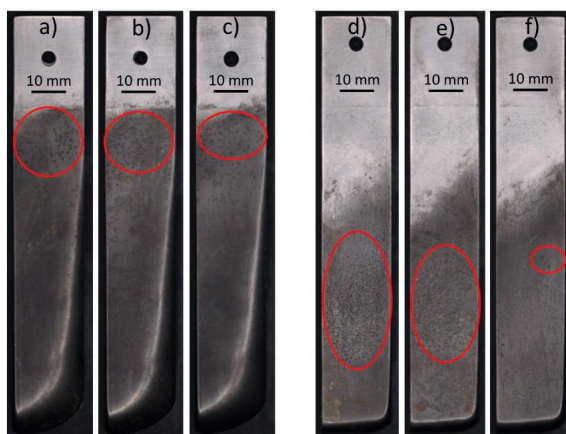


Figure 6-4 Worn slurry pot specimen after 180 hours operation of material FM (a, d), TM (b, e), and MP (c, f) on radius 105 and 125 mm, orientation 45° facing centre shaft and pot wall correspondingly

It is clear from the images that MP material did not experience so much pitting. This could be explained by its more ductile behaviour which originates from its microstructure. Its lower hardness helps to minimize the pitting formation, which is developed from the subsurface cracks, caused by the impacting particles. As a result of the wear test the specimens geometry changed, depending on their position, with edge rounding and shortening in total length. Due to the design configuration of the slurry pot tester, both pitting and abrasion were co-existing. The observed characteristic features were dependent on the zone on the specimen. The contact area between the specimen surface and the abrasive media increases as a function of the location radius. This increase comes from the effect of the centrifugal force on the slurry excluding samples mounted on radius 125 mm, where the abrasive particle movement has a different characteristic close to the pot wall. The observed characteristic wear mechanism features were dependent on the specimen zones. Two zones could be separated for each wear sample. On the bottom part of the specimen, under water level, where it is inside the abrasive media during operation, a polishing effect and severe material loss were observed. Furthermore, close to the rounded edges, small abrasion scars were noticed. Whereas in the upper zone of the specimen, where the contact is close to the surface level of the abrasive media, pitting was present. Pitting was found to be dominant in the upper part of the worn zone, which is in the lower pressure zone of the media. The pitting was present in the upper part of the worn zone in case of all specimens and materials. However, the material composition, the radius related to the specimen position, and the specimen orientation affected the severity of the pitting zones.

6.4.3 Pitting investigation

The pitting phenomenon was further investigated. The depth of the pits is connected to the impact speed of the particles. Figure 6-5 shows the comparison of the pits from radius 85 and 125 mm with their 3D model and height map.

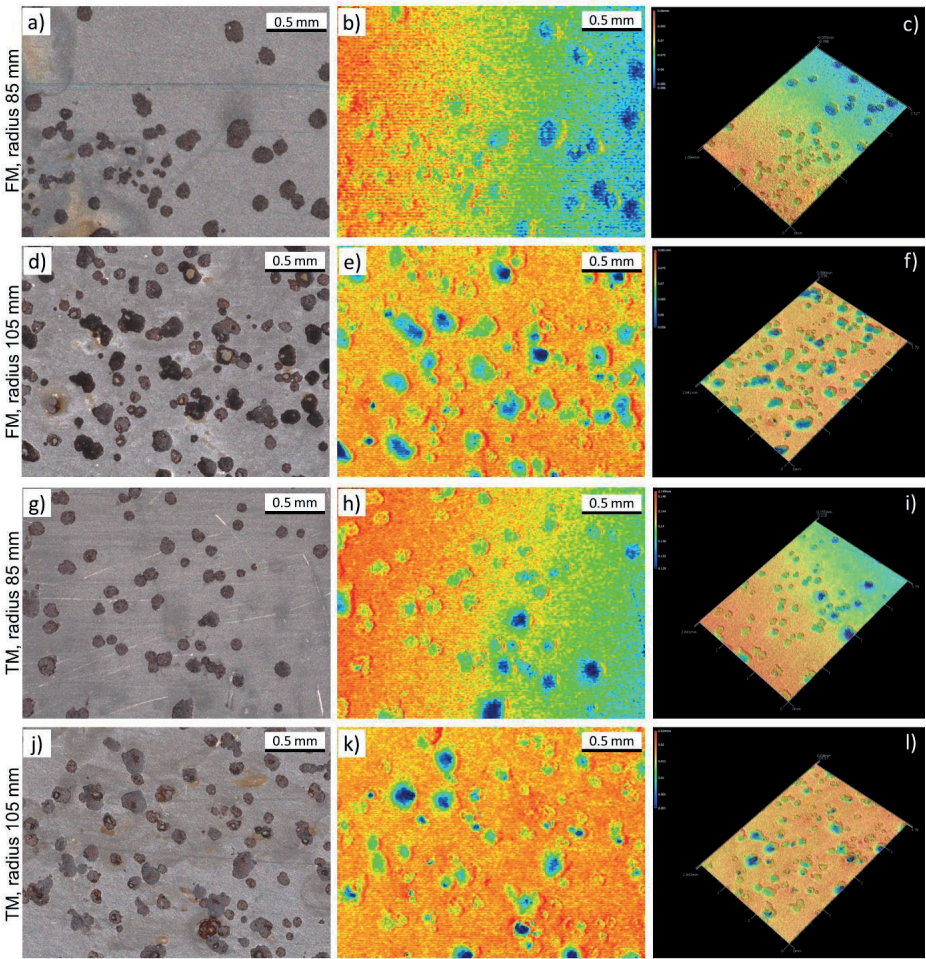


Figure 6-5 Pitting investigation of slurry pot specimen FM and TM (oriented 45 °to centre shaft): microscopy (a, d, g, j), pit dimensioning with corresponding height map (b, e, h, k), and quantifying pit depth with 3D model (c, f, i, l).

The samples mounted on radius 85 and 125 mm are oriented towards the pot wall and experienced the most significant pitting. The two most brittle materials, but overall best performing in terms of wear resistance were compared (material FM and TM). As Figure 6-5 shows, that pits were found to be deeper on the specimen surfaces which were mounted on radius 125 mm. The theoretical 0.6 m/s

difference in sliding speed and the more severe effect of the abrasive media due to the centrifugal force could be an explanation for the more severe pitting on the samples mounted on radius 125 mm. This observation is in line with the study of Shitole [134] regarding the effect of impacting particle kinetic energy on slurry erosive wear.

Pitting was observed to be a result of not a single, but repeated cyclic deformation. The investigation of the pit crater bottom surface showed the presence of micro-cracks and uneven material surface. Examples for these pit surfaces are shown in Figure 6-6.

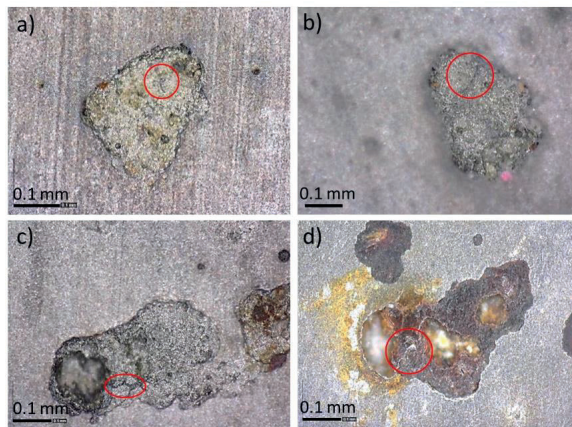


Figure 6-6 Pit surface microscopy (520x magnification): micro-crack initiation at the bottom pit surface (a), and more propagated cracks (b, c, d)

In contact mechanics, the highest stress in the material is below the contact surface with a few μm , according to Hertz contact theory [145]. Due to the dynamic loading, plastic deformation of the material occurs with dislocation formation leading to the spread of micro-cracks beneath the surface. These could merge and reach the surface resulting in a crater. The uneven, not polished surface with signs of micro-cracks of this crater/pit confirms the described formation process. These features (highlighted with red circles) could be identified on high magnification images taken from the bottom surface of the pits.

The pitting was found to be more significant with the circumferential distance travelled by specimen Figure 6-7. The number and the size of the pits grew in the function of the operation time. The higher impact (kinetic) energy on radius 125 mm resulted in larger pits than on radius 85 mm. The growth and spread of this phenomenon increase at the top part of the worn zone as the sliding distance increases. Hence, the pits are not a result of a single-cycle deformation and material is not removed through a single impact.

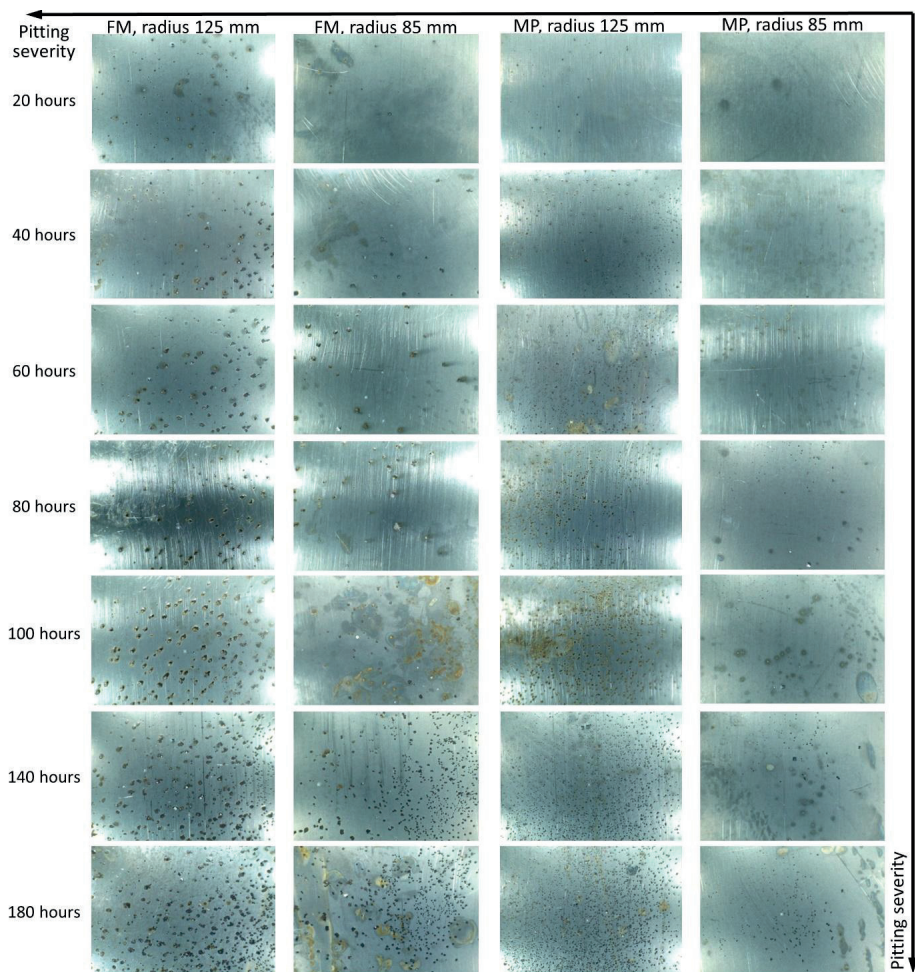


Figure 6-7 Progression of pitting on slurry pot specimen material FM and MP

High-speed camera videos made with 2000 fps on 1280x1024 resolution aids to understand the media equilibrium state during the operation with the media mixing and flowing back. The videos enable to track individual corundum particle motion (velocity vector: direction, sense and magnitude) and calculate/validate impact and impact energy. It was possible through painted corundum particles with i-SPEED pro program. The measurement set-up is shown in Figure 6-8.

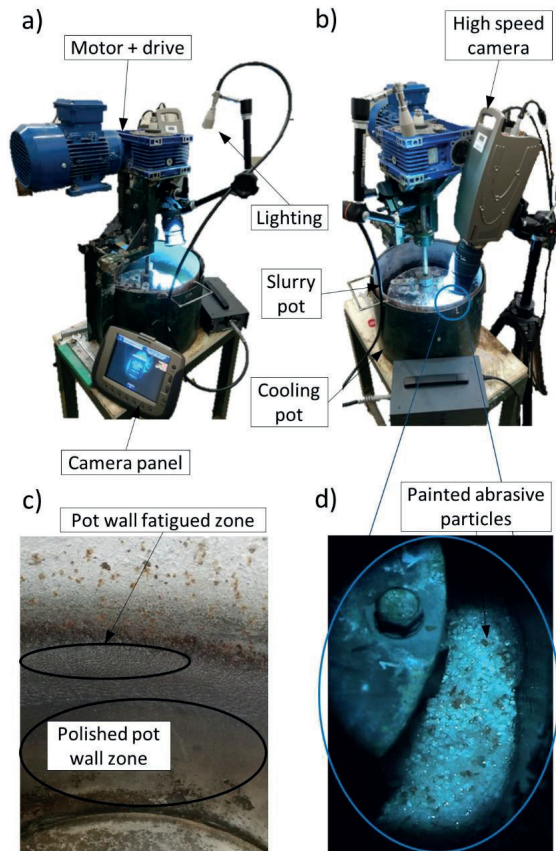


Figure 6-8 Slurry pot test set-up with high-speed camera (a, b), pot inside surface after wear tests (c), high-speed camera image (d)

Images from the high-speed camera recordings highlighting the movement of the tracked abrasive particles are shown in Figure 6-9. To be able to track individual particle movements, some corundum particles were painted for the high-speed camera recording. This contrast enables the software to keep track of the individual particle trajectory. After the given reference input, the software calculates the velocity vector for the given points/particles. This verified the surface speed and highlighted that the motion trajectory of the particles relative to the specimen results in impact with the top part of the specimen. The recordings confirmed the post-mortem identified wear mechanisms observed on the slurry pot specimen. Impact angle varies in real testing stochastically within the 3D turbulent flow. Using high-speed camera and painted corundum particles it was verified that specimen surface oriented in 135° suffered more frequent direct hit from the abrasive particles. Additionally, secondary impacts were also noted due to the bounce back of abrasives from the pot wall hitting back at the

specimen surface. In case of the 45° orientation the tangential slide of the particles on the specimen surface was found to be dominant.

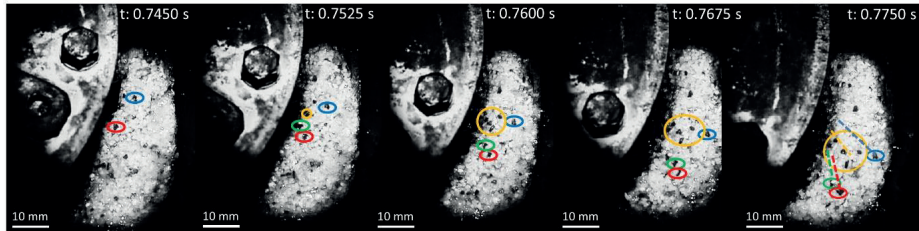


Figure 6-9 Images from high-speed camera recordings, highlighting the movement of the tracked painted abrasive particles

The summarized actions from the videos are described in this paragraph.

Setup: The specimens are circulating on their given radius in the slurry, while media backflow and abrasive media equalizing are observed in the void track of the specimen due to the 3D turbulent water flow.

Impact: The initial contact between an individual particle and the specimen happens on the top of the slurry level (in the low density media region) in the form of reverse impact.

The top specimen area rams in the lower density media part, where it hits different individual abrasive particles. Due to the chaotic, 3D turbulent flow of the slurry, the angle of these impacts vary stochastically. However, specimen oriented towards the pot wall was observed to suffer more direct impacts (see colored particle trajectories Figure 6-9).

After the impact: The particle gets a speed vector (direction, movement) from the contact and is bounced off from the specimen towards the pot wall. Because of this mechanism, a fatigued zone on the pot wall was also observed in the low density media level part (Figure 6-8-d).

After the collision, the specimen continues to run on its forced track on the given radius.

A void track is left after the specimen, but the cycle continues with the media re-equalization.

In parallel, the rest of the specimens below the water is continuously sliding and rolling/slipping in the packed and dense slurry.

6.4.4 Hardness investigation

The hardness of the worn zone of the specimens was monitored at regular intervals during the slurry pot tests. Figure 6-10 shows the hardness change of all tested materials as a function of the operating time.

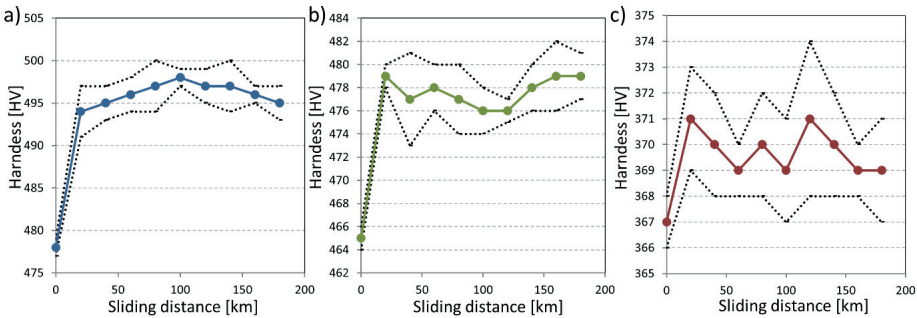


Figure 6-10 The hardness of tested slurry pot specimen in the function of wear testing time (sliding distance) (a) material FM, (b) material TM, (c) material MP [93]

The hardness gain was already present after the first 20 h of testing. The two best-performing martensitic materials experienced an average hardness gain of 15 HV. The MP steel experienced only a minor hardening and a more significant material removal through abrasion mechanism.

6.4.5 Multiple linear regression models and sensitivity analysis

Similar analysis based on multiple linear regression models were carried out to study the sensitivity of material properties and test system parameters on the wear. The independent variables were the sliding distance s , the sliding velocity v , and the orientation angle α , and furthermore the material properties and the indicators based on them. The mass loss is normalized Δm^* with the contact area to exclude the different areas of contact originating from the different radii. According to this, the best fitting model for the wear of the possible ones was

$$\Delta m^* = a_0 + a_1s + a_2\alpha + a_3v \tag{5.1}$$

Since $F = 65$ and $p < 0.001$, it means the model is relevant. The coefficients of it are presented in Table 6-2.

Table 6-2 Coefficients of the regression model for slurry pot test [93]

Model	Coefficient	Standardized Regression Coefficient, Beta	t	p
Constant	-0.854		-1.157	<0.001
s	0.00001	0.476	7.891	<0.001
α	-0.045	-0.680	-10.709	<0.001
v	3.336	0.378	5.663	<0.001

For this model, the goodness-of-fit is $R^2 = 0.626$. The sliding distance has the highest influence on the wear of the test sample, followed by the orientation angle and the velocity. The effect of material parameters is negligible. The model confirmed the less dominant role of the impact velocity compared to the orientation angle (as concluded from Figure 6-2) in this test system.

The best fitting model among the possible ones for the hardness gain was

$$\Delta H = a_0 + a_1 \frac{W\sigma_Y}{E} + a_2 s + a_3 \frac{E_c}{\sigma_c} \tag{5.2}$$

The model is relevant (F-value was 8959 and $p < 0.001$). The coefficients of the model are presented in detail in Table 6-3.

Table 6-3 Coefficients of the regression model for slurry pot test [93]

Model	Coefficient	Standardized Regression Coefficient, Beta	t	p
Constant	7541.733		12.438	<0.001
$\frac{W\sigma_Y}{E}$	-77,274.537	-1.275	-16.060	<0.001
s	0.001	0.030	4.965	<0.001
$\frac{E_c}{\sigma_c}$	-30.240	-0.279	-3.510	<0.001

For this model, the goodness-of-fit is $R^2 = 0.996$. From the material parameters ($W\sigma_Y/E$) had the highest effect on the hardness change. The compression strength and modulus (E_c/σ_c) also played a role as well as the time of the experiment (sliding distance).

The change in the surface topography of the tested specimens was investigated with an optical profilometer (Figure 6-11). Before testing, the surface roughness parameters of all specimens were similar due to the same manufacturing process. The surface roughness values after testing of the specimens experiencing largest wear are shown in Table 6-4. The surface of the contact area roughened and also experienced minor pitting due to the abrasive erosion. TM material surface roughened most, indicating a less effective material removal through abrasive polishing, which was confirmed by the mass loss plots (Figure 6-2).

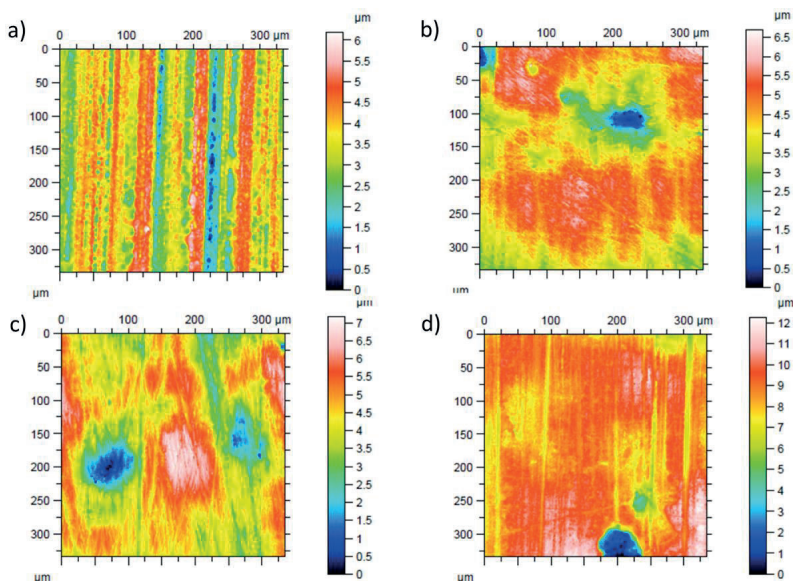


Figure 6-11 2D surface roughness of the tested materials from radius 105 mm, 45° after 11.4 km run
(a) unworn, (b) FM, (c) TM, (d) MP [93]

For all cases, the results are polished surfaces in different degrees with micro-cut grooves indicating abrasion, as well as co-existing micro-pits in different severity due to the abrasive erosion.

Table 6-4 Surface roughness parameters of the tested materials after 180 h testing on radius 105 mm with 45° impact angle and the change in %.

Parameter	Name	Unit	FM	%	TM	%	MP	%
Ra	Arithmetical mean height	[μm]	0.382	+5	0.4185	+24	0.410	+21
Rz	Max. height	[μm]	1.744	+4	1.929	+27	1.903	+23
Rp	Highest peak	[μm]	0.889	+8	0.9835	+29	0.987	+27
Rv	Lowest valley	[μm]	0.855	+1	0.946	+24	0.916	+19
Rt	Total height	[μm]	6.928	+184	12.0945	+483	10.763	+398
Rc	Average height of profile element	[μm]	1.215	-3	1.533	+30	1.42	+17
Rq	Root mean square height	[μm]	0.476	+6	0.5165	+27	0.506	+23
Rsm	Mean width of profile elements	[μm]	347.327	+3	354.292	+1	345.168	-2
Rsk	Skewness	-	0.108	-418	0.1055	+254	0.133	+359
Rku	Kurtosis	-	2.489	+1	2.5205	+5	2.508	+2

Similarly to the previous discussions, multiple linear regression models were evaluated to see the dependence of the surface roughness parameters on the duration of the test (sliding distance), the velocity of the test specimen, the orientation angle, and the material properties. Since the roughness parameters of the examined materials have a high deviation, for most of the models the goodness-of-fit varied in a large extent (between 0.27 and 0.72) and mostly, only one explanatory variable had a significant effect. Change in the surface roughness parameters of Ra, Rt, Rz, Rp, Rv Rc, Rq, and Rsm

followed the same trend, where the sliding distance in the experiment has the highest effect on the change of the roughness parameter, e.g., the best fitting model among the possible ones for Rt was

$$\Delta Rt = a_0 + a_1s \tag{5.3}$$

The model is relevant (F = 83 and *p* < 0.001). Table 6-5 summarizes the coefficients of the model.

Table 6-5 Coefficients of the regression model for slurry pot test [93]

Model	Coefficient	Standardized Regression Coefficient, Beta	t	p
Constant	2.504		3.592	<0.001
s	0.001	0.890	9.132	<0.001

For this model, the goodness-of-fit is R² = 0.782. The sliding distance in the experiment has the highest effect on the Rt. The effect of other parameters was negligible. However, the Rsk surface roughness parameter showed different results. The best fitting model among the possible ones for Rsk was

$$\Delta Rsk = a_0 + a_1v + a_2s \tag{5.4}$$

The model is relevant since F = 7 and *p* < 0.001. The coefficients of the model are presented in Table 6-6.


Table 6-6 Coefficients of the regression model for slurry pot test [93]

Model	Coefficient	Standardized Regression Coefficient, Beta	t	p
Constant	0.233		3.371	<0.001
v	-0.155	-0.555	-3.203	<0.001
s	0.001	0.452	2.609	0.001

For this model, the goodness-of-fit is R² = 0.401. The sliding velocity in the experiment has the highest effect on the Rsk of the worn surface followed by the sliding distance.

Table 6-7 summarizes the abrasive sensitivity for wear, hardness change, and the resulted surface roughness parameters based on the results of the above discussed linear models. The factors are presented in increasing order of effect.

Table 6-7 Abrasive sensitivity ranking to slurry pot system variables [93]

Effect of influencing factors 		$\frac{W\sigma_Y}{E}$	s				
	s					v	
	α	s				s	
	v	$\frac{E_c}{\sigma_c}$					
Independent variable	Δm^*	ΔH	$Ra, Rz, Rp, Rv, Rt, Rc, Rq, Rsm, Rku$				Rsk

6.5 Conclusions from multi-asperity slurry pot testing

This testing configuration served as an intermediate test between the real time application and the standardised lab-scale tests. Although the test system was not representative in terms of operating conditions to the field-tests, the co-existing wear mechanisms were reproduced and studied. The test configuration enabled to investigate the thin differentiation border between the experienced wear mechanisms in the same set-up. The developed slurry pot test rig enabled a comparison in wear rate and provided a quick ranking with adequate repetition for each test. The ranked materials resulted in the same wear resistance order in slurry abrasion-erosion conditions as in the standardised abrasion laboratory tests. The analysis was successful to highlight the appearance of different wear mechanisms and to investigate the effect of operational parameters on the wear damage. The sliding speed and the specimen orientation angle was found to have a significant effect on the wear, followed by the sliding distance. The effect of material factors was negligible.

The wear process was found to develop on a linear trend. A polished zone with abrasion scars was formed at the bottom of the samples, where sliding and rolling was the dominant contact mechanism below the surface level of the abrasive media. Pitting appeared as a characteristic feature on the specimen zone which was in contact with the top level of the abrasive media, where the dominant contact mechanism was repeated cyclic impact in the form of slurry erosion resulting in surface fatigue. Orientation of the specimen had more effect on the wear rate than the circumferential velocity. Specimen oriented towards the centre shaft experienced severe wear compared to the ones oriented to face the pot wall due to the particle flow characteristics and the effect of the centrifugal force. The orientation angle of the specimen, thus the impact angle of the particles influenced the appearance of surface fatigue in the form of pitting. The pitting was dominant on the specimen oriented towards the pot wall and was found to be more severe with increasing impact velocity and operation time as a result of the repeated cyclic impacts. More significant pitting surface damage was observed on the more brittle martensitic materials. Analysis with white light interferometer of the sample 3D geometry showed that the specimen shape change due to wear over time, confirming that abrasion resulted in more severe material loss than pitting. High-speed camera recordings highlighted the different specimen-particle contact mechanisms on the top of the slurry. The videos illustrate the different observed wear mechanisms. Repeated particle impingement was traced in the top specimen zone resulting in pitting in case of specimen surface oriented in 135° . In the 45° orientated specimen the tangential slide of the abrasive particles was found to be dominant. The wear from slurry pot testing is one order of magnitude less than the in-field and multi-asperity tests. The hardness gain was already present after the first 20 hours of run, which was the case for the tines during the in-field investigation. TM material performed best in terms of wear rate in the comparison, although it suffered significant pitting due to its more brittle characteristics than the MP steel.

7 CHAPTER 7

CONCLUSIONS

This chapter summarizes the connection of the multi-level investigation and the main conclusions of this research work. The conclusions are followed by recommendations for possible future work.



7.1 Connection of multi-scale testing

Besides the wear analysis on the tines the soil was also investigated for mineralogy with X-ray diffraction and mechanical analysis. The investigation pointed out, that the tines were tested in a soil with 32% of coarse sand (>0.25 mm) and 47% of fine sand (0.25-0.05 mm) (Table 7-1). Accordingly the selection of abrasive particle size for the laboratory tests was carried out to provide the same size range in grit diameter.

Table 7-1 Comparison of soil abrasive particle size with corresponding lab-test abrasive counterface

Soil sample			Abrasive size	
Mechanical analyses	Sandy loam	Loamy sand	Single-asperity Tip radius [μm]	Multi-asperity Grit size
>0.25 mm [m/m%] coarse sand	32.06	35.17	200	P80
0.25-0.05 mm [m/m%] fine sand	47.91	35.29	200	P80
0.05-0.02 mm [m/m%] sandy silt	6.51	5.65	100-50-25	P120-P180
0.02-0.01 mm [m/m%] silt	4.32	4.50	25	P800

The wear micro-mechanisms were replicated in both the micro-level (single asperity) testing and in the macro-level (multi-asperity) investigation. Both methods resulted in similar materials ranking in terms of wear rate. However, the single asperity test resulted in a bigger difference in the wear rate of the tested materials due to the difference of the material’s hardened surface state.

The degree of penetration is considered to be the bridging factor between the micro-and the macro-scale testing. The grooves profiles and geometry made with single-asperity tests were proportionally visualised and were compared to the average groove data obtained from the different tine segments from the in-field analysis (Figure 7-1).

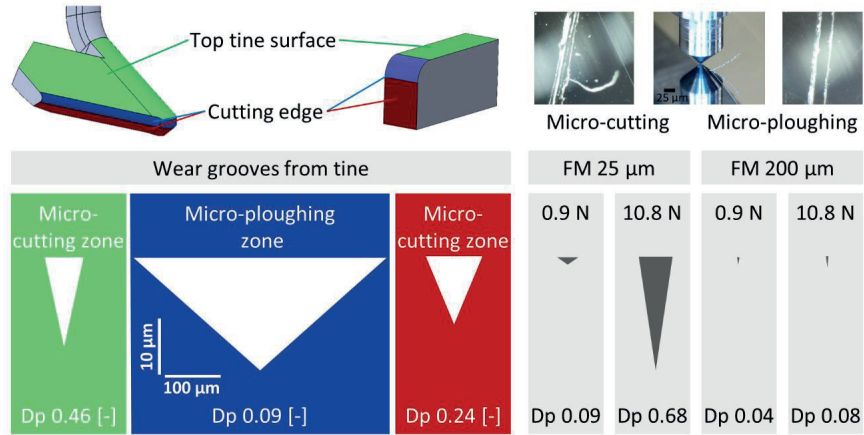


Figure 7-1 Average proportional groove profile comparison between differentiated tine surfaces and single-asperity test results

In case of single-asperity testing the micro-ploughing regime was achieved using low loads and hence material is plastically deformed and not removed in this case. At low contact pressures, the spherical part of the tip comes into contact with the worn surface. This results in low attack angles, leading to the micro-ploughing regime. Tests with 25 μm indenter tip radius and highest load (10.8 N) resulted in highest D_p .

The grooves profiles and geometry made with multi-asperity tests were proportionally visualised and were also compared to the average groove data obtained from the different tine segments from the in-field analysis. The comparison is shown in Figure 7-2. Regarding the multi-asperity tests, the groove geometries of the tine top surface and cutting edge are in the same order of magnitude as for the P80 tests. P80 test (200 μm) is most representative for the in-field test. All the D_p values of the tine surfaces are within the range of the P80 tests, hence each micro-mechanism regime of the tine surface was attained.

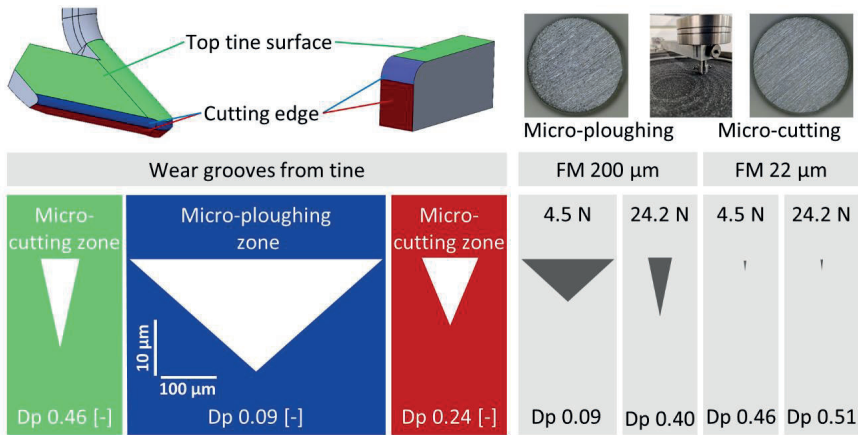


Figure 7-2 Average proportional groove profile comparison between differentiated tine surfaces and multi-asperity test results

A further connecting link between the testing methods is ensured by using the same abrading particle size range. In the single-asperity scratch testing, an advanced optical system was utilised for monitoring the wear particle generation. Both multi- and single-asperity contact was investigated in this study to make a connection between micro-and macro-scale of the abrasion process. The obtained results from both tests indicate the unnecessary character of performing both investigation methods; time and testing costs can thus be saved.

The differences in the results obtained in both single- and multi-asperity contact testing were studied. Single-asperity tests resulted in bigger differences in the wear rate of the tested materials compared to the multi-asperity tests. These were obtained with more ideal conditions of single-asperity lab

testing where the abrasive particle size and the attack angle are clearly defined as well as the load. In the multi-asperity testing more uncertainties are introduced with the abrasive papers having some distribution of abrasive particle size and statistically distributed attack angle. On the other hand, in the case of multi-asperity testing, samples experience work hardening at the contact surface due to multiple contacts. Subsurface work-hardening of the tested materials was observed through hardness measurements and SEM (tribo-layer). In this tribo-layer, plastic deformation observed through grain refinement underneath the contact surface indicated the predominant ploughing wear micro-mechanism in the materials. Low load test conditions resulted in a more wavy, plastically deformed contact surface with compressed grains in the tribo-layer. In the case of 24.2 N tests, traces of material shear was observed on the boundary of the contact surface indicating a dominant micro-cutting mechanism. In the case of the single-asperity test, the diamond indenter is in contact with the fresh material surface at every new contact. The ranking of the materials regarding wear resistance was the same under the testing conditions in both configurations.

The important factor for comparison of single-asperity and multi-asperity tests to the real application is D_p of wear grooves and the abrasion wear micro-mechanism. The calculated D_p values from the surface topographic measurement during the single-asperity tests are in the same range as that of the tines. All micro-mechanisms observed on the tine surface were experimentally simulated with the 25 μm tip radius single-asperity tests. The reproduced wear micro-mechanisms were verified via microscopic inspection of characteristic wear features, such as wedge and chip formation. The specific wear rate obtained from the single-asperity tests was in the same range as from the in-field test, shown in Table 7-2.

From the multi-asperity tests, it is evident that the wear of tine materials can be experimentally simulated using ASTM G132 pin abrasion testing. All the D_p values registered from the real tine component surfaces are within the range of the multi-asperity tests with P80 abrasive size. A comparison of average wear rate from multi-asperity tests with in field tests is shown in Table 7-2. The wear rate is in the same range as measured during the field investigation. Hardening effect was evident in case of all the tests, similar to the values measured on the tines.

The summary is shown in Table 7-2.

Table 7-2 Comparison of lab-scale tests with in-field results regarding wear micro-mechanisms and wear rate

Investigation	Type	Wear micro-mechanism	Wear rate [g/km] *specific wear rate [mm ³ /Nm]
In-field	Real component (tine)	Micro-ploughing, Wedge formation, Micro-cutting, Micro-fatigue	3.80 g/km *0.07 mm ³ /Nm
Single-asperity	Standardised lab-test simplified	Micro-ploughing, Wedge formation, Micro-cutting	*0.03-0.05 mm ³ /Nm
Multi-asperity	Standardised lab-scale test	Micro-ploughing, Wedge formation, Micro-cutting	2.7-4.1 g/km *0.013-0.10 mm ³ /Nm
Slurry pot	Intermediate custom made lab-test	Micro-ploughing, Wedge formation, Micro-cutting, Micro-fatigue	6.51-8.37 g/100 km

7.2 Main research conclusions

Based on the mass loss measurements and change in geometrical dimensions the wear trends obtained from the in-field test are in good agreement with literature of symmetrical goose foot tines. As an outcome of the in-field testing, sector specific wear mechanisms were identified in different regions of an individual tine. Two dominant micro-mechanisms, micro-cutting and micro-ploughing, were observed. The material removal was concluded to be dominant along the tine cutting edges in the form of micro-cutting ($D_p \sim 0.4$). This indicated that future design of tine materials should be focused to enhance the wear resistance against micro-cutting, which could prolong lifetime of the tines and hence reduce economic losses.

To understand the micro-mechanism and to relate them precisely between the different scales from single asperity to real application a multi-level investigation approach was used. This study investigated the abrasive wear behaviour of newly developed martensitic and multiphase steels and enabled their ranking in different abrasion conditions. Three different test systems represented a broad range of the abrasive wear mechanism, simulating different material responses to the complex appearance of abrasion in the targeted wear parts. Figure 7-3 highlights a brief overview of the investigation approach and the connection between the different test systems. Considering the three scales of testing, it was evident that the degree of penetration, wear micro-mechanism and wear rate are in-line with each other. Comparing the test systems, the tested materials ranked similarly based on their wear performance, however, in each configuration, the dominant variable of the wear mechanism differed.

The wear micro-mechanisms were replicated in both the micro-level (single asperity) testing and in the macro-level (multi-asperity) investigation. All methods resulted in similar materials ranking in terms of wear rate. However, the single asperity test resulted in a larger difference in the wear rate of the tested materials due to the difference of the material's hardened surface state. The martensitic materials with higher hardness reached micro-cutting regime in a more narrow range of testing conditions. Despite the similar microstructure and hardness, based on the “k” abrasive wear resistance rate, a clear difference was seen between TM and FM steels. The tempered martensitic TM material structure enabled smaller micro-cutting wear due to a good combination of initial hardness/strength and toughness, while the fresh martensitic structure showed 30% higher wear rate. It was confirmed that toughness/ductility does play a role in wear resistance (e.g. FM vs TM) but it has to be combined with sufficient hardness. The right balance of hardness-toughness needs to be found for each given type of application or wear test.

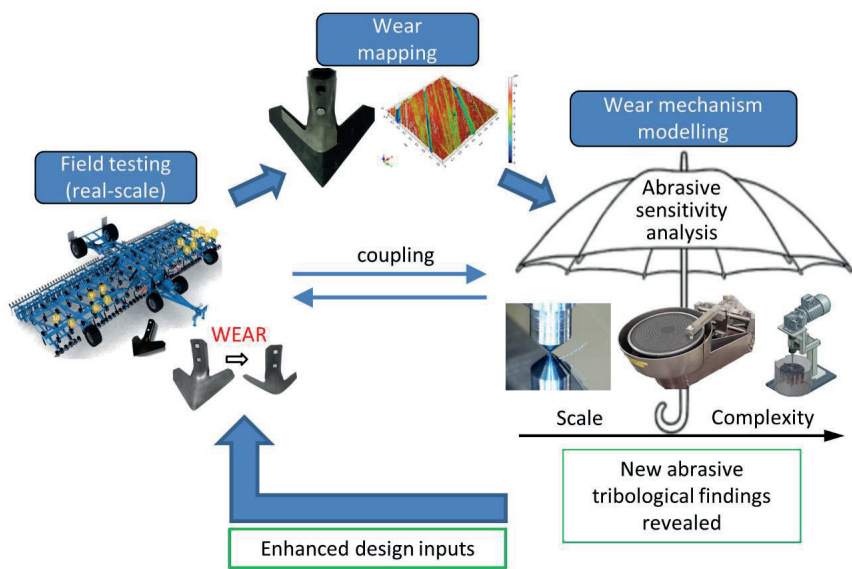


Figure 7-3 Connection of wear investigations

The significance and contribution of test parameters, extended material properties, and some derived dimensionless groups to wear behaviour and surface deformation were investigated. Correlation between parameters was obtained by multiple linear regression models.

In terms of wear resistance, the tempered martensitic steel performed best across all the investigated test systems, closely followed by the fresh martensitic structured material. The multiphase steel resulted in the most severe material loss.

The normal load was the driving factor in the material removal in the abrasive scratch tests, followed by the sliding distance. The dimensionless number $(WEH/\sigma_M\sigma_Y)$ had a moderate effect, while the indenter tip radius had a slight influence on the wear mechanism. The dominant variable affecting the surface topography of the materials in the scratch tests was found to be the normal load, followed by the tip radius. However, sensitivity to the material's compression properties (E_c, σ_c) was found in case of groove depth and groove area. The width of the scratch was influenced by the parameter $(W\sigma_Y/E)$.

In the abrasive pin-on-disk test system, the sliding distance and the abrasive particle size were found to be dominant on the wear severity, followed by the normal load. From the material parameters $(\sigma_Y/\sigma_c\epsilon_B)$ had a slight effect. Considering the worn surface topography, the particle size was found to be the dominant shaping factor followed by the sliding distance. The effect of $(\sigma_Y E/\sigma_M H)$ on the microgeometry was clear in the case of the parameters Rsm and Rsk. Considering the hardness change, the parameter $(W\sigma_Y/E)$ was found to have a significant effect, the model describing the hardness change resulted an R^2 value of 0.994. Proportional relations between the wear values of the materials and the dimensionless numbers of (σ_M/σ_Y) , as well as $(H\epsilon_B/\sigma_Y)$ were established in case of the most severe wear testing conditions (P80, 24.2 N). There are reciprocal relations between values (H/E) , $(\sigma_Y/\sigma_c\epsilon_B)$, (ϵ_B/ϵ_M) , (E_c/σ_c) and the wear of the materials. Increasing these dimensionless number values resulted in lower wear.

In the slurry pot test system, the sliding speed and the specimen orientation angle was found to have a significant effect on the wear, followed by the sliding distance. The effect of material factors was negligible in this case. Considering the surface deformation, only the sliding distance appeared to have a significant effect on the worn surface topography. Specimen experienced hardening of the abraded contact surface, which remained approximately constant afterward. Sensitivity analysis proved that for the hardness gain, the variable $(W\sigma_Y/E)$ had a significant influence. The material's compression properties (E_c, σ_c) were also found to have an effect.

Mathematical models were developed to determine the relationship between the wear, change of surface parameters and the test variables, material properties, and derived dimensionless groups. This investigation aids the design of an optimized tribo-system by enabling the prediction of the wear process in complex abrasive environment for the investigated steels.

7.3 Recommendations for further study

First, as an expansion of the current research work with the already used laboratory tests could focus on further material optimization of the tines. Application of hybrid materials, composites and coatings (e.g. ceramic coatings, welded hard layers) could be considered for further lifetime improvement.

A further possibility to improve the wear resistance is to change the tine geometry. The effects of change in cutting edge geometry can be investigated using the DEM model and evaluated with regards to the wear risk using the relative movement and the load on the tine. Therefore an accurate description of soil-tool interaction can help to reduce draft force through the optimization of tool geometry. Different simulation methods, FEA, DEM, and CFD have been already used over the years to simulate the soil-tool interaction and design agricultural tools based on the outcome of the simulations. The further extension of the initial DEM model mentioned in chapter 2.3.5 could help in understanding the physical test results by linking them through mechanisms as well as in leveraging the validated models for simulation-based optimization, thus reducing the number of costly physical experiments. In addition, the physics-based models could determine optimal conditions, which are far from the current operating regimes. However, investigation about precise input data and verification of the simulation would be needed. Therefore, extended data collection from the real parts is necessary.

Another possibility could be the further development of the tribological test systems. Traditionally, ground engaging tillage tools are developed by constructing parts and running physical tests in the field, resulting in adjustments of the design based on the obtained results. This ‘constructional design’ process is costly due to the manufacturing of the required parts and subsequently running the tests. An intermediate scale test, where the real tines could be investigated (e.g. large-scale soil bin tester) could provide beneficial data for the input for DEM. This method enables to perform repeatable tests that would be difficult to carry-out under real conditions in the field. Investigation could take place in a chosen soil with its fixed properties and composition as well as compaction on real tines with operation parameters matching the in-field run. Another advantage is the independence of the experimental procedure with respect to weather and season. Online data collection from this investigation would be beneficial. Equipping the investigated tines with sensors (e.g. pressure sensors to monitor draft force) would provide a crucial input data for the DEM simulation.

8 REFERENCES

- [1] H. P. Jost, "Tribology — Origin and future," *Wear*, vol. 136, no. 1, pp. 1–17, Feb. 1990, doi: 10.1016/0043-1648(90)90068-L.
- [2] G. Mohapatra and S. S. Sahay, "Wear and Tribology in Agricultural Machinery," *Friction, Lubrication, and Wear Technology*, pp. 984–1002, Dec. 2017, doi: 10.31399/ASM.HB.V18.A0006386.
- [3] A. Khan and A. Khan, "Tillage and Crop Production," *Agronomic Crops: Volume 1: Production Technologies*, pp. 115–129, Jan. 2019, doi: 10.1007/978-981-32-9151-5_7.
- [4] V. V. Singh, U. Kumar, and A. Kumar, "Tillage implements," *Data book for agricultural machinery design*, 2004. http://www.agritech.tnau.ac.in/agriculture/agri_tillage_tillageimplements.html (accessed Nov. 30, 2021).
- [5] R. Bednář, J. Votava, J. Červinka, and M. Fajman, "Suitability of technical materials for machinery subsoilers for soil tillage," *Acta Universitatis Agriculturae et Silviculturae Mendelianae Brunensis*, vol. 61, no. 1, pp. 9–16, Apr. 2013, doi: 10.11118/actaun201361010009.
- [6] "Solis Tractor Implements | The Best Tractor Implements." <https://solisworld.com/complete-implements-solution/> (accessed Dec. 13, 2021).
- [7] K. Kato and K. Adachi, "Wear mechanisms," in *Modern Tribology Handbook*, CRC Press, 2001, pp. 273–300.
- [8] J. A. Williams, "Wear and wear particles—some fundamentals," *Tribology International*, vol. 38, no. 10, pp. 863–870, Oct. 2005, doi: 10.1016/j.triboint.2005.03.007.
- [9] T. S. Eyre, "Wear characteristics of metals," *Tribology International*, vol. 9, no. 5, pp. 203–212, Oct. 1976, doi: 10.1016/0301-679X(76)90077-3.
- [10] K.-H. Zum Gahr, *Microstructure and Wear of Materials*, 1st ed. Elsevier Science Publishers, 1987.
- [11] S. J. Rosenber, *Resistance of steels to abrasion by sand*. Forgotten Books, 2018.
- [12] H. J. Yu and S. D. Bhole, "Development of a prototype abrasive wear tester for tillage tool materials," *Tribology International*, vol. 23, no. 5, pp. 309–316, Oct. 1990, doi: 10.1016/0301-679X(90)90004-9.
- [13] E. Rabinowicz, L. A. Dunn, and P. G. Russell, "A study of abrasive wear under three-body conditions," *Wear*, vol. 4, no. 5, pp. 345–355, Sep. 1961, doi: 10.1016/0043-1648(61)90002-3.
- [14] J. H. Tylczak and A. Oregon, "Abrasive wear," in *ASM Handbook - Friction, Lubrication, and Wear Technology*, P. J. Blau, Ed. ASM International, 1992, pp. 184–190.
- [15] G. K. Budinski, *Guide to friction, wear and erosion testing*. ASTM International, 2007.
- [16] Canadian National Research Council Associate Committee on Tribology, "A Strategy for Tribology in Canada: Enhancing Reliability and Efficiency Through the Reduction of Wear and Friction," Ottawa, ON, 1986.
- [17] D. Gupta and A. K. Sharma, "Investigation on sliding wear performance of WC10Co2Ni cladding developed through microwave irradiation," *Wear*, vol. 271, no. 9–10, pp. 1642–1650, Jul. 2011, doi: 10.1016/j.wear.2010.12.037.
- [18] S. Ma, S. Zheng, D. Cao, and H. Guo, "Anti-wear and friction performance of ZrO₂ nanoparticles as lubricant additive," *Particuology*, vol. 8, no. 5, pp. 468–472, Oct. 2010, doi: 10.1016/j.partic.2009.06.007.
- [19] A. D. Sarkar and J. Clarke, "Friction and wear of aluminium-silicon alloys," *Wear*, vol. 61, no. 1, pp. 157–167, Jun. 1980, doi: 10.1016/0043-1648(80)90120-9.
- [20] "Sustainability is Driving the Future of Agriculture | Bayer." <https://www.bayer.com/en/investors/agriculture-megatrends> (accessed Mar. 12, 2022).
- [21] Á. Kalácska, P. De Baets, D. Fauconnier, F. Schramm, L. Frerichs, and J. Sukumaran, "Abrasive wear behaviour of 27MnB5 steel used in agricultural tines," *Wear*, vol. 442–443, p. 203107, Feb.

- 2020, doi: 10.1016/j.wear.2019.203107.
- [22] J. Rendón and M. Olsson, "Abrasive wear resistance of some commercial abrasion resistant steels evaluated by laboratory test methods," *Wear*, vol. 267, no. 11, pp. 2055–2061, Oct. 2009, doi: 10.1016/j.wear.2009.08.005.
 - [23] Y. Xie, J. (Jimmy) Jiang, K. Y. Tufa, and S. Yick, "Wear resistance of materials used for slurry transport," *Wear*, vol. 332–333, pp. 1104–1110, May 2015, doi: 10.1016/j.wear.2015.01.005.
 - [24] S. Ahmed, O. P. Thakare, R. Shrivastava, S. Sharma, and S. G. Sapate, "A Review On Slurry Abrasion Of Hard Faced Steels," *Materials Today: Proceedings*, vol. 5, no. 2, pp. 3524–3532, 2018, doi: 10.1016/j.matpr.2017.11.600.
 - [25] S. G. Sapate, A. D. Chopde, P. M. Nimbalkar, and D. K. Chandrakar, "Effect of microstructure on slurry abrasion response of En-31 steel," *Materials & Design*, vol. 29, no. 3, pp. 613–621, Jan. 2008, doi: 10.1016/j.matdes.2007.02.014.
 - [26] M. Bootle, "Wear in rotodynamic (centrifugal) slurry pumps," *Proceedings of the Calgary Pump Symposium*, 2009.
 - [27] V. Javaheri, D. Porter, and V.-T. Kuokkala, "Slurry erosion of steel – Review of tests, mechanisms and materials," *Wear*, vol. 408–409, pp. 248–273, Aug. 2018, doi: 10.1016/j.wear.2018.05.010.
 - [28] J. Camacho, R. Lewis, and R. S. Dwyer-Joyce, "Solid particle erosion caused by rice grains," *Wear*, vol. 267, no. 1–4, pp. 223–232, Jun. 2009, doi: 10.1016/j.wear.2008.12.034.
 - [29] H. Muhandes, Á. Kalácska, L. Székely, R. Keresztes, and G. Kalácska, "Abrasive Sensitivity of Engineering Polymers and a Bio-Composite under Different Abrasive Conditions," *Materials*, vol. 13, no. 22, p. 5239, Nov. 2020, doi: 10.3390/ma13225239.
 - [30] K. Májlinger, G. Kalácska, I. N. Orbulov, L. Zsidai, B. Bozóki, and R. Keresztes, "Global Approach of Tribomechanical Development of Hybrid Aluminium Matrix Syntactic Foams," *Tribology Letters*, vol. 65, no. 1, p. 16, Mar. 2017, doi: 10.1007/s11249-016-0798-0.
 - [31] S. A. Sidorov, V. K. Khoroshenkov, Y. P. Lobachevskii, and T. S. Akhmedova, "Improving Wear Resistance of Agricultural Machine Components by Applying Hard-Alloy Thick-Layer Coatings Using Plasma Surfacing," *Metallurgist*, vol. 60, no. 11–12, pp. 1290–1294, Mar. 2017, doi: 10.1007/S11015-017-0443-7.
 - [32] R. G. Bayer, *Mechanical Wear Fundamentals and Testing*, 2nd ed. New York, USA: Marcel Dekker, 2004.
 - [33] P. J. Blau, *ASM Handbook Volume 18—Friction, Lubrication, and Wear Technology*. Ohio: ASM International, 1992.
 - [34] X. Xu, F. H. Ederveen, S. van der Zwaag, and W. Xu, "Correlating the abrasion resistance of low alloy steels to the standard mechanical properties: A statistical analysis over a larger data set," *Wear*, vol. 368–369, pp. 92–100, Dec. 2016, doi: 10.1016/j.wear.2016.09.014.
 - [35] M. M. Khrushchov, "Principles of abrasive wear," *Wear*, vol. 28, no. 1, pp. 69–88, Apr. 1974, doi: 10.1016/0043-1648(74)90102-1.
 - [36] G. K. Nathan and W. J. D. Jones, "The empirical relationship between abrasive wear and the applied conditions," *Wear*, vol. 9, no. 4, pp. 300–309, Jul. 1966, doi: 10.1016/0043-1648(66)90004-4.
 - [37] J. Goddard and H. Wilman, "A theory of friction and wear during the abrasion of metals," *Wear*, vol. 5, no. 2, pp. 114–135, Mar. 1962, doi: 10.1016/0043-1648(62)90235-1.
 - [38] O. A. Zambrano, Y. Aguilar, J. Valdés, S. A. Rodríguez, and J. J. Coronado, "Effect of normal load on abrasive wear resistance and wear micromechanisms in FeMnAlC alloy and other austenitic steels," *Wear*, vol. 348–349, pp. 61–68, Feb. 2016, doi: 10.1016/j.wear.2015.11.019.
 - [39] X. Ma, R. Liu, and D. Y. Li, "Abrasive wear behavior of D2 tool steel with respect to load and sliding speed under dry sand/rubber wheel abrasion condition," *Wear*, vol. 241, no. 1, pp. 79–85, Jun. 2000, doi: 10.1016/S0043-1648(00)00351-3.
 - [40] T. O. Mulhearn and L. E. Samuels, "The abrasion of metals: A model of the process," *Wear*, vol. 5, no. 6, pp. 478–498, Nov. 1962, doi: 10.1016/0043-1648(62)90064-9.
 - [41] J. Larsen-Badse, "Influence of grit size on the groove formation during sliding abrasion," *Wear*, vol. 11, no. 3, pp. 213–222, Mar. 1968, doi: 10.1016/0043-1648(68)90559-0.

- [42] R. Gåhlin and S. Jacobson, "The particle size effect in abrasion studied by controlled abrasive surfaces," *Wear*, vol. 224, no. 1, pp. 118–125, 1999.
- [43] H. Sin, N. Saka, and N. P. Suh, "Abrasive wear mechanisms and the grit size effect," *Wear*, vol. 55, no. 1, pp. 163–190, Jul. 1979, doi: 10.1016/0043-1648(79)90188-1.
- [44] M. Baig, R. Cook, J. Pratten, and R. Wood, "The effect of shape and size distribution of abrasive particles on the volume loss of enamel using micro-abrasion," *Wear*, vol. 448–449, p. 203212, May 2020, doi: 10.1016/j.wear.2020.203212.
- [45] K. H. Z. Gahr, "Modelling of two-body abrasive wear," *Wear*, vol. 124, no. 1, pp. 87–103, May 1988, doi: 10.1016/0043-1648(88)90236-0.
- [46] P. J. Mutton and J. D. Watson, "Some effects of microstructure on the abrasion resistance of metals," *Wear*, vol. 48, no. 2, pp. 385–398, Jun. 1978, doi: 10.1016/0043-1648(78)90234-X.
- [47] A. Sundström, J. Rendón, and M. Olsson, "Wear behaviour of some low alloyed steels under combined impact/abrasion contact conditions," *Wear*, vol. 250, no. 1–12, pp. 744–754, Oct. 2001, doi: 10.1016/S0043-1648(01)00712-8.
- [48] X. Deng, Z. Wang, Y. Tian, T. Fu, and G. Wang, "An investigation of mechanical property and three-body impact abrasive wear behavior of a 0.27% C dual phase steel," *Materials & Design*, vol. 49, pp. 220–225, Aug. 2013, doi: 10.1016/j.matdes.2013.01.024.
- [49] O. P. Modi, D. P. Mondal, B. K. Prasad, M. Singh, and H. K. Khaira, "Abrasive wear behaviour of a high carbon steel: effects of microstructure and experimental parameters and correlation with mechanical properties," *Materials Science and Engineering: A*, vol. 343, no. 1–2, pp. 235–242, Feb. 2003, doi: 10.1016/S0921-5093(02)00384-2.
- [50] M. Aksoy, M. B. Karamiş, and E. Evin, "An evaluation of the wear behaviour of a dual-phase low-carbon steel," *Wear*, vol. 193, no. 2, pp. 248–252, May 1996, doi: 10.1016/0043-1648(95)06796-5.
- [51] A. K. Jha, B. K. Prasad, O. P. Modi, S. Das, and A. H. Yegneswaran, "Correlating microstructural features and mechanical properties with abrasion resistance of a high strength low alloy steel," *Wear*, vol. 254, no. 1–2, pp. 120–128, Jan. 2003, doi: 10.1016/S0043-1648(02)00309-5.
- [52] X. Xu, S. van der Zwaag, and W. Xu, "The effect of martensite volume fraction on the scratch and abrasion resistance of a ferrite–martensite dual phase steel," *Wear*, vol. 348–349, pp. 80–88, Feb. 2016, doi: 10.1016/j.wear.2015.11.017.
- [53] W. Chen, S. Biswas, A. Roberts, J. O'Shea, and K. Williams, "Abrasion wear resistance of wall lining materials in bins and chutes during iron ore mining," *International Journal of Mineral Processing*, vol. 167, pp. 42–48, Oct. 2017, doi: 10.1016/j.minpro.2017.08.002.
- [54] F. Aydin, "The investigation of the effect of particle size on wear performance of AA7075/Al2O3 composites using statistical analysis and different machine learning methods," *Advanced Powder Technology*, vol. 32, no. 2, pp. 445–463, Feb. 2021, doi: 10.1016/j.appt.2020.12.024.
- [55] W. Tsai, J. A. C. Humphrey, I. Cornet, and A. V. Levy, "Experimental measurement of accelerated erosion in a slurry pot tester," *Wear*, vol. 68, no. 3, pp. 289–303, May 1981, doi: 10.1016/0043-1648(81)90178-2.
- [56] A. H. S. Rahiman *et al.*, "Dry sliding wear analysis OF Al5083/CNT/Ni/MoB hybrid composite using DOE Taguchi method," *Wear*, vol. 460–461, p. 203471, Nov. 2020, doi: 10.1016/j.wear.2020.203471.
- [57] A. Bustillo, D. Y. Pimenov, M. Matuszewski, and T. Mikolajczyk, "Using artificial intelligence models for the prediction of surface wear based on surface isotropy levels," *Robotics and Computer-Integrated Manufacturing*, vol. 53, pp. 215–227, Oct. 2018, doi: 10.1016/j.rcim.2018.03.011.
- [58] M. Matuszewski, M. Słomion, A. Mazurkiewicz, and D. Y. Pimenov, "Mathematical models of changes in the surface layer of frictional pairs as a tool to optimize the wear process," *MATEC Web of Conferences*, vol. 182, p. 02008, Jul. 2018, doi: 10.1051/mateconf/201818202008.
- [59] "Allrounder-classic
Köckerling." <https://www.koeckerling.de/en/produkte/tillage/cultivator/allrounder-classic> (accessed Nov. 15, 2021).

- [60] E. McKyes, *Soil Cutting and Tillage*. Amsterdam, The Netherlands: Elsevier Science Publishers, 1985.
- [61] Z. Owsiak, "Wear of symmetrical wedge-shaped tillage tools," *Soil and Tillage Research*, vol. 43, no. 3–4, pp. 295–308, Nov. 1997, doi: 10.1016/S0167-1987(97)00020-2.
- [62] G. Kalacska, "Laboratory modelling of abrasive wear effects of soils," *Cereal Research Communications*, vol. 36, pp. 907–910, 2008.
- [63] S. A. Ferguson, J. M. Fielke, and T. W. Riley, "Wear of cultivator shares in abrasive South Australian soils," *Journal of Agricultural and Engineering Research*, vol. 69, no. 2, pp. 99–105, 1998, doi: 10.1006/jaer.1997.0182.
- [64] A. Natsis, G. Petropoulos, and C. Pandazaras, "Influence of local soil conditions on mouldboard ploughshare abrasive wear," *Tribology International*, vol. 41, no. 3, pp. 151–157, Mar. 2008, doi: 10.1016/j.triboint.2007.06.002.
- [65] J. M. Fielke, T. W. Riley, M. G. Slattery, and R. W. Fitzpatrick, "Comparison of tillage forces and wear rates of pressed and cast cultivator shares," *Soil and Tillage Research*, vol. 25, no. 4, pp. 317–328, Jan. 1993, doi: 10.1016/0167-1987(93)90030-5.
- [66] J. M. Fielke, "Interactions of the Cutting Edge of Tillage Implements with Soil," *Journal of Agricultural Engineering Research*, vol. 63, no. 1, pp. 61–71, Jan. 1996, doi: 10.1006/jaer.1996.0008.
- [67] A. Misra and I. Finnie, "A classification of three-body abrasive wear and design of a new tester," *Wear*, vol. 60, no. 1, pp. 111–121, Apr. 1980, doi: 10.1016/0043-1648(80)90252-5.
- [68] P. Swanson, "Comparison of Laboratory Abrasion Tests and Field Tests of Materials Used in Tillage Equipment," in *Tribology: Wear Test Selection for Design and Application*, no. 1199, 100 Barr Harbor Drive, PO Box C700, West Conshohocken, PA 19428-2959: ASTM International, 1993, pp. 80–80–20.
- [69] H. M. Taylor and H. R. Gardner, "Penetration of cotton seedling taproots as influenced by bulk density, moisture content, and strength of soil," *Soil Science*, vol. 96, pp. 153–156, 1963.
- [70] R. L. Raper, "Subsoiler shapes for site-specific tillage," *Applied Engineering in Agriculture*, vol. 21, no. 1, pp. 25–30, 2005, doi: 10.13031/2013.17906.
- [71] J. G. Hendrick and A. C. Bailey, "Determining Components of Soil-Metal Sliding Resistance," *Transactions of the ASAE*, vol. 25, no. 4, pp. 845–849, Jul. 1982, doi: 10.13031/2013.33625.
- [72] T. Fouda and M. El-Tarhuny, "A Study on Plowshares Wearing Behavior under Conditions of Sandy Loam Soil," *Jordan Journal of Agricultural Sciences*, vol. 6, no. 3, pp. 2010–423, Nov. 2010.
- [73] T. A. Abisuwa and S. I. Manuwa, "Development of Instrumentation System for Evaluating Draught of Tillage Tools Under Indoor Soil Bin Conditions," *Proceedings of the International Soil Tillage Research Organisation*, pp. 50–61, 2014.
- [74] S. Derafshpour and P. A. Mogaddam, "Chisel Plow Blades' Wear Modeling and the Determination of Wear Sensitive Points," *ResearchGate*, 2013.
- [75] S. A. Al-Suhaibani and A. E. Ghaly, "Comparative Study of the Kinetic Parameters of Three ChiselPlows Operating At DifferentDepthsand Forward Speed In A Sandy Soil," *The International Journal Of Engineering And Science*, vol. 2, no. 7, pp. 42–59, 2013.
- [76] P. Novák, J. Chyba, F. Kumhála, and P. Procházka, "Measurement of stubble cultivator draught force under different soil conditions," *Agronomy Research*, vol. 12, no. 1, pp. 135–142, 2014.
- [77] L. Naderloo, R. Alimadani, A. Akram, P. Javadikia, and H. Z. Khanghah, "Tillage depth and forward speed effects on draft of three primary tillage implements in clay loam soil," *International journal of food, agriculture and environment*, 2009.
- [78] R. G. Bayer, *Wear Analysis for Engineers*. New York: HNB, 2002.
- [79] K. Hokkirigawa, K. Kato, and Z. Z. Li, "The effect of hardness on the transition of the abrasive wear mechanism of steels," *Wear*, vol. 123, no. 2, pp. 241–251, Apr. 1988, doi: 10.1016/0043-1648(88)90102-0.
- [80] K. Hokkirigawa and K. Kato, "An experimental and theoretical investigation of ploughing, cutting and wedge formation during abrasive wear," *Tribology International*, vol. 21, no. 1, pp. 51–57, Feb. 1988, doi: 10.1016/0301-679X(88)90128-4.

- [81] J. J. Coronado and A. Sinatora, "Effect of abrasive size on wear of metallic materials and its relationship with microchips morphology and wear micromechanisms: Part 1," *Wear*, vol. 271, no. 9–10, pp. 1794–1803, Jul. 2011.
- [82] T. Kayaba, K. Hokkirigawa, and K. Kato, "Analysis of the abrasive wear mechanism by successive observations of wear processes in a scanning electron microscope," *Wear*, vol. 110, no. 3–4, pp. 419–430, Aug. 1986, doi: 10.1016/0043-1648(86)90115-8.
- [83] F. Schramm, Kalácska, V. Pfeiffer, J. Sukumaran, P. De Baets, and L. Frerichs, "Modelling of abrasive material loss at soil tillage via scratch test with the discrete element method," *Journal of Terramechanics*, vol. 91, pp. 275–283, Oct. 2020, doi: 10.1016/J.JTERRA.2020.08.002.
- [84] P. A. Cundall and O. D. L. Strack, "A discrete numerical model for granular assemblies," *Géotechnique*, vol. 29, no. 1, pp. 47–65, May 1979, doi: 10.1680/GEOT.1979.29.1.47.
- [85] Y. Prawoto, N. Jasmawati, and K. Sumeru, "Effect of Prior Austenite Grain Size on the Morphology and Mechanical Properties of Martensite in Medium Carbon Steel," *Journal of Materials Science & Technology*, vol. 28, no. 5, pp. 461–466, May 2012, doi: 10.1016/S1005-0302(12)60083-8.
- [86] S. Morito, H. Yoshida, T. Maki, and X. Huang, "Effect of block size on the strength of lath martensite in low carbon steels," *Materials Science and Engineering: A*, vol. 438–440, no. SPEC. ISS., pp. 237–240, Nov. 2006, doi: 10.1016/j.msea.2005.12.048.
- [87] Y. F. Shen, L. N. Qiu, X. Sun, L. Zuo, P. K. Liaw, and D. Raabe, "Effects of retained austenite volume fraction, morphology, and carbon content on strength and ductility of nanostructured TRIP-assisted steels," *Materials Science and Engineering: A*, vol. 636, pp. 551–564, Jun. 2015, doi: 10.1016/j.msea.2015.04.030.
- [88] M. Lindroos, K. Valtonen, A. Kemppainen, A. Laukkanen, K. Holmberg, and V.-T. Kuokkala, "Wear behavior and work hardening of high strength steels in high stress abrasion," *Wear*, vol. 322–323, pp. 32–40, Jan. 2015, doi: 10.1016/j.wear.2014.10.018.
- [89] P. V. Moghaddam, J. Hardell, E. Vuorinen, and B. Prakash, "The role of retained austenite in dry rolling/sliding wear of nanostructured carbide-free bainitic steels," *Wear*, vol. 428–429, pp. 193–204, Jun. 2019, doi: 10.1016/j.wear.2019.03.012.
- [90] G. Saha, K. Valtonen, A. Saastamoinen, P. Peura, and V.-T. Kuokkala, "Impact-abrasive and abrasive wear behavior of low carbon steels with a range of hardness-toughness properties," *Wear*, vol. 450–451, p. 203263, Jun. 2020, doi: 10.1016/j.wear.2020.203263.
- [91] G. Krauss, "Heat Treated Martensitic Steels: Microstructural Systems for Advanced Manufacture.," *ISIJ International*, vol. 35, no. 4, pp. 349–359, Apr. 1995, doi: 10.2355/isijinternational.35.349.
- [92] Á. Kalácska, P. De Baets, H. Ben Hamouda, K. Theuwissen, and J. Sukumaran, "Tribological investigation of abrasion resistant steels with martensitic and retained austenitic microstructure in single- and multi-asperity contact," *Wear*, vol. 482–483, p. 203980, Oct. 2021, doi: 10.1016/j.wear.2021.203980.
- [93] Á. Kalácska, L. Székely, R. Z. Keresztes, A. Gábora, T. Mankovits, and P. De Baets, "Abrasive Sensitivity of Martensitic and a Multi-Phase Steels under Different Abrasive Conditions," *Materials*, vol. 14, no. 6, p. 1343, Mar. 2021, doi: 10.3390/ma14061343.
- [94] A. Saastamoinen, A. Kaijalainen, T. T. Nyo, P. Suikkanen, D. Porter, and J. Kömi, "Direct-quenched and tempered low-C high-strength structural steel: The role of chemical composition on microstructure and mechanical properties," *Materials Science and Engineering A*, vol. 760, pp. 346–358, Jul. 2019, doi: 10.1016/j.msea.2019.06.018.
- [95] G. Krauss, "Martensite in steel: Strength and structure," *Materials Science and Engineering A*, vol. 273–275, pp. 40–57, Dec. 1999, doi: 10.1016/S0921-5093(99)00288-9.
- [96] G. Krauss, "Tempering of Lath Martensite in Low and Medium Carbon Steels: Assessment and Challenges," *Steel Research International*, vol. 88, no. 10, Oct. 2017, doi: 10.1002/srin.201700038.
- [97] B. Bushan, *Modern Tribology Handbook*. Boca Raton: CRC Press, 2001.
- [98] A. Ghaderi, G. Saha, T. Guo, D. Fabijanic, and M. R. Barnett, "Material wear map for ground-

- engaging steels based on scratch tests," *Wear*, vol. 404–405, pp. 153–165, Jun. 2018, doi: 10.1016/j.wear.2018.03.017.
- [99] N. Ojala *et al.*, "Effects of composition and microstructure on the abrasive wear performance of quenched wear resistant steels," *Wear*, vol. 317, no. 1–2, pp. 225–232, Sep. 2014, doi: 10.1016/j.wear.2014.06.003.
- [100] X. Xu, S. van der Zwaag, and W. Xu, "A novel multi-pass dual-indenter scratch test to unravel abrasion damage formation in construction steels," *Wear*, vol. 322–323, pp. 51–60, Jan. 2015, doi: 10.1016/j.wear.2014.10.011.
- [101] M. Shah and S. Das Bakshi, "Three-body abrasive wear of carbide-free bainite, martensite and bainite-martensite structure of similar hardness," *Wear*, vol. 402–403, pp. 207–215, May 2018, doi: 10.1016/j.wear.2018.02.020.
- [102] C. Trevisiol, A. Jourani, and S. Bouvier, "Effect of hardness, microstructure, normal load and abrasive size on friction and on wear behaviour of 35NCD16 steel," *Wear*, vol. 388–389, pp. 101–111, Oct. 2017, doi: 10.1016/j.wear.2017.05.008.
- [103] ASTM, "G171 – 03 Standard Test Method for Scratch Hardness of Materials Using a Diamond Stylus," vol. 03, no. Reapproved 2017, p. 7, 2017, doi: 10.1520/G0171-03R09E02.2.
- [104] M. Woldman, E. Van Der Heide, T. Tinga, and M. A. Masen, "The influence of abrasive body dimensions on single asperity wear," *Wear*, vol. 301, no. 1–2, pp. 76–81, Apr. 2013, doi: 10.1016/j.wear.2012.12.009.
- [105] S. Mezlini, M. Zidi, H. Arfa, M. Ben Tkaya, and P. Kapsa, "Experimental, numerical and analytical studies of abrasive wear: correlation between wear mechanisms and friction coefficient," *Comptes Rendus Mécanique*, vol. 333, no. 11, pp. 830–837, Nov. 2005, doi: 10.1016/j.crme.2005.09.005.
- [106] A. R. Chintha, K. Valtonen, V.-T. Kuokkala, S. Kundu, M. J. Peet, and H. K. D. H. Bhadeshia, "Role of fracture toughness in impact-abrasion wear," *Wear*, vol. 428–429, pp. 430–437, Jun. 2019, doi: 10.1016/j.wear.2019.03.028.
- [107] F.-J. Ulm and S. James, "The scratch test for strength and fracture toughness determination of oil well cements cured at high temperature and pressure," *Cement and Concrete Research*, vol. 41, no. 9, pp. 942–946, Sep. 2011, doi: 10.1016/j.cemconres.2011.04.014.
- [108] A.-T. Akono and F.-J. Ulm, "Scratch test model for the determination of fracture toughness," *Engineering Fracture Mechanics*, vol. 78, no. 2, pp. 334–342, Jan. 2011, doi: 10.1016/j.engfracmech.2010.09.017.
- [109] A. R. Chintha, "Metallurgical aspects of steels designed to resist abrasion, and impact-abrasion wear," *Materials Science and Technology*, vol. 35, no. 10, pp. 1133–1148, Jul. 2019, doi: 10.1080/02670836.2019.1615669.
- [110] V. Abouei, H. Saghafian, S. Kheirandish, and K. Ranjbar, "An investigation of the wear behaviour of 0.2% C dual phase steels," *Journal of Materials Processing Technology*, vol. 203, no. 1–3, pp. 107–112, Jul. 2008, doi: 10.1016/j.jmatprotec.2007.09.044.
- [111] G. W. Stachowiak and A. W. Batchelor, *Engineering tribology*. Amsterdam, The Netherlands, 2014.
- [112] W. Y. Ali and F. M. H. Ezzat, "Wear of tillage tools coated by thermoplastic coatings," *Wear*, vol. 173, no. 1–2, pp. 115–119, 1994, doi: 10.1016/0043-1648(94)90263-1.
- [113] J. K. Fulcher, T. H. Kosel, and N. F. Fiore, "The effect of carbide volume fraction on the low stress abrasion resistance of high Cr-Mo white cast irons," *Wear*, vol. 84, no. 3, pp. 313–325, Feb. 1983, doi: 10.1016/0043-1648(83)90272-7.
- [114] K. Grigoroudis and D. J. Stephenson, "Modelling low stress abrasive wear," *Wear*, vol. 1–2, no. 213, pp. 103–111, Dec. 1997, doi: 10.1016/S0043-1648(97)00170-1.
- [115] A. N. J. Stevenson and I. M. Hutchings, "Development of the dry sand/rubber wheel abrasion test," *Wear*, vol. 195, no. 1–2, pp. 232–240, Jul. 1996, doi: 10.1016/0043-1648(96)06965-7.
- [116] R. Dasgupta, B. K. Prasad, O. P. Modi, and A. K. Jha, "A comparison of material removal mechanism under low stress abrasive condition of steel and hardfacing alloys," *Journal of Materials Engineering and Performance* 1999 8:4, vol. 8, no. 4, pp. 437–442, Aug. 1999, doi:

- 10.1361/105994999770346738.
- [117] N. B. Dube and I. M. Hutchings, "Influence of particle fracture in the high-stress and low-stress abrasive wear of steel," *Wear*, vol. 233–235, pp. 246–256, Dec. 1999, doi: 10.1016/S0043-1648(99)00297-5.
 - [118] L. Bourithis and G. Papadimitriou, "Three body abrasion wear of low carbon steel modified surfaces," *Wear*, vol. 258, no. 11–12, pp. 1775–1786, Jun. 2005, doi: 10.1016/j.wear.2004.12.013.
 - [119] E. Y. H. Bobobee *et al.*, "Wear rate of animal-drawn ploughshares in selected Ghanaian soils," *Soil and Tillage Research*, vol. 93, no. 2, pp. 299–308, Apr. 2007, doi: 10.1016/j.still.2006.05.004.
 - [120] Z. Horvat, D. Filipovic, S. Kosutic, and R. Emert, "Reduction of mouldboard plough share wear by a combination technique of hardfacing," *Tribology International*, vol. 41, no. 8, pp. 778–782, Aug. 2008, doi: 10.1016/j.triboint.2008.01.008.
 - [121] D. Singh, K. P. Saha, and D. P. Mondal, "Development of mathematical model for prediction of abrasive wear behaviour in agricultural grade medium carbon steel," *Indian Journal of Engineering and Materials Sciences*, vol. 18, no. 2, pp. 125–136, 2011.
 - [122] ASTM International, "ASTM G132-96. Standard Test Method for Pin Abrasion Testing,," vol. 96, no. Reapproved 2018, p. 8, 2013.
 - [123] J. D. Huffington, "Abrasion groove sizes and shapes in relation to the mechanism of abrasion," *Wear*, vol. 49, no. 2, pp. 327–337, 1978.
 - [124] M. G. Hamblin and G. W. Stachowiak, "A multi-scale measure of particle abrasivity, and its relation to two-body abrasive wear," *Wear*, vol. 190, no. 2, pp. 190–196, 1995.
 - [125] "Silicon Carbide Paper, Grit 120. 32 mm (1¼") dia. 100 pcs. (40400129)." [https://e-shop.struers.com/CA/EN/products/Miscellaneous/Non-destructive_Testing/Silicon_Carbide_Paper_Grit_120_32_mm_\(1_dia_100_pcs\(40400129\).aspx](https://e-shop.struers.com/CA/EN/products/Miscellaneous/Non-destructive_Testing/Silicon_Carbide_Paper_Grit_120_32_mm_(1_dia_100_pcs(40400129).aspx) (accessed Nov. 03, 2021).
 - [126] M. R. Thakare, J. A. Wharton, R. J. K. Wood, and C. Menger, "Effect of abrasive particle size and the influence of microstructure on the wear mechanisms in wear-resistant materials," *Wear*, vol. 276–277, pp. 16–28, Feb. 2012, doi: 10.1016/J.WEAR.2011.11.008.
 - [127] M. Adamiak, *Abrasion Resistance of Materials*. Rijeka: InTech, 2012.
 - [128] B. W. E. Avient, J. Goddard, and H. W. Ilm An, "An experimental study of friction and wear during abrasion of metals," *Proceedings of the Royal Society of London. Series A. Mathematical and Physical Sciences*, vol. 258, no. 1293, pp. 159–180, Oct. 1960, doi: 10.1098/rspa.1960.0180.
 - [129] S. W. Date and S. Malkin, "Effects of grit size on abrasion with coated abrasives," *Wear*, vol. 40, no. 2, pp. 223–235, Nov. 1976, doi: 10.1016/0043-1648(76)90100-9.
 - [130] R. F. Smart and J. C. Moore, "Materials selection for wear resistance," *Wear*, vol. 56, no. 1, pp. 55–67, Sep. 1979, doi: 10.1016/0043-1648(79)90006-1.
 - [131] A. Misra and I. Finnie, "On the size effect in abrasive and erosive wear," *Wear*, vol. 65, no. 3, pp. 359–373, Jan. 1981, doi: 10.1016/0043-1648(81)90062-4.
 - [132] L. . Whittaker and A. Matthews, "Comparison of a simulated 'in-service' rig test with a standardised laboratory abrasion test," *Surface and Coatings Technology*, vol. 177–178, pp. 603–610, Jan. 2004, doi: 10.1016/j.surfcoat.2003.08.060.
 - [133] T. H. Kosel, "Solid particle erosion," *ASM Handbook on Friction, Lubrication and Wear Technology*, vol. 18, p. 199, 1992.
 - [134] P. P. Shitole, S. H. Gawande, G. R. Desale, and B. D. Nandre, "Effect of Impacting Particle Kinetic Energy on Slurry Erosion Wear," *Journal of Bio- and Tribo-Corrosion*, vol. 1, no. 4, pp. 1–9, Dec. 2015, doi: 10.1007/s40735-015-0028-6.
 - [135] M. Arora, C. D. Ohl, and K. A. Mørch, "Cavitation inception on microparticles: A self-propelled particle accelerator," *Physical Review Letters*, vol. 92, no. 17, p. 174501, Apr. 2004, doi: 10.1103/PhysRevLett.92.174501.
 - [136] A. A. Gadhihar, A. Sharma, D. B. Goel, and C. P. Sharma, "Fabrication and testing of slurry pot erosion tester," *Transactions of the Indian Institute of Metals*, vol. 64, no. 4–5, pp. 493–500, Oct. 2011, doi: 10.1007/s12666-011-0075-8.

- [137] S. N, "Theoretical modelling of slurry erosive wear testing of HVOF thermally sprayed Inconel-Titania coatings," *Indian Journal of Science and Technology*, vol. 5, no. 6, pp. 1–5, Jun. 2012, doi: 10.17485/ijst/2012/v5i6.17.
- [138] H.-N. Liu, M. Nomura, K. Ogi, and M. Sakamoto, "Abrasion resistance of high Cr cast irons at an elevated temperature," *Wear*, vol. 250, no. 1–12, pp. 71–75, Oct. 2001, doi: 10.1016/S0043-1648(01)00665-2.
- [139] M. H. Buszko and A. K. Krella, "Slurry Erosion – Design of Test Devices," *Advances in Materials Science*, vol. 17, no. 2, pp. 5–17, Jun. 2017, doi: 10.1515/adms-2017-0007.
- [140] H. S. Grewal, A. Agrawal, and H. Singh, "Design and development of high-velocity slurry erosion test rig using CFD," *Journal of Materials Engineering and Performance*, vol. 22, no. 1, pp. 152–161, Jan. 2013, doi: 10.1007/s11665-012-0219-y.
- [141] B. T. Lu, J. F. Lu, and J. L. Luo, "Erosion–corrosion of carbon steel in simulated tailing slurries," *Corrosion Science*, vol. 53, no. 3, pp. 1000–1008, Mar. 2011, doi: 10.1016/j.corsci.2010.11.034.
- [142] N. Ojala *et al.*, "Wear performance of quenched wear resistant steels in abrasive slurry erosion," *Wear*, vol. 354–355, pp. 21–31, May 2016, doi: 10.1016/j.wear.2016.02.019.
- [143] R. Macchini, M. S. A. Bradley, and T. Deng, "Influence of particle size, density, particle concentration on bend erosive wear in pneumatic conveyors," *Wear*, vol. 303, no. 1–2, pp. 21–29, Jun. 2013, doi: 10.1016/j.wear.2013.02.014.
- [144] C. Song *et al.*, "Effect of multiphase microstructure on fatigue crack propagation behavior in TRIP-assisted steels," *International Journal of Fatigue*, vol. 133, p. 105425, Apr. 2020, doi: 10.1016/j.ijfatigue.2019.105425.
- [145] K. L. Johnson, *Contact Mechanics*. Cambridge: Cambridge University Press, 1985.
- [146] C. J. Coetzee and D. N. J. Els, "Calibration of granular material parameters for DEM modelling and numerical verification by blade-granular material interaction," *Journal of Terramechanics*, vol. 46, no. 1, pp. 15–26, Feb. 2009, doi: 10.1016/j.jterra.2008.12.004.
- [147] J. B. Barr, M. Ucgul, J. M. A. Desbiolles, and J. M. Fielke, "Simulating the effect of rake angle on narrow opener performance with the discrete element method," *Biosystems Engineering*, vol. 171, pp. 1–15, Jul. 2018, doi: 10.1016/j.biosystemseng.2018.04.013.
- [148] I. Shmulevich, Z. Asaf, and D. Rubinstein, "Interaction between soil and a wide cutting blade using the discrete element method," *Soil and Tillage Research*, vol. 97, no. 1, pp. 37–50, Nov. 2007, doi: 10.1016/j.still.2007.08.009.
- [149] C. Hang, X. Gao, M. Yuan, Y. Huang, and R. Zhu, "Discrete element simulations and experiments of soil disturbance as affected by the tine spacing of subsoiler," *Biosystems Engineering*, vol. 168, pp. 73–82, Apr. 2018, doi: 10.1016/j.biosystemseng.2017.03.008.
- [150] R. Zhang, B. Chen, J. qiao Li, and S. cai Xu, "DEM Simulation of Clod Crushing by Bionic Bulldozing Plate," *Journal of Bionic Engineering*, vol. 5, no. SUPPL., pp. 72–78, Sep. 2008, doi: 10.1016/S1672-6529(08)60075-X.
- [151] L. Graff, M. Roberge, and T. Crowe, "Application of Discrete Element Method (DEM) simulations as a tool for predicting tillage tool wear," *XVIIth World Congress of the International Commission of Agricultural and Biosystems Engineering*, 2010.
- [152] J. Tong *et al.*, "DEM Numerical simulation of abrasive wear characteristics of a bioinspired ridged surface," *Journal of Bionic Engineering*, vol. 7, no. 2, pp. 175–181, Jun. 2010, doi: 10.1016/S1672-6529(09)60206-7.

9 APPENDIX

Parts of the thesis work (tine wear characterisation, single-asperity and pin-abrasion tests) were performed in the framework of the Integrated Material Modelling for Abrasion Resistant Steels (IMMARS) project work (RFSR-CT-2015-00010) funded by Research Fund for Coal and Steel (RFCS). All the conducted investigations are personal and original contributions. The referred DEM model was developed at TUBS (Braunschweig, Germany) in the research collaboration described in [21]. The most frequent investigations concern the parameterisation of the soil and the resulting forces and loads on the tools to be investigated. Relative particle-geometry displacements were used by Coetzee and Els [146] to predict the position and shape of the shear lines in front of the geometry in the form of a horizontally aligned plate. Soil mixing is an essential task of soil tillage; the mixing effects were investigated by process and tool parameters with the DEM. Barr *et. al* [147] investigates the effect of narrow point openers on the basis of the parameters of the furrow profile such as the loosened area, ridge height, immersion area, furrow backfilling and lateral soil insertion. The tool shape was used by Shmulevich *et. al* [148] with the DEM to optimize soil tillage tools. It was based on four designs, which were evaluated with regard to the forces occurring but also on the basis of the mixing performance. In addition to the effect of a single tool in the soil, Hang *et. al* [149] investigated the influence of the lateral distance between two tools for optimal soil mixing. Zhang *et. al* [150] analysed adjustments of the geometry for a better working pattern in soil tillage with regard to better clod crushing. Graff *et. al* [151] focuses fundamentally on the modelling of wear in the DEM. The model is validated using a cylindrical solid as a reference that has been moved through the soil [24]. Tong *et. al* [152] investigates the effect of a change in the surface morphology on the wear behaviour of a Farrer's scallop.

Only individual particles from the particle bed are monitored at one time step (Figure 9-1). At this time the submerging phase of the tine into the particle bed is completed and a constant flow has formed. The particles under consideration are initially in contact with the cutting edge of the tine and move away from the tool on its path through the particles. The angle of the cutting edge to the tine top surface (tine wing) is 90°, with the exception of the tip. As a result, the cutting edge is inclined backwards in the mounting position. When looking at the particle movement in the top view (z-axis), as shown in the figure, it can be seen that the particles are covered by the geometry during the tine movement. The tine is shown with reduced opacity. The particle movement mainly below the cutting edge can also be seen in the Figure 9-2 in the frontal view.

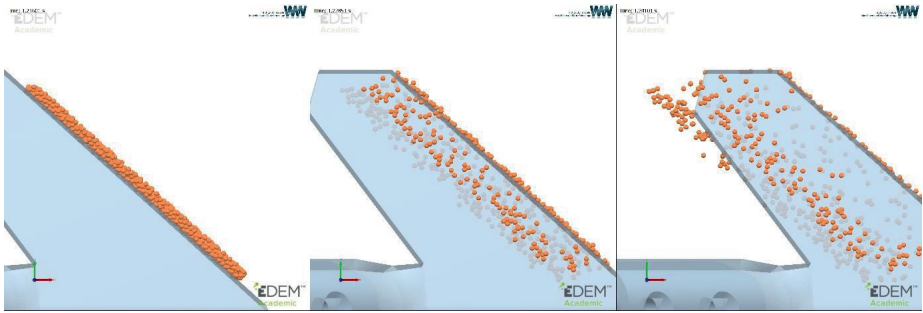


Figure 9-1 Soil particle movement along the cutting edge in the DEM analysis [21]

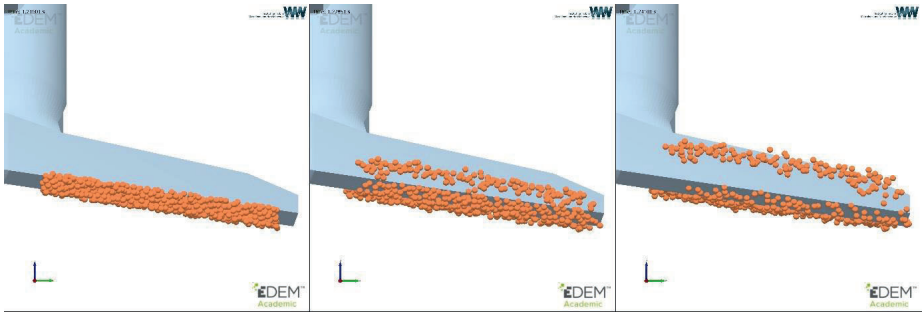


Figure 9-2 Frontal view of the particle movement along the cutting edge [21]

10 CURRICULUM VITAE

Contact and personal information

Name	Ádám Kalácska
Date of birth	19 December 1990
Place of birth	Budapest
Nationality	Hungarian
E-mail	adam.kalacska@UGent.be kalacsadam@hotmail.com

Education

2016-2022	PhD student: Ghent University (UGent), Faculty of Engineering and Architecture, Department of Electromechanical, Systems and Metal Engineering
2014-2016	MSc in Mechanical Engineering, Budapest University of Technology and Economics (BME), Faculty of Mechanical Engineering
2009-2014	BSc in Mechanical Engineering, Budapest University of Technology and Economics (BME), Faculty of Mechanical Engineering
2001-2009	Premonstratensian St. Norbert High School, Gödöllő

Scientific awards

2019	Best Poster award: Wear of Materials, 22nd International Conference, USA.
------	---------------------------------------------------------------------------

Teaching experience (2015-2021)

Advanced Machine Design (lab practices, UGent, 2016-2017, 2020-2021)

Engineering Project (lab practices, UGent, 2019-2022)

Supervised students (2016-2021)

2017	Fabien Taillieu	UGent, MSc thesis
2020	Laurens Descamps	UGent, MSc thesis
2021	Dries Van Acker	UGent, MSc thesis

A1 - Peer-reviewed journal articles included in Science Citation Index

- 1 Zoltán Károly, Gábor Kalácska, Jacob Sukumaran, Dieter Fauconnier, **Ádám Kalácska**, Miklós Mohai, Szilvia Klébert: *Effect of atmospheric cold plasma treatment on the adhesion and tribological properties of Polyamide 66 and Poly(Tetrafluoroethylene)*. *Materials*, 14(4), 658, 2019, DOI 10.3390/ma12040658. IF 3.057 (2019).
- 2 Jacob Sukumaran, **Ádám Kalácska**, Patric Daniel Neis, Dieter Fauconnier, Patrick De Baets: From single asperity to real scale in the wear of agricultural tine. *Wear*, 426, 14-26, 2019. DOI 10.1016/j.wear.2018.12.014. IF 4.108 (2019).
- 3 **Ádám Kalácska**, Patrick De Baets, Dieter Fauconnier, Florian Schramm, Ludger Frerichs, Jacob Sukumaran: Abrasive wear behaviour of 27MnB5 steel used in agricultural tines. *Wear*, 442, 2020. DOI 10.1016/j.wear.2019.203107. IF 3.892 (2020).
- 4 Levente Ferenc Tóth, Jacob Sukumaran, Gábor Szabó, **Ádám Kalácska**, Dieter Fauconnier, Rajini Nagarajan, Patrick De Baets: *Large-scale tribological characterisation of eco-friendly basalt and jute fibre reinforced thermoset composites*. *Wear*, 450, 2020. DOI 10.1016/j.wear.2020.203274. IF 3.892 (2020).
- 5 Florian Schramm, **Ádám Kalácska**, Valentin Pfeiffer, Jacob Sukumaran, Patrick De Baets, Ludger Frerichs: Modelling of abrasive material loss at soil tillage via scratch test with the discrete element method. *Journal of Terramechanics*, 91, 275-283, 2020. DOI 10.1016/j.jterra.2020.08.002. IF 2.446 (2020).
- 6 Hasan Muhandes, **Ádám Kalácska**, László Székely, Róbert Keresztes, Gábor Kalácska: Abrasive sensitivity of engineering polymers and a bio-composite under different abrasive conditions. *Materials*, 13(22), 5239, 2020. DOI 10.3390/ma13225239. IF 3.623 (2020).
- 7 **Ádám Kalácska**, László Székely, Róbert Zolt Keresztes, András Gábora, Tamás Mankovits, Patrick De Baets: Abrasive sensitivity of martensitic and a multiphase steels under different abrasive conditions. *Materials*, 14(6), 1343, 2021. DOI 10.3390/ma14061343. IF 3.601
- 8 **Ádám Kalácska**, Patrick De Baets, Haithem Ben Hamouda, Koenraad Theuwsen, Jacob Sukumaran: Tribological investigation of abrasion resistant steels with martensitic and retained austenitic microstructure in single- and multi-asperity contact. *Wear*, 482, 2021. DOI 10.1016/j.wear.2021.203980. IF 3.601

A2 - Peer-reviewed journal articles not included in Science Citation Index

- 1 Jacob Sukumaran, **Ádám Kalácska**, Patrick De Baets, Kannaki Shanmugham Pondicherry: Wear mechanisms prevalent in agricultural tines. Mechanical Engineering Letters, 2017, 15, 87-93, ISSN 2060-3789.
- 2 Gábor Kalácska, László Székely, **Ádám Kalácska**: Multiple linear regression method for deeper analyses of abrasive tribological behaviour of engineering materials. Modern concepts in material science, 3(4), 2020. DOI 10.33552/MCMS.2020.03.000569.

C1 - Articles in conference proceedings

- 1 Peerapon Wechsuwanmanee, Junhe Lian, Jacob Sukumaran, **Ádám Kalácska**, Haithem Ben Hamouda, Patrick De Baets, Sebastian Münstermann: Finite element model in Abrasion analysis for single-asperity scratch test. Proceedings of the 7th International Conference on Fracture Fatigue and Wear, 768-779, 2018. DOI 10.1007/978-981-13-0411-8_68.
- 2 Hasan Muhandes, **Ádám Kalácska**, Gábor Kalácska: Analyses of abrasive wear behaviour in pin-on-plate tribo-system for several materials. IOP Conf. Ser.: Material Science and Engineering, 749, 2020. DOI 10.1088/1757-899x/749/1/012020.

C3 - Conference abstracts

- 1 Hayder Al-Maliki, Gábor Kalácska, **Ádám Kalácska**, Jacob Sukumaran: Influence of atmospheric DBD plasma on 3D topography of polymers. 2nd Danube Vltava Sava Polymer Meeting, Vienna (Austria), 05-08 September 2017. ISBN 978-9504017-6-9.
- 2 Hayder Al-Maliki, Zoltán Károly, Szilvia Klébert, Gábor Kalácska, **Ádám Kalácska**, Jacob Sukumaran: Surface characterization of Polytetrafluoroethylene treated by atmospheric plasma. 5th International Scientific Conference on Advances in Mechanical Engineering, Debrecen (Hungary), 12-14 October 2017. ISBN 978-963-473-304-1.
- 3 **Ádám Kalácska**, Jacob Sukumaran, Patrick De Baets: Tribological investigation of tillage tools. 19th FEA Research Symposium, 19 February 2019. Id 8609674.
- 4 **Ádám Kalácska**, Jacob Sukumaran, Haithem Ben Hamouda, Patrick De Baets: Abrasive slurry testing of different type of steels used in agricultural machinery. Wear of Materials, 22nd International Conference, Miami (USA), 14-19 April 2019. Id 8615318.



Abraded agricultural cultivator tine.